Copy 5
RM L52H01

NACA

RESEARCH MEMORANDUM

AN INVESTIGATION OF A 0.16-SCALE MODEL OF THE DOUGLAS X-3 AIRPLANE TO DETERMINE MEANS OF IMPROVING THE LOW-SPEED LONGITUDINAL STABILITY AND CONTROL CHARACTERISTICS

By John W. McKee and John M. Riebe

Langley Aeronautical Laboratory
Langley Field, Va.

FOR REFERENCE

NATIONAL ADVISORY COMMITTEE
FOR AERONAUTICS

WASHINGTON

November 5, 1952

NATIONAL ADVISORY COMMITTEE FOR AERONAUTICS

RESEARCH MEMORANDUM

AN INVESTIGATION OF A 0.16-SCALE MODEL OF THE DOUGLAS X-3 AIRPLANE TO DETERMINE MEANS OF IMPROVING THE LOW-SPEED LONGITUDINAL STABILITY AND CONTROL CHARACTERISTICS

By John W. McKee and John M. Riebe

SUMMARY

An investigation of a 0.16-scale model of the Douglas X-3 airplane was made in the Langley 300 MPH 7- by 10-foot tunnel to determine means of improving the low-speed longitudinal stability and control characteristics. Various high-lift devices in the form of plain and slotted leading-edge flaps and plain, split, and slotted trailing-edge flaps were also tested on the model.

The model in the original condition, flaps up, had unstable pitching-moment characteristics near the stall (0.6 lift coefficient) which were caused by an unstable break in the pitching-moment characteristics of the wing at the stall and by the fact that the relatively large fuselage continued to increase the downwash angle at the tail location as the angle of attack was increased above that at which wing stall occurred. The severity of the unstable break in the pitching-moment curve was reduced, or the break eliminated, as the span of the horizontal tail was increased. The largest static margin and one of the smoothest pitching-moment-coefficient variations with lift coefficient occurred for the highest-aspect-ratio tail (4.76) tested on the model in the position of the original tail. Raising the wing for one of the tail configurations (aspect ratio 4) so that the tail was 4 percent wing mean aerodynamic chord above the wing-chord line extended, compared with 53 percent mean aerodynamic chord for the low wing position, resulted in a decided improvement in longitudinal stability at the stall. A model configuration which had a high wing and a low tail with a moment arm about half the moment arm of the original tail generally had good stability characteristics through the lift range. The large differences in longitudinal stability at the stall for the X-3 model with various tail configurations resulted primarily from large spanwise variations in effective downwash angle.

The highest trimmed maximum lift coefficient was obtained with a slotted leading-edge flap deflected 45° combined with either a slotted or a split trailing-edge flap deflected 50°.

INTRODUCTION

An investigation of a 0.16-scale model of the Douglas X-3 research airplane to determine means of improving the low-speed longitudinal stability and control characteristics has been made in the Langley 300 MPH 7- by 10-foot tunnel.

Previous investigations of preliminary models of the X-3 research airplane, such as that of reference 1, have indicated longitudinal instability for the airplane at the stall at both low speed (ref. 1) and high subsonic speeds (unpublished). The primary objective of the present investigation, which was made on a later and more complete model version of the airplane having a canopy and a ducting system, was to determine the factors in the airplane design that were resulting in unstable pitching-moment characteristics of the model at the stall and to provide corrective measures that generally would necessitate the least possible change in design. Various high-lift devices in the form of plain and slotted leading-edge flaps and plain, split, and slotted trailing-edge flaps were also tested on the model.

SYMBOLS

The system of axes used, together with an indication of the positive forces, moments, and angles, is presented in figure 1. Pitching-moment coefficients are given about the center-of-gravity location shown in figure 2 (0 percent of the mean aerodynamic chord). The symbols used in this paper are defined as follows:

C_L	lift coefficient, Lift/qS
C_m	pitching-moment coefficient, $M/qS\bar{c}$
C_D	drag coefficient, Drag/qS
X	longitudinal force along X-axis, lb
Z	force along Z-axis (lift equals -Z), lb

[redacted]

M	pitching moment about Y-axis, ft-lb
q	free-stream dynamic pressure, $\rho V^2/2$, lb/sq ft
S	wing area, sq ft
$\bar{c}$	wing mean aerodynamic chord, ft
c	local chord
b	wing span, ft
V	free-stream velocity, ft/sec
A	aspect ratio
λ	taper ratio
Λ	sweep angle, deg
ρ	mass density of air, slugs/cu ft
α	angle of attack of fuselage reference line, deg
i_t	deflection angle of all-movable tail with respect to fuselage reference line, deg (hinge line located at 25 percent $\bar{c}$ of original tail)
δ	flap deflection measured in a plane perpendicular to hinge line, deg (fig. 4)
ϵ	downwash angle, deg

Subscripts:

LE	leading edge
TE	trailing edge
t	tail
0.25c	25-percent-chord line
max	maximum

[redacted]

MODEL AND APPARATUS

The physical characteristics of the 0.16-scale model of the Douglas X-3 research airplane are presented in figure 2 and a photograph of the model mounted in the Langley 300 MPH 7- by 10-foot tunnel is shown as figure 3. The model was constructed by the Douglas Aircraft Company and is one of a series of models used by the Langley Pilotless Aircraft Research Division for a high-speed investigation. A second wing was constructed of wood with the same airfoil section and plan form as the original wing for the investigation of the various leading- and trailing-edge high-lift devices shown in figure 4. Dimensions of the various revised all-movable horizontal-tail arrangements, which were constructed by adding $\frac{1}{32}$-inch sheet brass to the original tail, are given in figure 5 and the geometric characteristics of the wing-tip tail arrangement are shown in figure 6. Several auxiliary horizontal surfaces which were added separately to the model and various fuselage-nose arrangements tested are shown in figures 7 and 8, respectively. A rather crude high-wing—low-tail model configuration that was devised during the test program is shown in figure 9, and dimensions of the rounded wing-leading-edge arrangement are given in figure 10.

The twin air ducts were normally open with no air-flow restriction. For some tests the ducts were plugged at the duct inlets. Plug fairings used at the duct inlets of the model were of two shapes, flat and hemispherical with surfaces tangent to the inlet lips.

CORRECTIONS

Jet-boundary corrections have been applied to the angles of attack, the drag coefficients, and the tail-on pitching-moment coefficients. The corrections, computed by use of reference 2, were as follows:

$$\Delta\alpha = 0.410C_L$$

$$\Delta C_D = 0.0071C_L^2$$

$$\Delta C_m = 0.0121C_L$$

where $\Delta\alpha$ is measured in degrees. All jet-boundary corrections were added to the test data.

[redacted]

Corrections due to blocking by the model and its wake as well as tare corrections resulting from the support strut have not been applied. Previous tests on other models indicate that these corrections would be small except for the drag tare correction. Estimates made from previous investigations of similar complete-model setups in the Langley 300 MPH 7- by 10-foot tunnel indicate that the drag coefficients for the 0.16-scale X-3 model would be lower by about 0.01 if the effects of the model support struts were considered.

The test data have been corrected for horizontal buoyancy and airflow misalinement in the tunnel.

The tests were made in the Langley 300 MPH 7- by 10-foot tunnel at a dynamic pressure of 99.75 pounds per square foot (except where noted otherwise) which corresponds to a Mach number of 0.264 and a Reynolds number of 2.23×10^6 based on the wing mean aerodynamic chord of 1.254 feet.

RESULTS AND DISCUSSION

Table I is an index of figures 11 to 30, which present the results of the investigation.

The results of longitudinal tests of the original model configuration (fig. 2) showing unstable pitching-moment characteristics at the stall of the model (at about 12° angle of attack and near 0.6 trim lift coefficient for a tail setting of -4°) are shown in figure 11. The model with the tail off was unstable in about the same angle-of-attack and lift-coefficient range. A large loss in stabilizing influence from the tail occurred near the stall region, as shown by the tail-on and tail-off pitching-moment-coefficient curves which became nearly parallel at the higher lift coefficients.

In order to determine the factors in the airplane design that were resulting in unstable pitching-moment characteristics of the model at the stall, the longitudinal stability characteristics of component parts of the original model were determined and are presented in figure 12. The figure shows the large unstable contribution of the fuselage to the pitching moment throughout the angle-of-attack range. In the lower angle-of-attack range, the wing alone was longitudinally stable to the extent that, when combined with the fuselage, the combination was only slightly unstable. The pitching-moment-coefficient curve of the wing alone broke unstable at the stall (about 14° angle of attack). The pitching-moment-coefficient curve of the combined wing-fuselage configuration broke unstable at a smaller angle of attack and lift coefficient than the pitching-moment coefficient of wing alone plus fuselage alone; thus

[redacted]

some deleterious effect from wing-fuselage interference is indicated. However, at higher angles of attack, wing-fuselage interference was stabilizing.

The addition of the horizontal tail of the original model was not only unsuccessful in removing the longitudinal instability at the stall of the wing-fuselage combination but also made the instability in about the 16° to 19° angle-of-attack range slightly greater, as shown by the curve for the complete model minus fuselage and wing which corresponds to the condition for the tail alone in the presence of wing and fuselage. The tail with only the interference effects from the fuselage was generally stabilizing throughout the angle-of-attack range as shown by the curve for (fuselage + tail) - (fuselage alone).

Effect of Various Factors on Longitudinal Stability

In order to provide corrective measures to the unstable pitching-moment characteristics of the model at the stall that would generally necessitate the least possible change in design, the following various test conditions and configurations were applied to the model.

Reynolds number effect.- As shown by figure 14, Reynolds number had no large effect on the longitudinal instability of the model at the stall in the range of Reynolds numbers investigated.

Air flow over fuselage in vicinity of ducts.- Air-flow studies of the original model by means of wool tufts (fig. 13) showed unsteady flow on the fuselage in the region above the duct lips as well as early wing stall. In order to determine whether fuselage air-flow separation was contributing to the longitudinal instability, smooth flow, as shown by unpublished tuft studies, was established over the fuselage by plugging the duct with a rounded fairing; however, the longitudinal instability was still present (fig. 15). The fact that the instability was little affected by separation over the duct is seen from similar pitching-moment data for the configuration with a flat plug across the duct entrance. The results of tuft studies for this configuration, not presented herein, showed a much larger air-flow separation commencing at a lower angle of attack than that which existed for the original model. Similar tests at other Reynolds numbers, not presented herein, show the same lack of effect of air-flow separation on the abrupt reversal of pitching moment. It can be noted, however, that the largest instability occurred with the duct open, particularly in the range of $\alpha = 14°$, $C_L = 0.6$ to $\alpha = 22°$, $C_L = 0.8$ (figs. 15 and 11).

Wing incidence.- Some additional evidence that the unstable break in the pitching-moment curve is directly associated with wing stall rather than fuselage attitude is presented in figure 16(a) where it is shown that

changing the wing incidence from 0° to 2.5° had little effect on the variation of the pitching-moment coefficient with lift coefficient and that the unstable break occurred at about the same wing angle of attack (fig. 16(b)).

Some effects of wing incidence on the change in pitching-moment coefficient at a given lift coefficient (which would apply to airplanes and missile configurations with longitudinal control provided by means of an all-movable wing) are shown in figure 16(a). The wing-incidence increase for the condition with tail off resulted in a negative increment in pitching moment at a given lift coefficient; whereas only a small change in pitching-moment coefficient occurred with tail on. Wing-incidence change did affect both tail-on and tail-off pitching moment when plotted against angle of attack of the fuselage reference line (fig. 16(b)). These differences in pitching-moment-coefficient increments resulted from the pitching-moment-coefficient contribution from the longitudinally unstable fuselage alone (fig. 12), the pitching-moment-coefficient contribution from the tail resulting from angle-of-attack change of the model, and the pitching-moment-coefficient contribution from the tail caused by change in wing downwash at the tail.

The fuselage effect can be shown by considering at a given lift coefficient the difference in pitching-moment-coefficient increment from wing-incidence change for tail on and off. For the tail-off condition the wing may be considered as held at a given angle of attack (in order to hold the lift coefficient constant) and the fuselage attitude changed 2.5° inasmuch as the fuselage lift-curve slope is very small (fig. 12). For the tail-off condition, the 2.5° wing-incidence change corresponds to about -0.04 pitching-moment-coefficient increment (fig. 16), which agrees very nearly with the pitching-moment-coefficient increment for negative 2.5° change of fuselage-alone attitude (fig. 12). For the tail-on condition, and with the wing held at a given angle of attack in order to obtain constant lift coefficient (a condition which is only approximated because of the increased lift-curve slope of the fuselage plus tail, compared to that of the fuselage, fig. 12) a negative 2.5° shift of fuselage-plus-tail attitude resulted in a 0.15 positive increment of pitching-moment coefficient (fig. 12). This positive increment, which partially offsets the negative pitching-moment increment of the fuselage alone, was a contributing factor for the small change in pitching-moment coefficient caused by wing-incidence change with tail on. However a constant lift coefficient as assumed above to explain fuselage effect on the difference in pitching-moment-coefficient increment, tail on and off, cannot be realized because of the negative lift of the fuselage plus tail for negative shift in fuselage-plus-tail attitude. It is therefore necessary also to consider a positive angle-of-attack shift for the wing-fuselage-tail combination. Since wing angle-of-attack change will have the largest effect on lift, the pitching-moment-coefficient change resulting from wing-incidence change at a fixed

[redacted]

fuselage angle of attack might be considered, (fig. 16(b)). With the center of moment at 0 percent $\bar{c}$, an increase of wing incidence for the tail-off condition might be expected to result in the diving moment at a given fuselage angle of attack (fig. 16(b)). However with the tail on, the diving moment from the wing-incidence change was smaller and was evidently compensated by a download on the tail resulting from increased downwash from the wing. The downwash effect on the tail is shown in figure 12 by the difference in slopes of the pitching-moment-coefficient curves for (complete model) - (fuselage + wing) and (fuselage + tail) - (fuselage alone).

Fuselage-nose shape.- Shortening the fuselage nose (fig. 8) did not alleviate the pitching-moment-coefficient break (fig. 17).

Wing-leading-edge shape.- Extending the angle of attack at which wing stall occurred by use of the rounded wing leading edge altered the model pitching-moment characteristics (fig. 18). Rounding only the outboard section of the wing did not have very much effect on the pitching-moment characteristics; whereas rounding only the inboard section delayed the unstable pitching-moment break to higher lift coefficients. A full-span rounding of the wing leading edge resulted in a general smoothing of the pitching-moment curve, delayed the stall lift coefficient from about 0.6 lift coefficient to 1.1 lift coefficient, and resulted in a stable but erratic break of the pitching-moment curve at the wing stall for the tail incidence angle of -4°. However, the model with the full-span rounded wing leading edge and with tail incidence angle of -4° was slightly unstable in the 0.7 to 1.1 lift-coefficient range.

Wing-tip tail and fillets.- The addition of the wing-tip tail (fig. 6) to the original model did not improve the unstable break at the stall (fig. 19) but resulted in a stable shift of the pitching-moment curves, tail on and off. The wing fillet had a smoothing effect on the pitching-moment curve; however, the model was still unstable at the stall. The horizontal fin and tail fillet had very little effect on the pitching-moment characteristics.

Tail size and aspect ratio.- The severity of the break in the pitching-moment curve of the model (fig. 20) was dependent upon the span of the horizontal tail used, which was larger for the higher aspect ratios (fig. 5). With either the tail configuration of aspect ratio 4.0 or of 4.76, the model was generally longitudinally stable throughout the lift-coefficient range tested. Some instability occurred at about 0.62 lift coefficient and 15° angle of attack for the aspect-ratio-4.0 tail at -4° incidence angle, (fig. 20); however, for tail incidence angles nearer trim for 0.62 lift coefficient (fig. 25(a)) the model was longitudinally stable. An unstable break in the pitching-moment curve near 0.6 lift coefficient was still present with the tail configuration of

aspect ratio 3, $\frac{b_t}{b} = 0.52$ but it was much less severe than the unstable break of the original model configuration which had the same aspect ratio but a shorter span.

The variation of effective downwash angle with angle of attack computed from the tail-incidence and tail-off tests for the model with various tail configurations (fig. 21) indicates that the stability of the model was severely affected by spanwise downwash-distribution variation. The effective downwash for the original tail configuration continued to increase rapidly at angles of attack far above wing stall (approximately 11° for the wing in the presence of the fuselage) primarily because the lift of the fuselage which held to angles of attack beyond that of the wing (fig. 12); the fuselage width (fig. 2) was relatively large compared to the tail span. Increasing the tail aspect ratio and the ratio of tail span to wing span resulted in a larger part of the tail being in a more favorable downwash region where the variation of effective downwash angle with angle of attack, $d\epsilon/d\alpha$, was reduced.

Wake surveys behind a somewhat similar model of the X-3 airplane in reference 1 showed a large reduction of downwash angle and an increase of dynamic-pressure ratio in the region of the tail with increasing distance from the plane of symmetry at high angles of attack. The reference paper also showed that the effect of the fuselage downwash was destabilizing after the wing stalled.

Relative position of wing and tail.- Raising the wing for the aspect-ratio-4.0 tail configuration so that the tail was $0.04\bar{c}$ above the chord line extended, compared to $0.53\bar{c}$ above the chord line extended for the low wing position, resulted in increased longitudinal stability above 0.7 lift coefficient (fig. 22(a)).

The configuration with the high wing and low tail (fig. 9) had stable pitching-moment curves which for all cases near trimmed values of pitching-moment coefficient were free of reversals or sudden changes in slopes (fig. 22(b)). This high-wing—low-tail configuration, which had a moment arm about half the moment arm of the original tail, appears to offer one means of reducing the longitudinal-stability problems associated with airplanes having low-aspect-ratio wings and horizontal tails. The variation of effective downwash angle with angle of attack was very favorable for good stability at high angles of attack for the tail configurations with high wing location (fig. 21). The upwash shown for the high-wing—low-tail configuration at 0° angle of attack was probably due to upflow around the fuselage.

A comparison of the neutral points of the model with the various tail arrangements is presented in figure 23. The discontinuities that occurred for some of the tail configurations resulted from unstable

[redacted]

breaks in the pitching-moment curves of the tail-incidence tests from which the neutral points were determined. As might be expected, the static margin for the model increased with aspect ratio and area of the horizontal tail tested in the position of the original tail. The smallest and smoothest neutral-point shift with lift coefficient in the 0 to 0.6 lift-coefficient range, about 15 percent $\bar{c}$, occurred for the configuration having the high wing and low tail. Neutral points are not given above 0.6 lift coefficient for the tail configurations which have pitching-moment data far from trim conditions.

Leading- and trailing-edge flaps.- As shown in figures 24(a) and 26, deflecting the plain leading-edge and trailing-edge flaps on the model with the original tail generally increased the longitudinal stability in the low positive lift-coefficient range and delayed the unstable break in the pitching-moment curve to higher values of lift coefficient. The configuration with a slotted leading-edge flap deflected 45° and a split trailing-edge flap deflected 50° also had increased stability at low lift coefficients but had neutral stability and an unstable break in the pitching-moment coefficient at high lift (fig. 26(e)). With the slotted leading-edge flap deflected 45° and trailing-edge flap at zero deflection, a stable break occurred at high lift coefficients, but the model had some instability in about the 0.5 to 0.8 lift-coefficient range (fig. 26(f)).

Flap characteristics on the wing alone (fig. 24(b)) also showed with leading-edge flap deflection an increase in maximum lift coefficient at which the pitching moment became unstable.

With the aspect-ratio-4.0 tail configuration the model was generally stable throughout the lift-coefficient range, regardless of the type and deflection of the leading- and trailing-edge flaps tested (figs. 25 and 27). Some instability did occur at the stall for the configuration with a split trailing-edge flap and with plain leading-edge flap (fig. 25(c)); however, these data are for tail incidence angles which are far out of trim.

For the tail of aspect ratio 3 and $\frac{b_t}{b} = 0.52$ a slight unstable break occurred in the 0.7 to 0.8 lift-coefficient range with trailing-edge flap at zero deflection and the leading-edge flap deflected 10° (fig. 28(b)). Deflecting the plain leading-edge flap 30° with split trailing-edge flap deflected 50° produced stability throughout the lift range for negative tail incidence angles which would be required for trim (fig. 28(c)). Deflecting a plain leading-edge flap 30° in conjunction with a split trailing-edge flap deflected 50° produced about neutral stability of the model with negative tail incidence angles for the $A = 4.76$ tail at intermediate lift coefficients of 0.8 to 1.1 (fig. 29(c)), but for this model configuration a stable break occurred at the stall.

Flap Characteristics

Effect on $C_{L_{max}}$.- The lift-coefficient curves presented in figure 24(a) show the beneficial effect of deflecting the leading-edge flap in extending the linear portion of the lift curve to higher values of lift coefficient by delaying leading-edge separation. The maximum lift coefficient (defined as that lift coefficient at which the slope of the lift curve first became zero) was extended from 0.63 at $\alpha = 11.5^\circ$ for the model with plain wing to 1.0 at $\alpha = 20^\circ$ for the model with the leading-edge flap deflected 30°. An index of the various flap arrangements tested for various tail configurations on the model is given in table II. Included in the table are values of maximum trim lift coefficient obtained for the various model configurations by either interpolating the data for various tail incidences or by estimating the loss in lift caused by download on the tail for trim.

Because the tail moment arm was essentially constant, the tail configuration generally had negligible effect on trimmed $C_{L_{max}}$ for a given leading- and trailing-edge flap configuration. The unstable break in pitching-moment coefficient was considered as the factor limiting the maximum trim lift coefficient for the original model and wing-alone configuration. For the model with revised tail configurations, a sudden stable break in pitching-moment coefficient might be the limiting factor, but higher trim lift coefficients might be obtained, depending on the effectiveness of the tail at incidence angles higher than those tested. For example, the data of figure 27(b), (the model with the A = 4.0 tail with leading-edge flap undeflected and slotted trailing-edge flap undeflected) show that the model might be capable of being trimmed at lift coefficients above the stable break in pitching moment. The trim lift coefficient of the model at the stable break in pitching moment with either the split or slotted trailing-edge flap was about the same. The highest trimmed maximum lift coefficient was obtained on the model with a slotted leading-edge flap deflected 45° combined with either a slotted or a split trailing-edge flap deflected 50°. The slotted leading-edge flap configuration on the model was optimum in a two-dimensional investigation (ref. 3); however, the configurations may not be optimum for the present three-dimensional investigation. At the time of testing, the single slotted trailing-edge flap configuration (fig. 4(b)) was believed optimum. However, recent unpublished data on other wings have indicated that better lift effectiveness can be obtained with gaps other than that tested.

Effect on tail effectiveness and minimum flying speed.- A comparison of the tail incidence required for steady, straight, unyawed flight of the X-3 model with various tail arrangements and various leading- and trailing-edge flap configurations is given in figure 30. The minimum velocities for the model with the original tail configuration were

generally determined by the lift coefficients at which the model became longitudinally unstable. The minimum velocities for the model with the revised tail configurations correspond to the lift coefficients at which a loss of tail effectiveness occurred because of a sudden rapid increase in longitudinal stability such as shown in figure 27(h). The limit minimum speeds for some of the configurations were not determined because it would have been necessary to extrapolate the tail-effectiveness data, such as shown in figure 28(a), to tail deflection angles far beyond those investigated.

The lowest minimum speed occurred for the model with the A = 4.0 tail configuration with the slotted leading-edge flap deflected 45° and split trailing-edge flap deflected 50°. The use of a slotted trailing-edge flap deflected 50° in place of the split trailing-edge flap deflected 50° produced about the same variation of i_t with airspeed. However, the minimum speed might actually be slightly lower, depending upon how tail effectiveness varies at tail deflection angles beyond those tested in the present investigation.

These data generally show only a small change in tail incidence angle required when the various flaps are deflected from the zero position.

CONCLUSIONS

Results of longitudinal stability tests on a 0.16-scale model of the Douglas X-3 research airplane in the Langley 300 MPH 7- by 10-foot tunnel indicate the following conclusions:

1. The original model configuration had unstable pitching-moment characteristics at the stall which were caused by an unstable break in the pitching-moment characteristic of the wing at the stall and by the fact that the relatively large fuselage continued to increase the downwash angle at the tail location as the angle of attack was increased above that at which wing stall occurred. Air flow through the duct and separation on the fuselage at the entrance location had negligible effects on the unstable pitching-moment break.

2. The severity of the unstable break in the pitching-moment curve was reduced or the break eliminated as the span of the horizontal tail was increased so that a larger part of the tail was in a more favorable downwash region.

3. The largest static margin and one of the smoothest variations of pitching-moment coefficient with lift coefficient for the case with no flaps deflected occurred with the highest-aspect-ratio and largest-span tail tested on the model at the original tail location.

[redacted]

4. Raising the wing for the aspect-ratio-4.0 tail configuration so that the tail was 4 percent wing mean aerodynamic chord above the wing-chord line extended, compared to 53 percent mean aerodynamic chord for the low wing position, resulted in a decided improvement in longitudinal stability at the stall.

5. A model configuration which had a high wing and a low tail with a moment arm about half the moment arm of the original tail generally had good stability characteristics through the lift range.

6. For the model with tail configurations having unstable breaks in the pitching-moment curves, various arrangements of the leading- and trailing-edge flaps generally increased the stability in the low lift-coefficient range and delayed the unstable break to higher lift coefficients.

7. The highest trimmed maximum lift coefficient was obtained on the model with a slotted leading-edge flap deflected 45° combined with either a slotted or a split trailing-edge flap deflected 50°.

Langley Aeronautical Laboratory,
National Advisory Committee for Aeronautics,
Langley Field, Va.

REFERENCES

1. Delany, Noel K., and Hayter, Nora-Lee F.: Low-Speed Investigation of a 0.16-Scale Model of the X-3 Airplane - Longitudinal Characteristics. NACA RM A50G06, 1950.

2. Gillis, Clarence L., Polhamus, Edward C., and Gray, Joseph L., Jr.: Charts for Determining Jet-Boundary Corrections for Complete Models in 7- by 10-Foot Closed Rectangular Wind Tunnels. NACA ARR L5G31, 1945.

3. McKee, Paul B.: Preliminary Report of an Investigation on the Maximum Lift Coefficient of a 4.5 Percent Thick Supersonic Airfoil Equipped With High Lift Devices. Part II - Various Double Slotted Trailing Edge Flaps Combined With Plain and Slotted Leading Edge Flaps. MR No. MCREXA9-4482-5-27, Air Materiel Command, U.S. Air Force, Nov. 2, 1950.

[redacted]

TABLE I.- INDEX OF FIGURES PRESENTING

RESULTS OF INVESTIGATION

Figure	Data presented
11	Longitudinal aerodynamic characteristics of the original model. Reynolds number, 2.23×10^6.
12	Longitudinal stability characteristics of component parts of the model.
13	Air-flow studies of the original model. Flaps zero; ducts open.
14	Effect of Reynolds number on the longitudinal stability of the model. Original configuration; $i_t = -4^\circ$.
15	Effect of plugging the duct inlets on the longitudinal stability of the model. Original configuration; $i_t = -4^\circ$.
16	Effect of wing incidence on the longitudinal stability of the model. Original configuration.
17	Effect of altering the fuselage-nose configuration on the longitudinal stability of the model. $i_t = -4^\circ$.
18	Effect of rounding the wing leading edge on the longitudinal stability of the model.
19	Effect of auxiliary fillets and a wing-tip tail on the longitudinal stability of the model. $i_t = 0^\circ$.
20	Effect of various tail arrangements on the longitudinal stability characteristics of the model. $i_t = -4^\circ$.
21	Effective downwash angles and dynamic-pressure ratio q_t/q for various tail arrangements of a 0.16-scale model of the Douglas X-3 airplane.
22	Effect of tail location on the longitudinal stability characteristics of the model with high and low wing.
23	All-movable-tail-fixed neutral points of the Douglas X-3 airplane as determined from wind-tunnel test of a 0.16-scale model.

[redacted]

TABLE I - Concluded

INDEX OF FIGURES PRESENTING RESULTS OF INVESTIGATION

Figure	Data presented
24	Effect of various leading- and trailing-edge flap configurations on the longitudinal stability of the original model.
25	Effect of various leading- and trailing-edge flap configurations on the longitudinal stability characteristics of the model with the A = 4.0, $\frac{b_t}{b}$ = 0.59 tail.
26	Effect of various leading- and trailing-edge flap configurations on the tail effectiveness of the model. Original tail configuration.
27	Effect of various leading- and trailing-edge flap configurations on the tail effectiveness of the model with the A = 4.0, $\frac{b_t}{b}$ = 0.59 tail.
28	Effect of various leading- and trailing-edge flap arrangements on the tail effectiveness of the model with the A = 3.0, $\frac{b_t}{b}$ = 0.52 tail.
29	Effect of various leading- and trailing-edge flap arrangements on the tail effectiveness of the model with the A = 4.76, $\frac{b_t}{b}$ = 0.73 tail.
30	Effect of various flap arrangements on the variation of horizontal-tail incidence with indicated airspeed of the airplane for steady flight conditions. Wing loading, 100 pounds per square foot.

TABLE II.- INDEX OF FIGURES HAVING DATA ON HIGH-LIFT DEVICES AND ESTIMATED MAXIMUM TRIM LIFT COEFFICIENTS

Model configuration	Flap configuration		Maximum trim C_L	Factor limiting maximum trim C_L (*)	Figure
	δ_{LE}	δ_{TE}			
Original model	0°	0°	0.62	a	11, 24(a)
Original model	10° plain	0°	.72	a	24(a), 26(a)
Original model	30° plain	0°	.99	a	24(a), 26(b)
Original model	30° plain	60° plain	1.23	a	24(a), 26(c)
Original model	30° plain	50° split	1.30	a	24(a), 26(d)
Original model	45° slotted	0°		c	24(a), 26(f)
Original model	45° slotted	50° split	1.65	a	24(a), 26(e)
Wing alone	0°	0°	.61	a	24(b)
Wing alone	10° plain	0°	.72	a	24(b)
Wing alone	30° plain	0°	.90	a	24(b)
Wing alone	30° plain	60° plain	1.25	a	24(b)
Model with A = 4 tail	0°	0°	.59	b	25(a), 25(b), 25(c), 27(a)
Model with A = 4 tail	0°	0° slotted		c	27(b)
Model with A = 4 tail	10° plain	0°		c	25(b), 25(c), 27(f)
Model with A = 4 tail	10° plain	20° slotted		c	25(b)
Model with A = 4 tail	10° plain	30° slotted		c	25(b)
Model with A = 4 tail	30° plain	30° slotted		c	25(b)
Model with A = 4 tail	30° plain	40° slotted	1.26	b	25(b), 27(h)
Model with A = 4 tail	30° plain	50° slotted			25(b)
Model with A = 4 tail	30° plain	50° split	1.31	b	25(c), 27(g)
Model with A = 4 tail	45° slotted	0°		c	25(c), 27(c)
Model with A = 4 tail	45° slotted	20° slotted		c	25(a)
Model with A = 4 tail	45° slotted	30° slotted		c	25(a)
Model with A = 4 tail	45° slotted	40° slotted	1.63	b	25(a)
Model with A = 4 tail	45° slotted	50° slotted	1.65	b	25(a), 27(d)
Model with A = 4 tail	45° slotted	50° split	1.67	b	25(c), 27(e)
Model with A = 3 tail	0°	0°	.60	b	28(a)
Model with A = 3 tail	10° plain	0°	.71	b	28(b)
Model with A = 3 tail	30° plain	50° split	1.30	b	28(c)
Model with A = 4.7 tail	0°	0°	.61	b	29(a)
Model with A = 4.7 tail	10° plain	0°	.71	b	29(b)
Model with A = 4.7 tail	30° plain	50° split	1.31	b	29(c)

*a - C_m breaks unstable.

b - C_m has sudden stable break in pitching moment but maximum trim C_L might be higher, depending on tail effectiveness (for example, see fig. 27(b)).

c - Undetermined (will depend on tail effectiveness at high incidence angles).

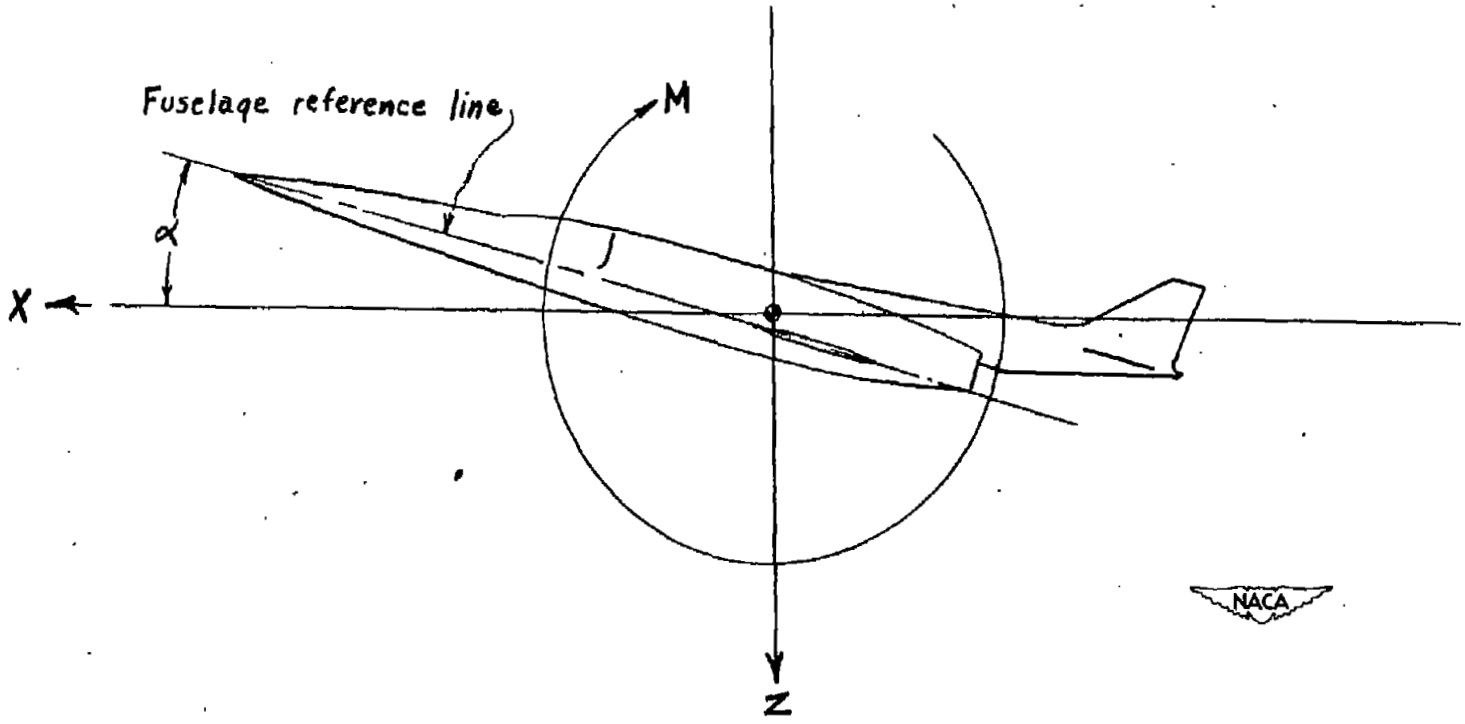

Figure 1.- System of longitudinal stability axes.

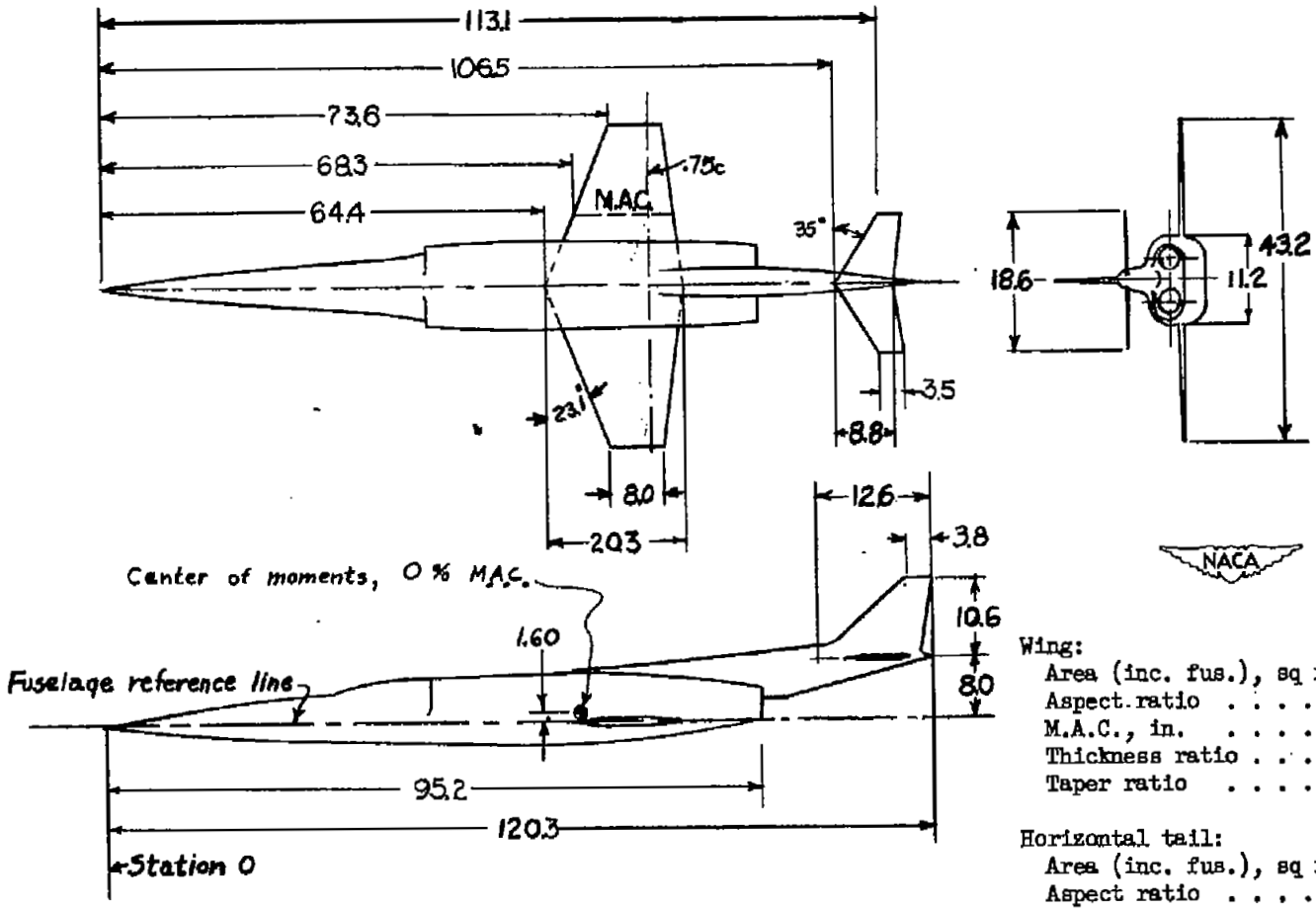

Wing:

Area (inc. fus.), sq ft	4.25
Aspect ratio	3.0
M.A.C., in.	15.05
Thickness ratio	0.045c
Taper ratio	0.4

Horizontal tail:

Area (inc. fus.), sq ft	0.79
Aspect ratio	3.0
M.A.C., in.	6.54
Taper ratio	0.4

$\frac{b_t}{b} = 0.43$

Figure 2.- General arrangement of the model, original condition. (All dimensions are in inches.)

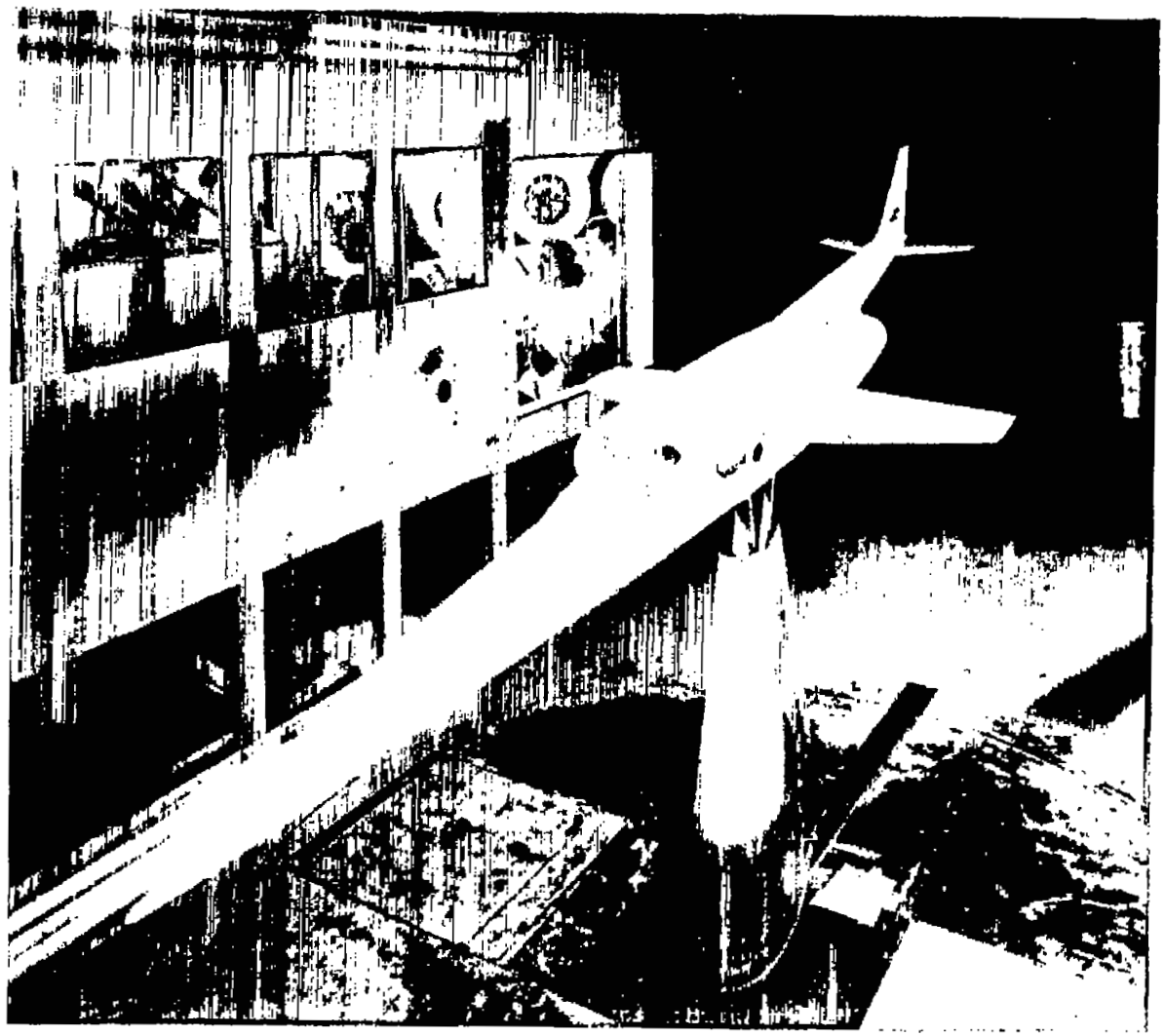

Figure 3.- The 0.16-scale model of the Douglas X-3 airplane in the Langley 300 MPH 7- by 10-foot tunnel.

NACA L-67617

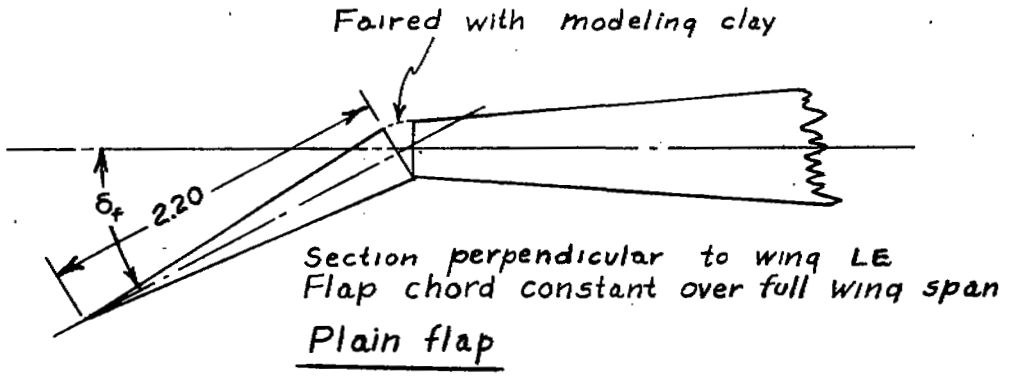

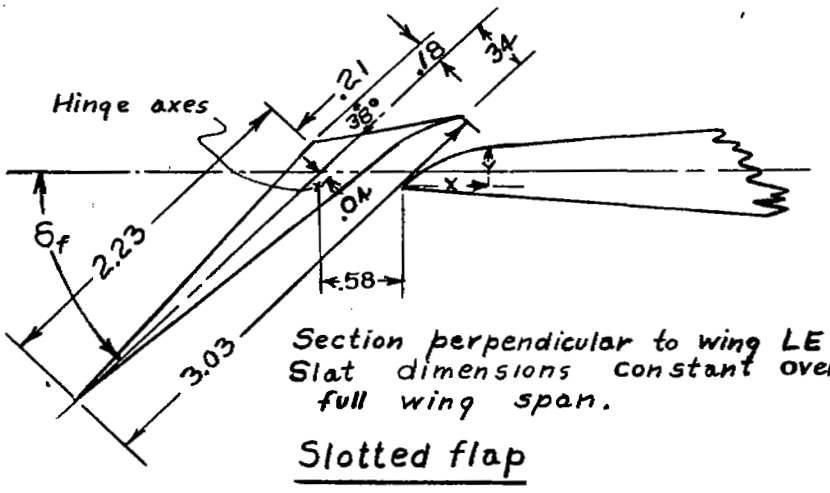

X	Y_{root}	Y_{tip}
0	0	0
.1	.20	.18
.2	.27	.25
.3	.35	.30
.4	.39	.35
.5	.42	.36
.6	.44	.37
.7	.46	.38
.8	.47	

NACA

(a) Leading-edge flaps.

Figure 4.- Leading- and trailing-edge flap arrangements tested on model.

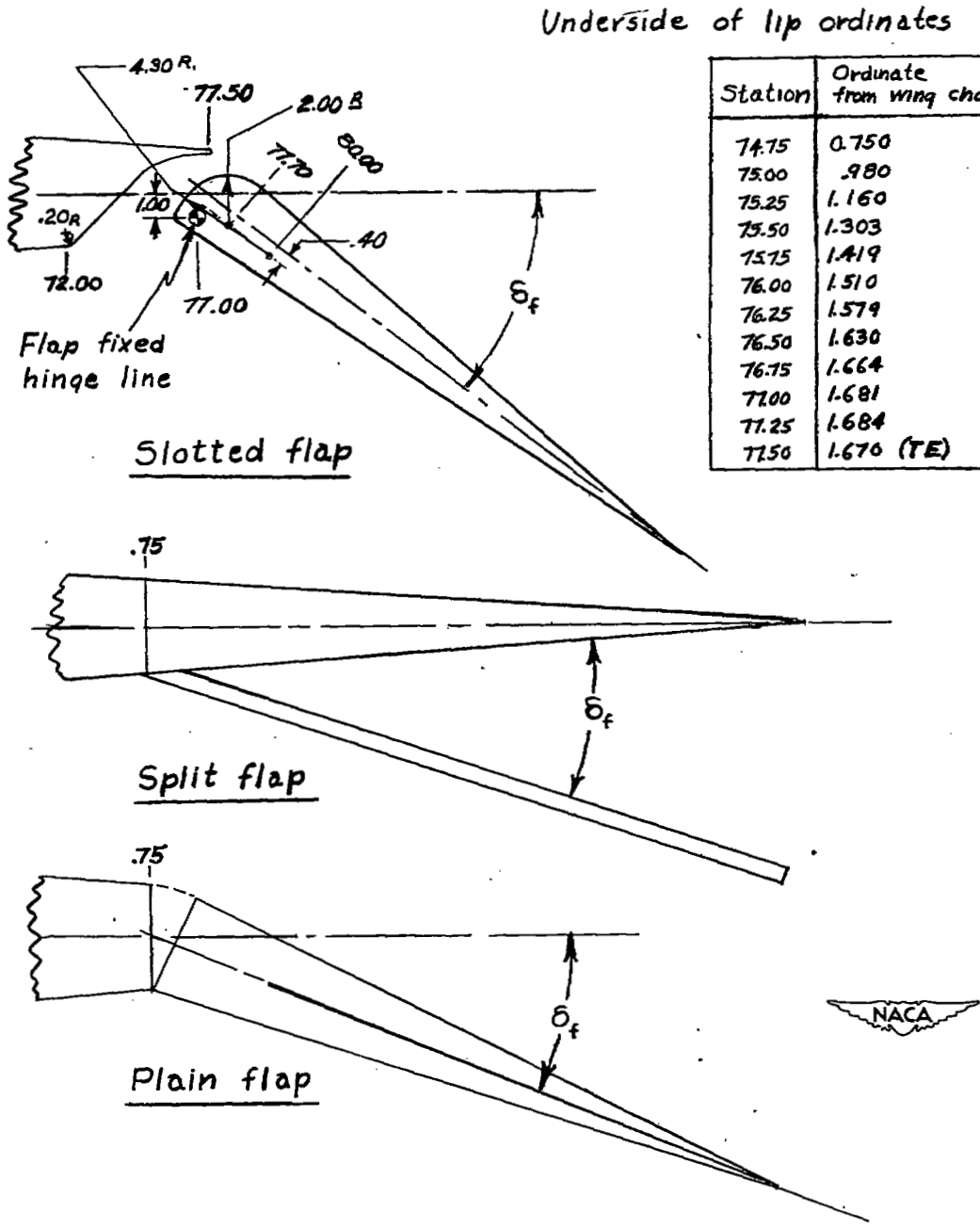

(b) Trailing-edge flaps. All dimensions are in percent of wing chord. Flap spans extended from fuselage to 70 percent wing semispan and from plane of symmetry to 70 percent wing semispan for wing-alone tests.

Figure 4.- Concluded.

[redacted]

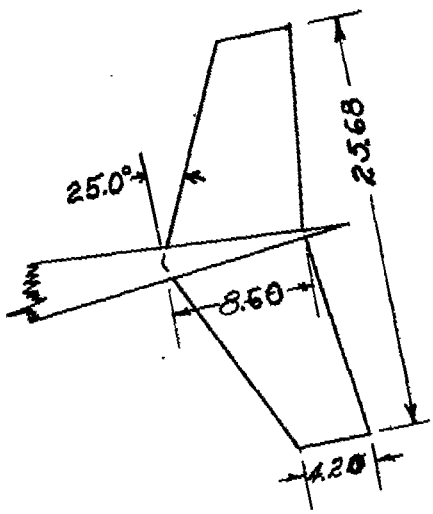

$A_t = 4.0$

$\lambda = .49$

$\Lambda_{.25c} = 20.9°$

$S_t = 1.14\ ft^2$

$\frac{b_t}{b} = .59$

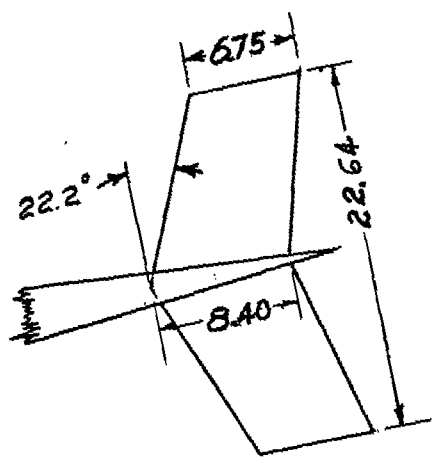

$A_t = 3.0$

$\lambda = .80$

$\Lambda_{.25c} = 20.4°$

$S_t = 1.19\ ft^2$

$\frac{b_t}{b} = .52$

Leading edge of root chord of tails located 1/32" ahead of original tail root chord shown in figure 2, vertical location of tails same as original tail.

Figure 5.- Revised horizontal-tail arrangements tested on the model.

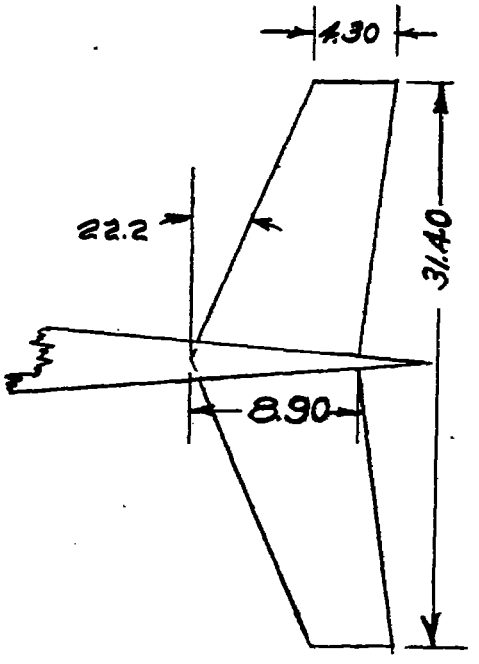

$A_t = 4.76$

$\lambda = .48$

$\Lambda_{.25c} = 18.5°$

$S_t = 1.44\ ft^2$

$\frac{b_t}{b} = .73$

$\frac{S_t}{S} = .339$

Figure 5.- Concluded.

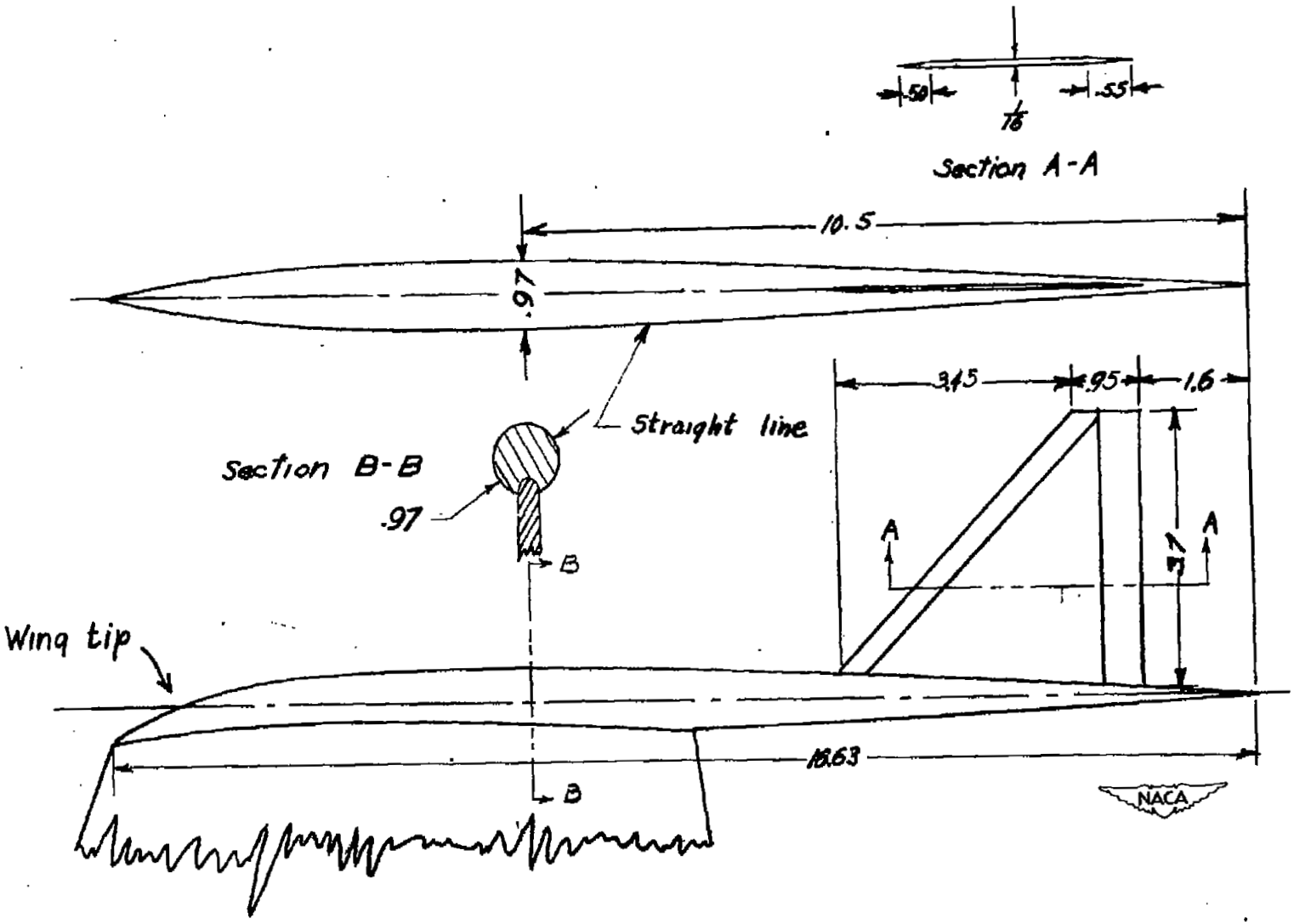

Figure 6.- Wing-tip tail configuration tested on the model. (All dimensions are in inches.)

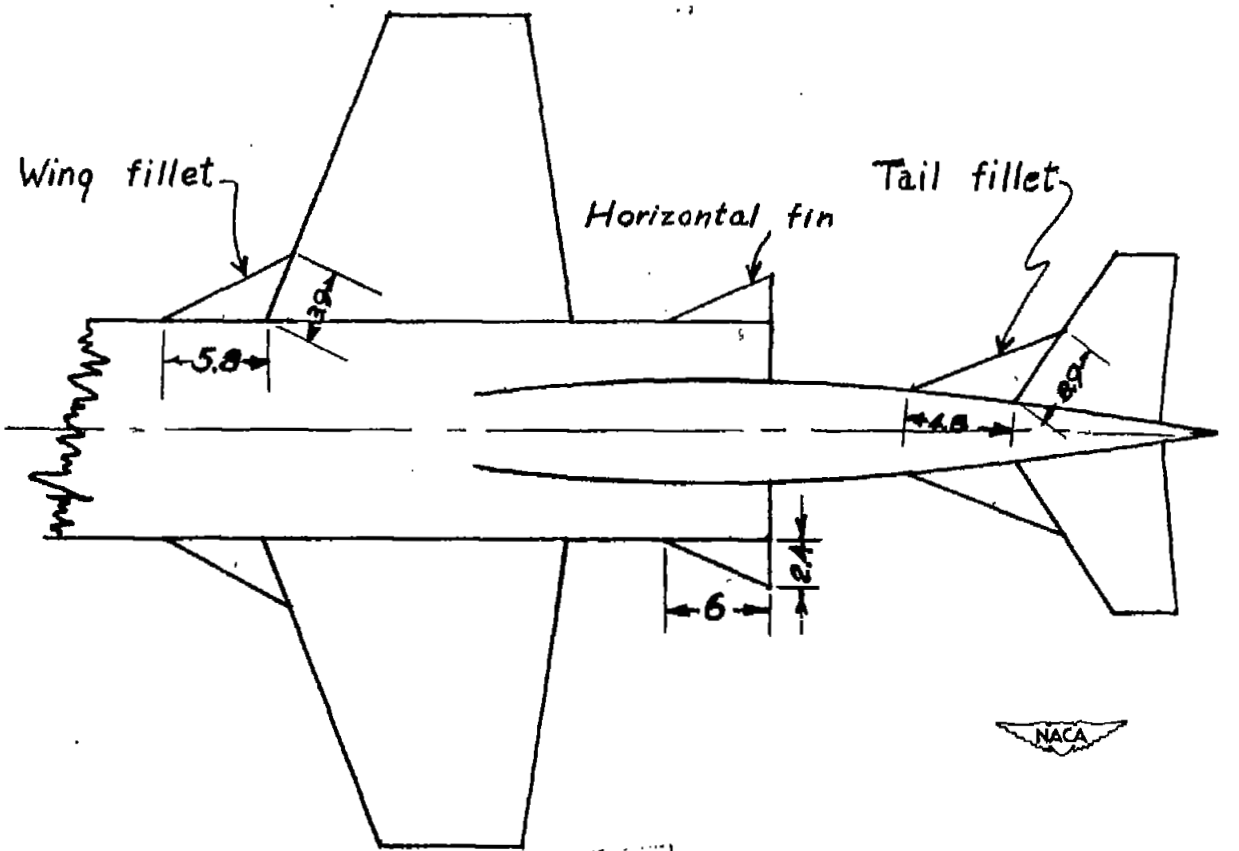

Figure 7.- Fin and fillet arrangements of the model. (All dimensions are in inches.)

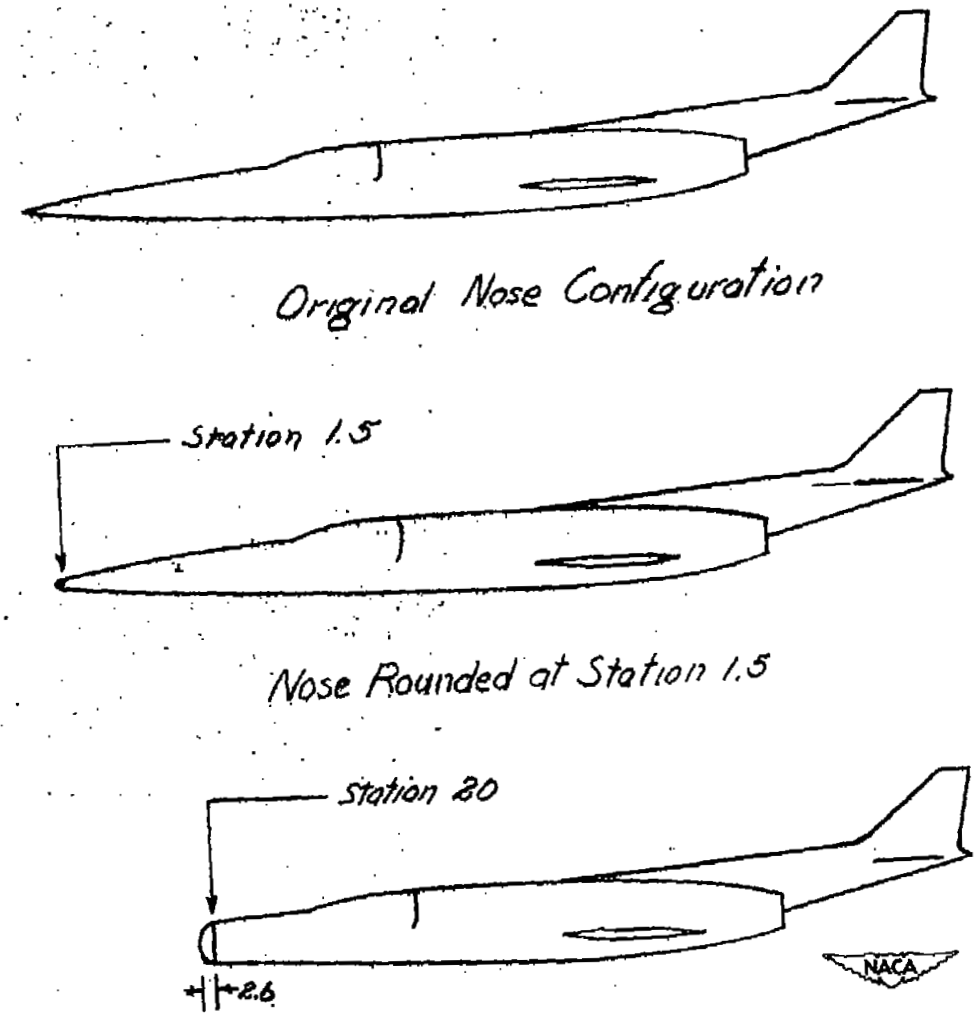

Figure 8.- Fuselage-nose configurations tested on the model. (All dimensions are in inches.)

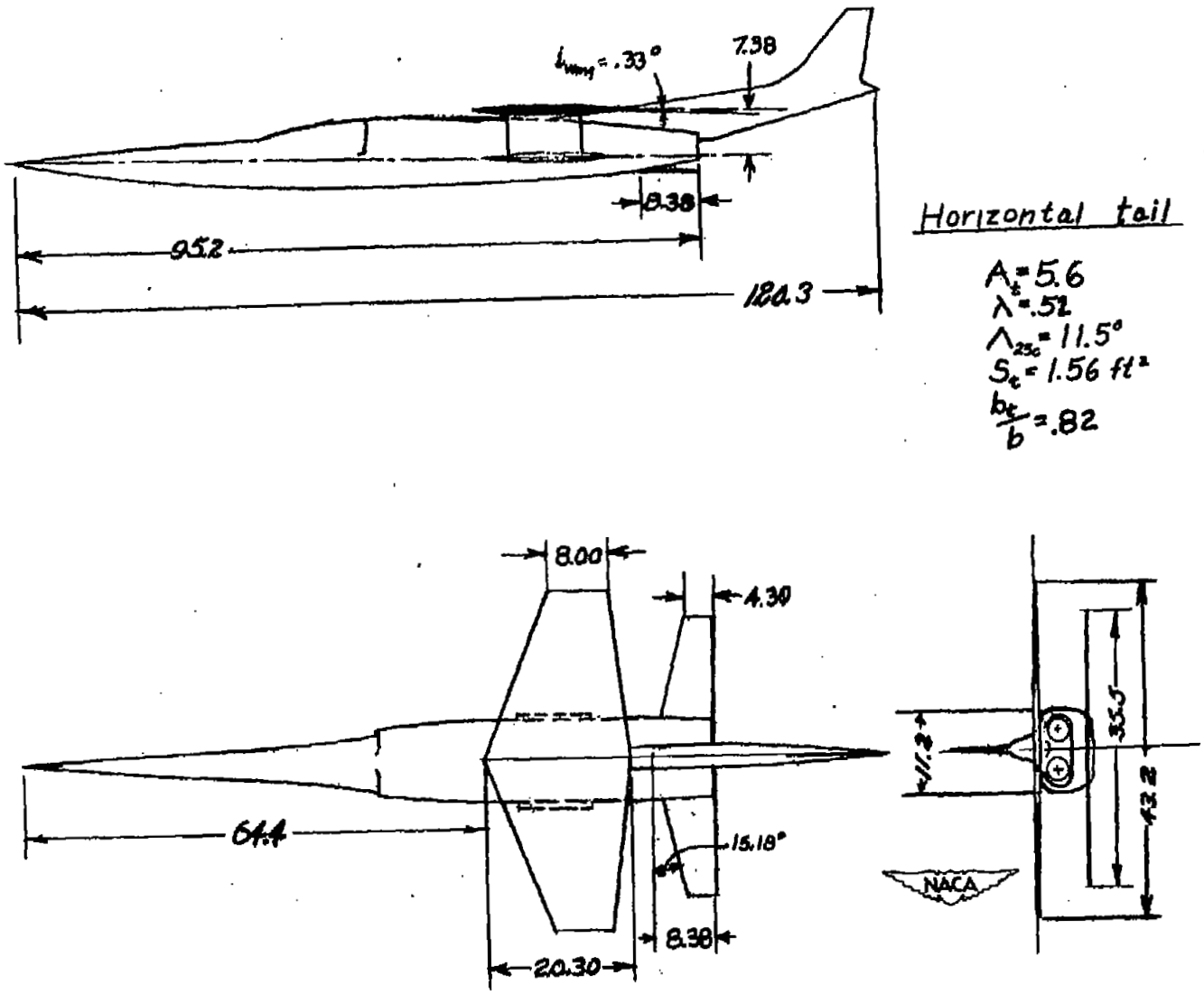

Figure 9.- The high-wing-low-tail model configuration.

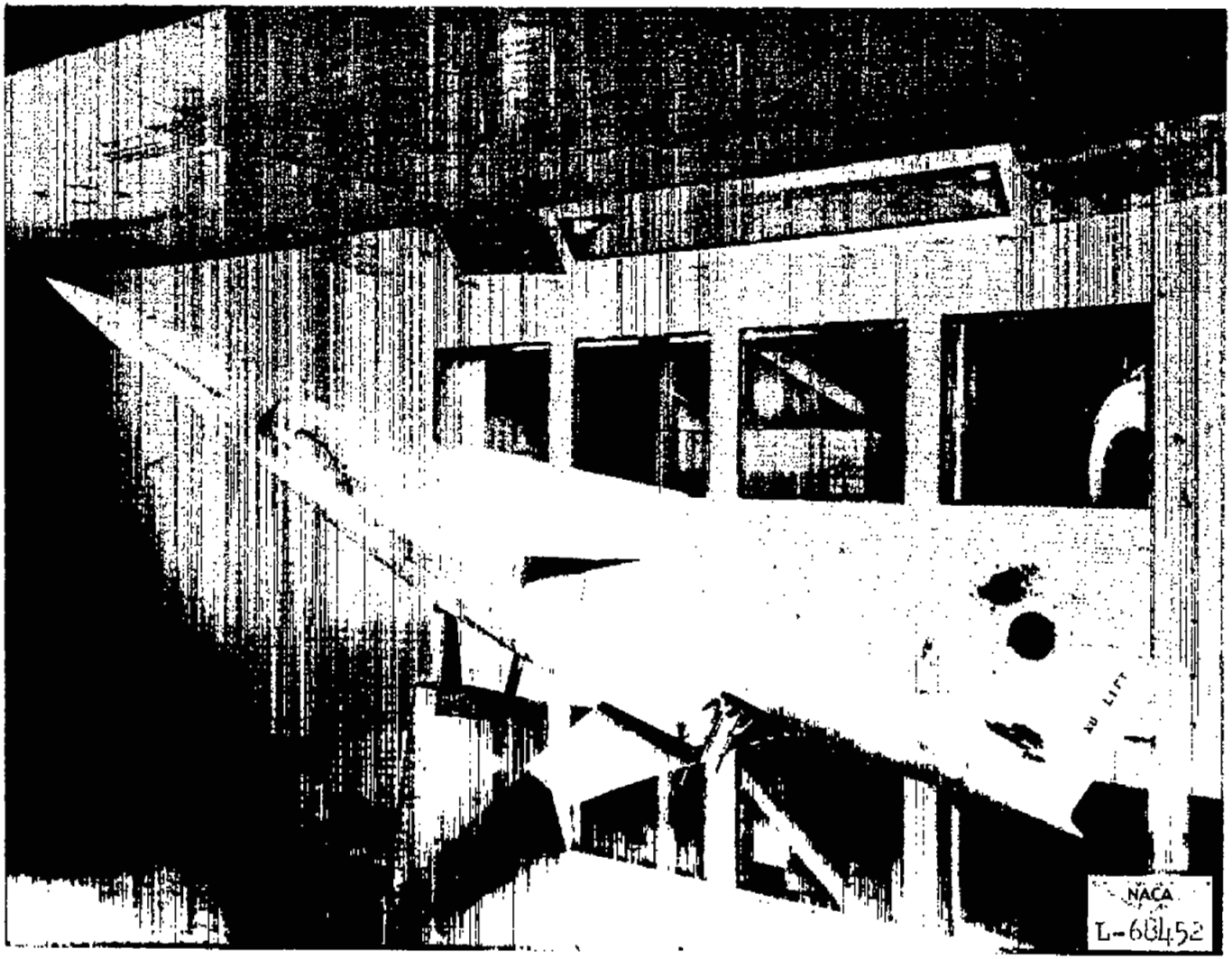

Figure 9.- Concluded.

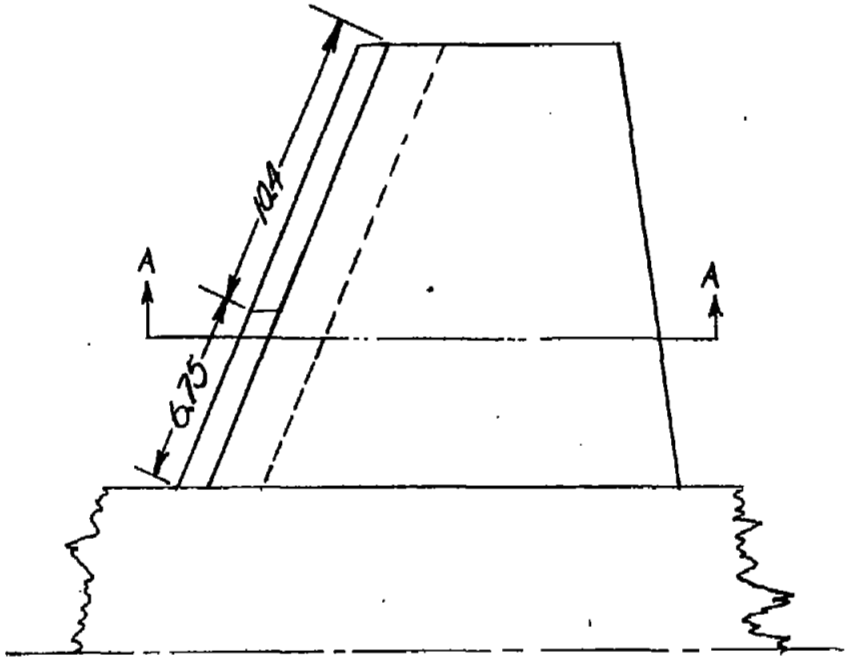

Ordinates for rounded leading edge given in inches

X	Y
0	0
.15	.025
.35	.070
.55	.14
.75	.23
.95	.38
1.11	

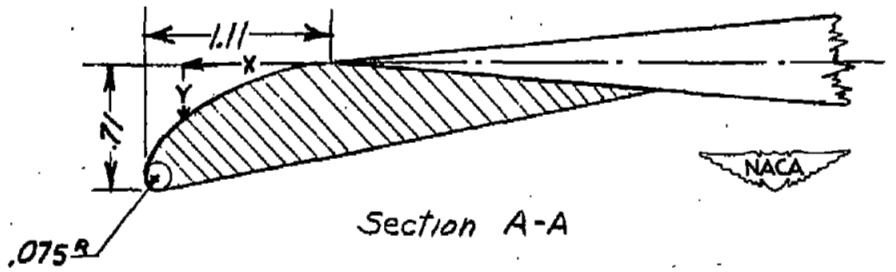

Section A-A

Figure 10.- Rounded wing-leading-edge configuration of the model. (All dimensions are in inches.)

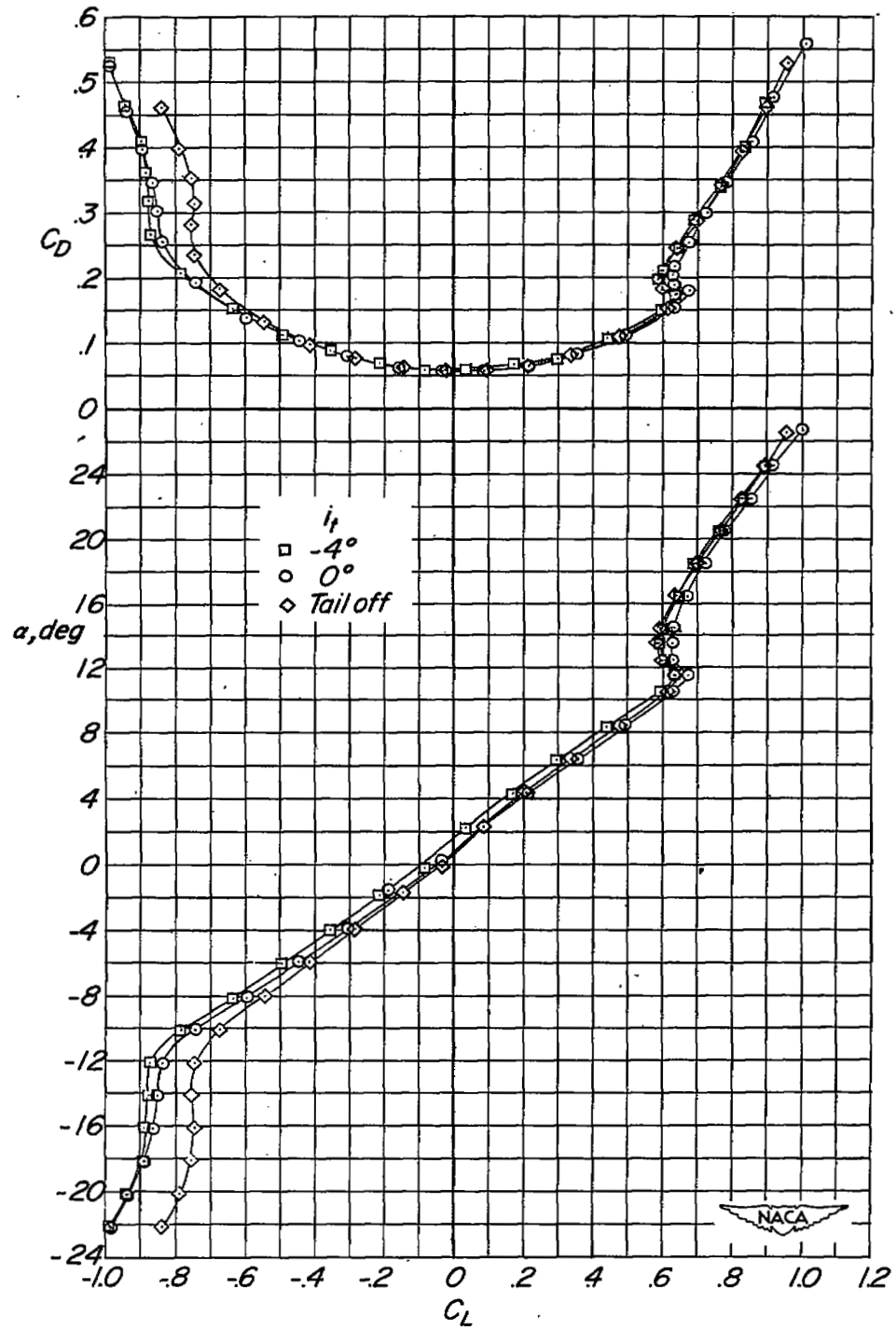

Figure 11.- Longitudinal aerodynamic characteristics of the original model. Reynolds number, 2.23×10^6.

[redacted]

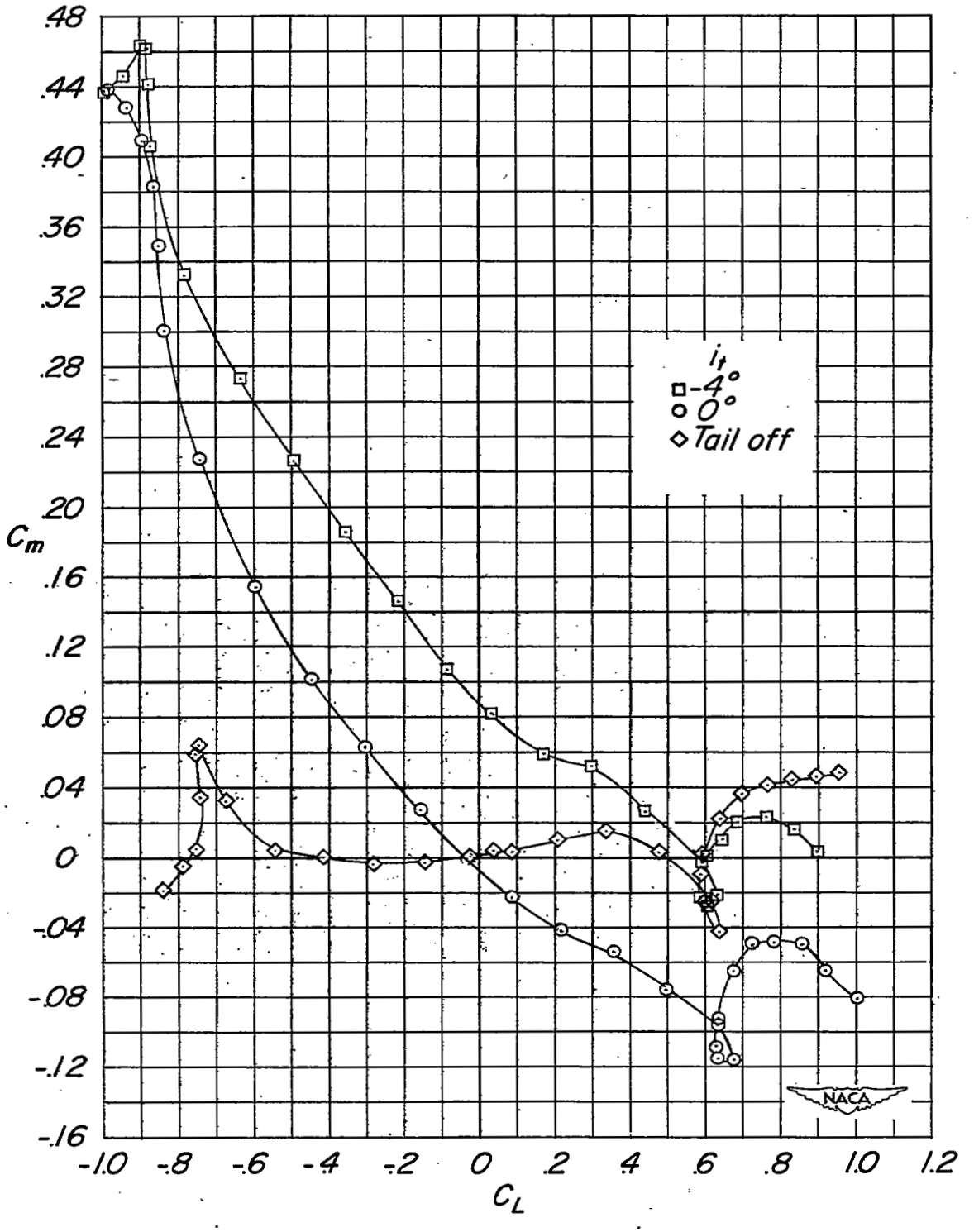

Figure 11.- Continued.

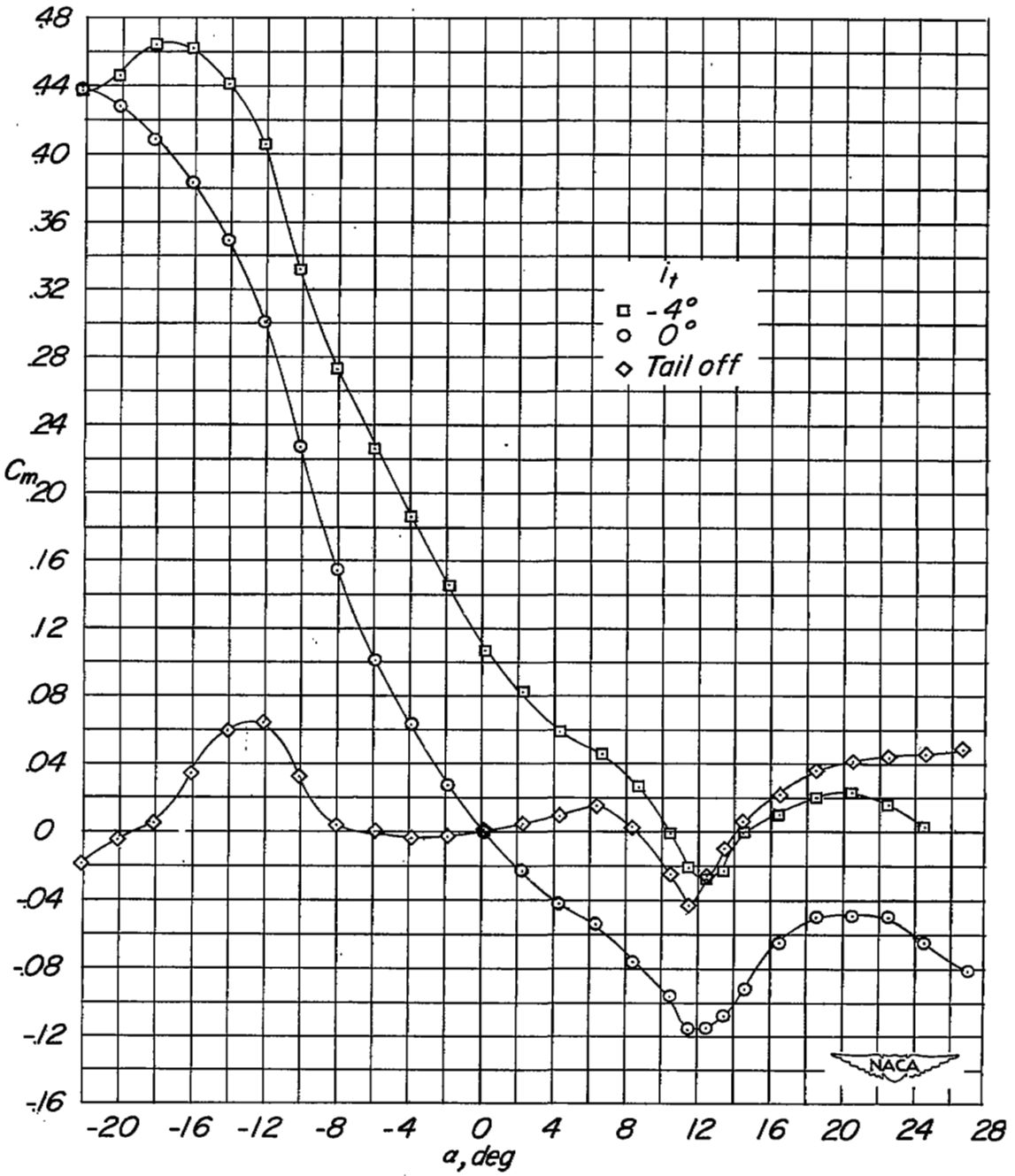

Figure 11.- Concluded.

[redacted]

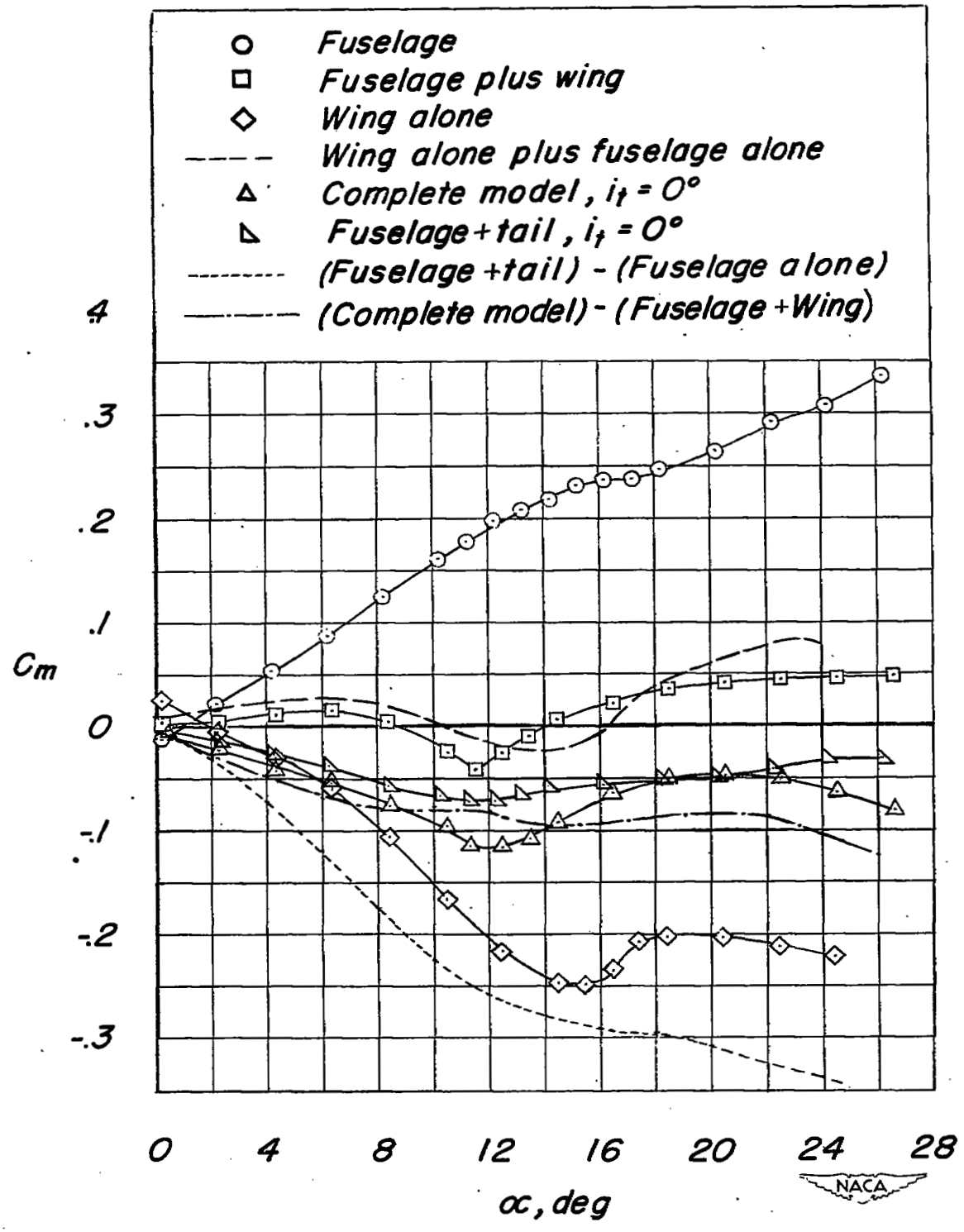

Figure 12.- Longitudinal stability characteristics of component parts of the model.

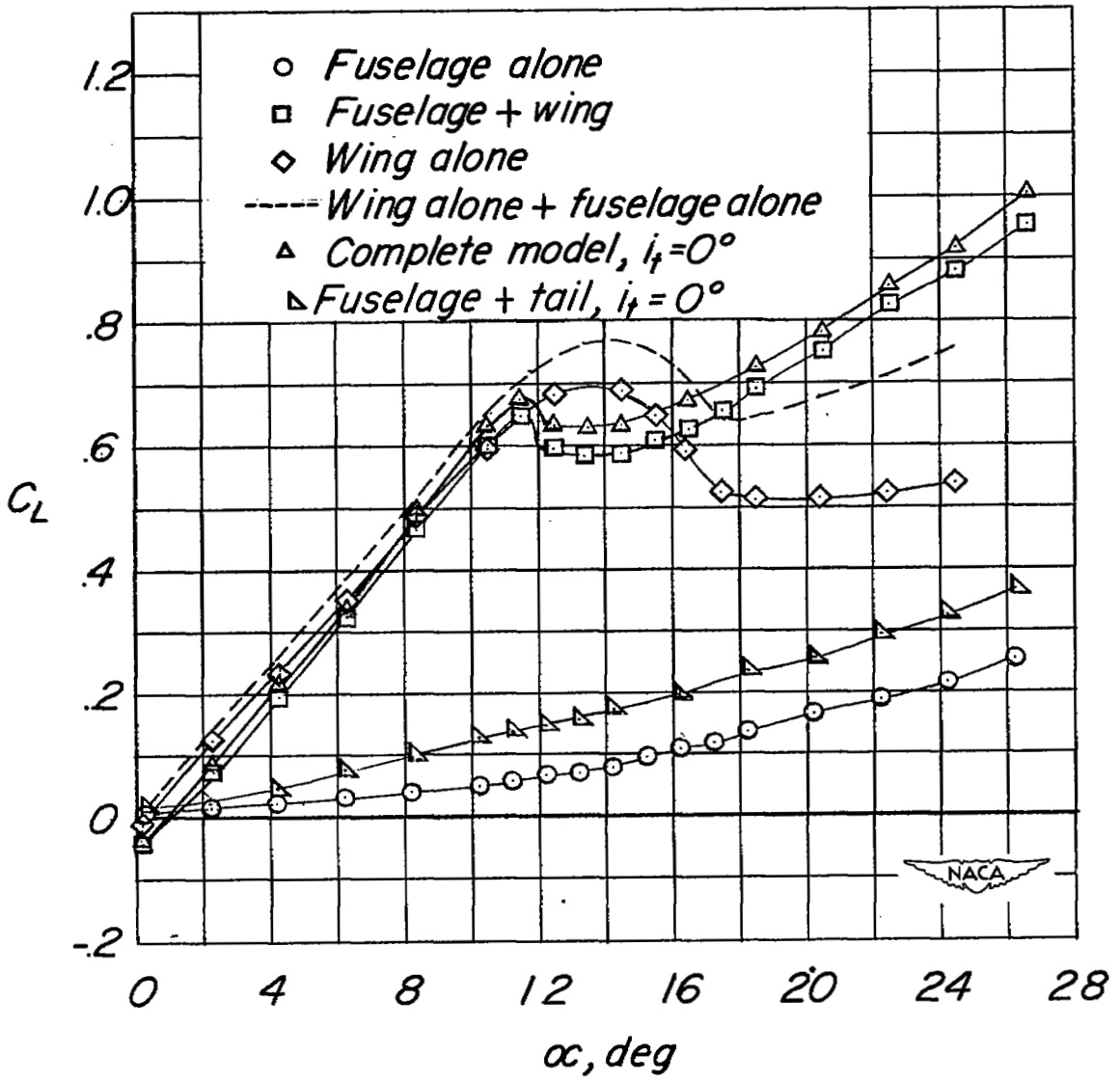

Figure 12.- Concluded.

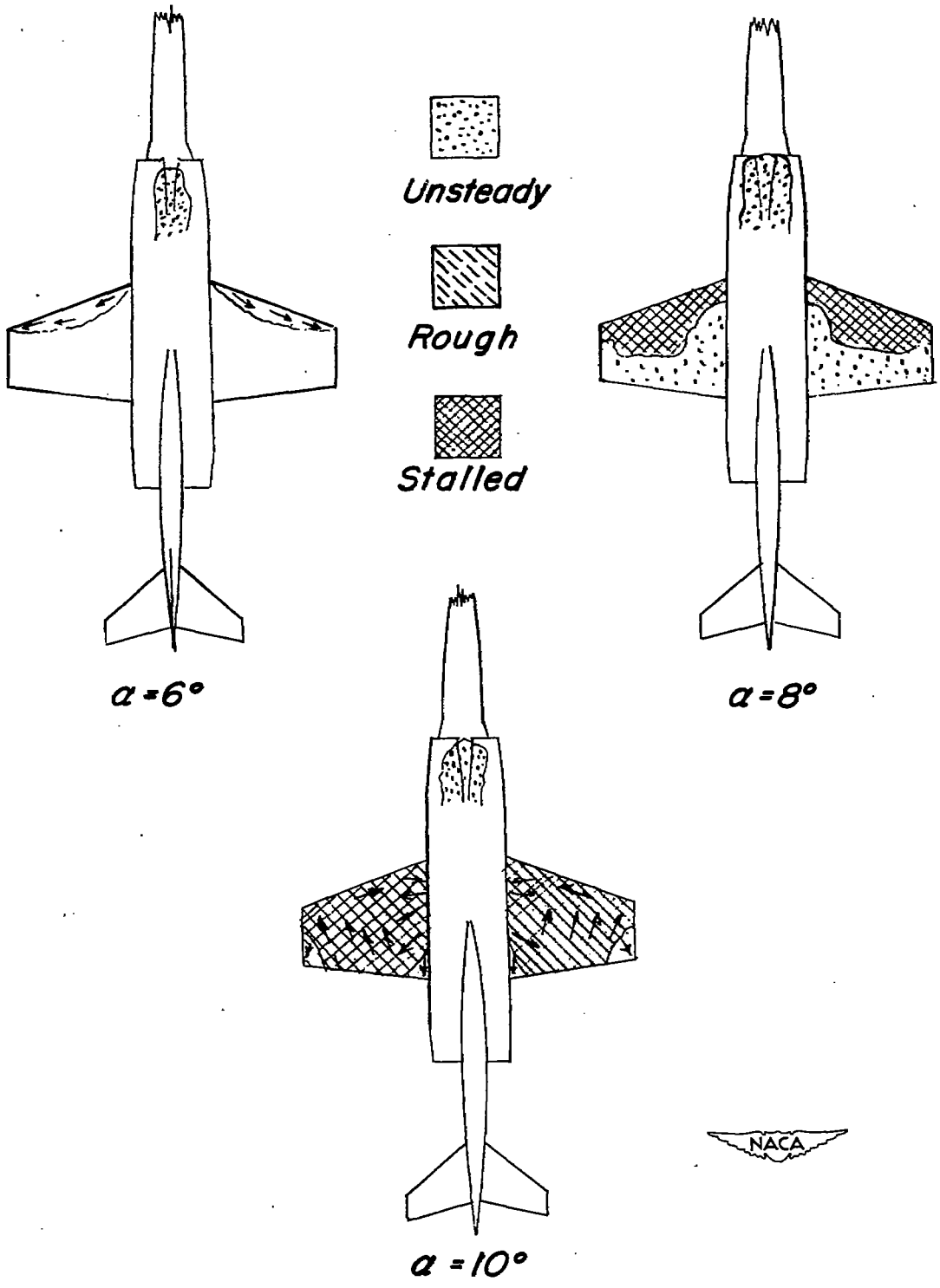

Figure 13.- Air-flow studies of the original model. Flaps zero; ducts open.

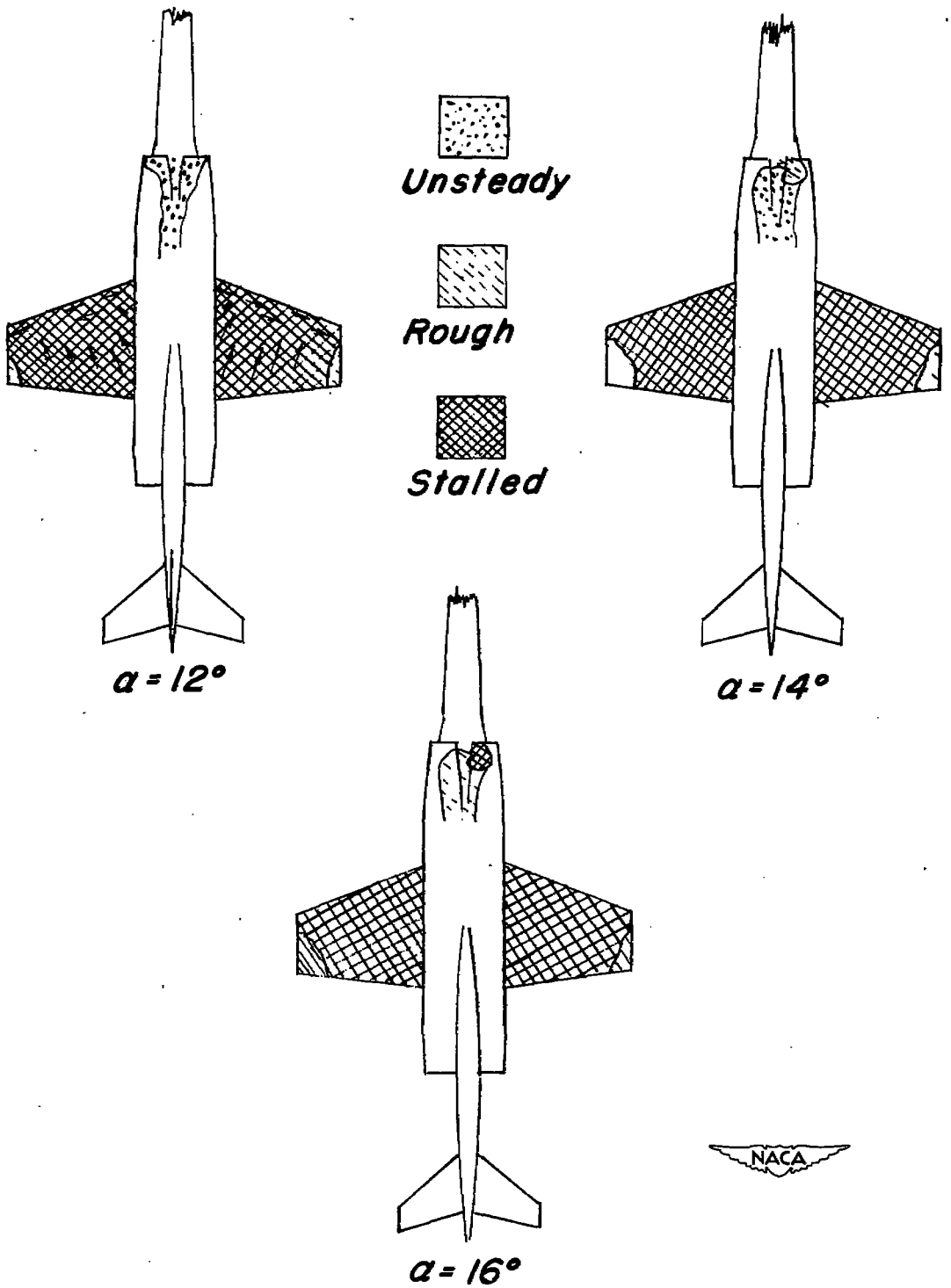

Figure 13.- Concluded.

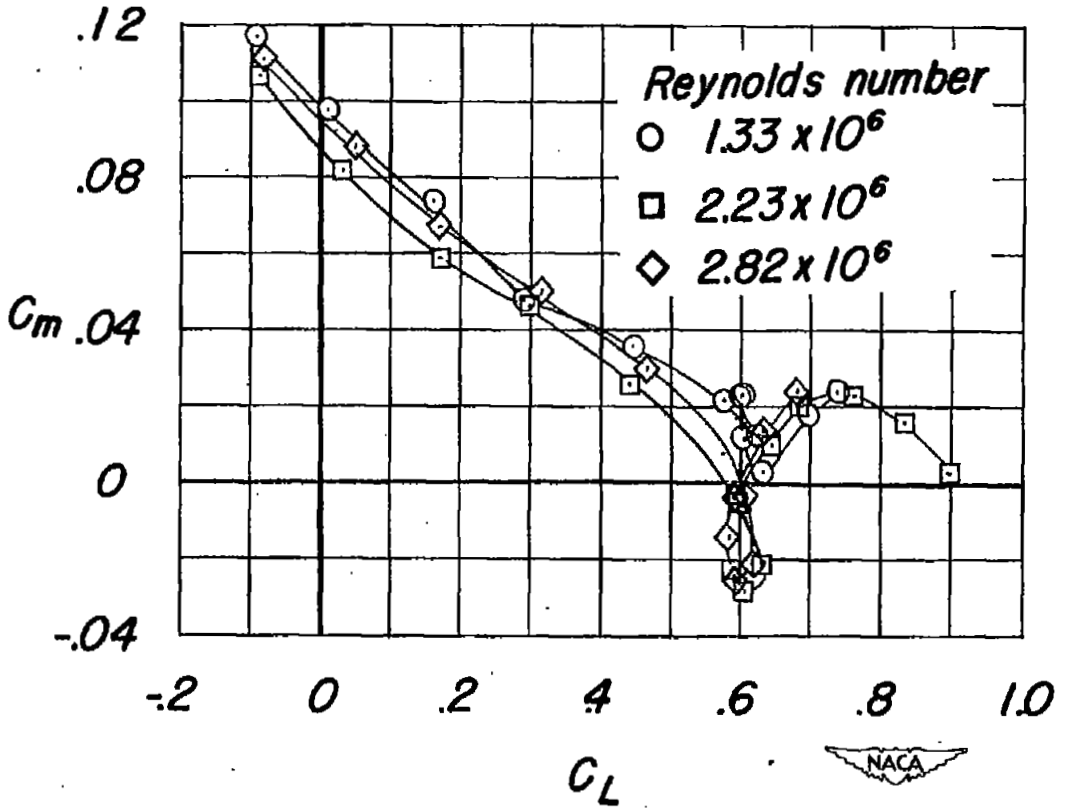

Figure 14.- Effect of Reynolds number on the longitudinal stability of the model. Original configuration; $i_t = -4^\circ$.

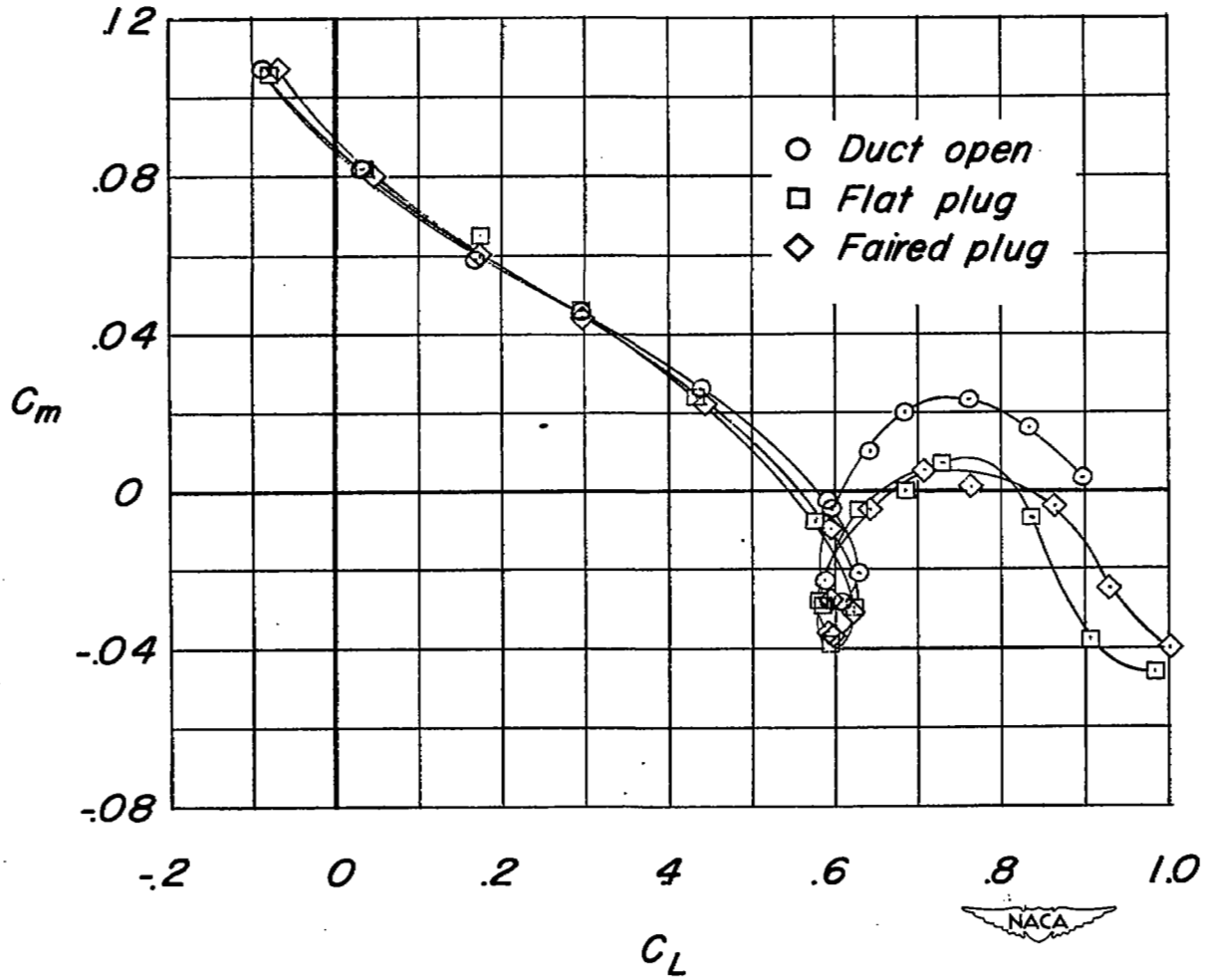

Figure 15.- Effect of plugging the duct inlets on the longitudinal stability of the model. Original configuration; $i_t = -4^\circ$.

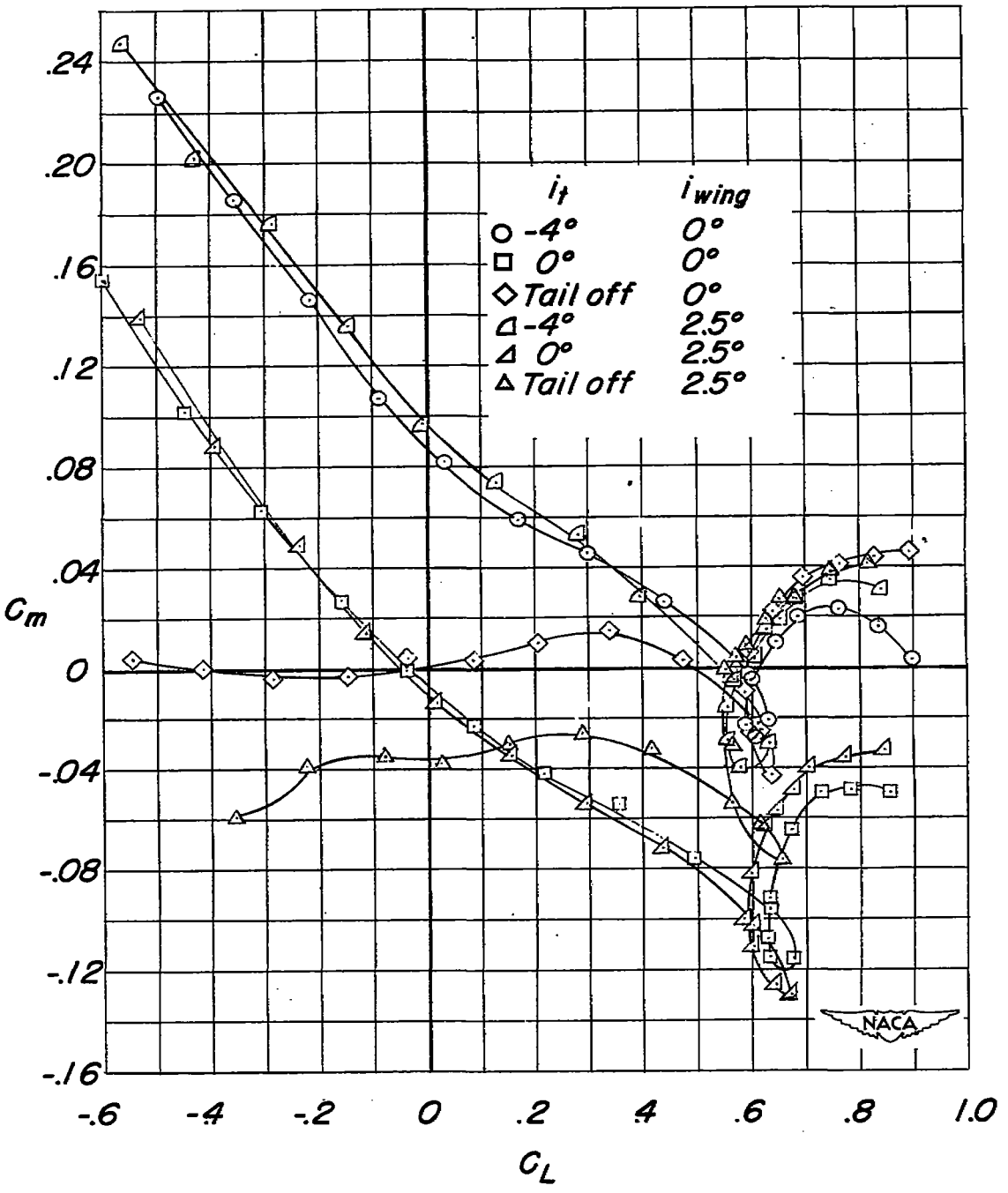

(a) Variation of C_m with C_L.

Figure 16.- Effect of wing incidence on the longitudinal stability of the model. Original configuration.

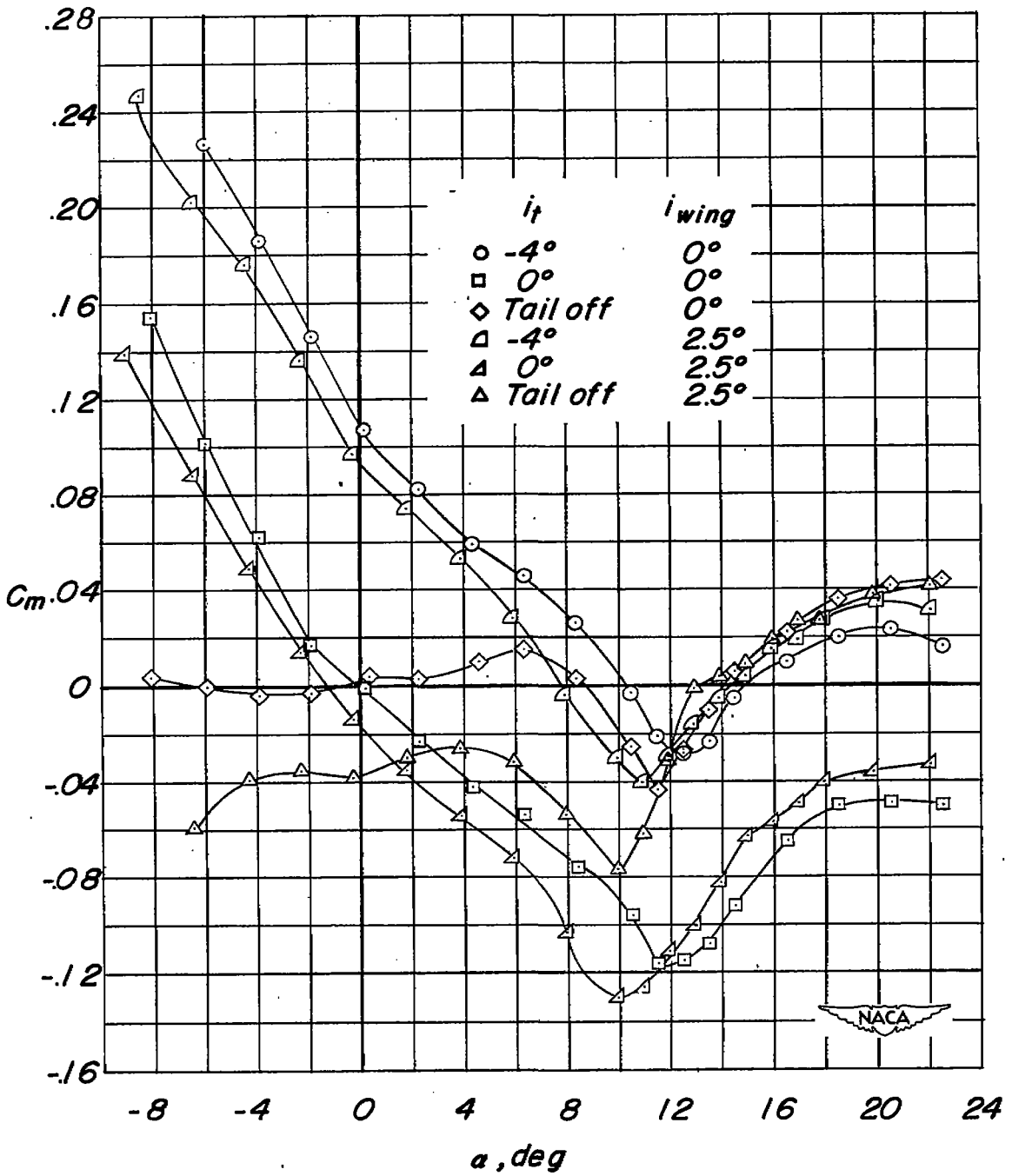

(b) Variation of C_m with α.

Figure 16.- Concluded.

[redacted]

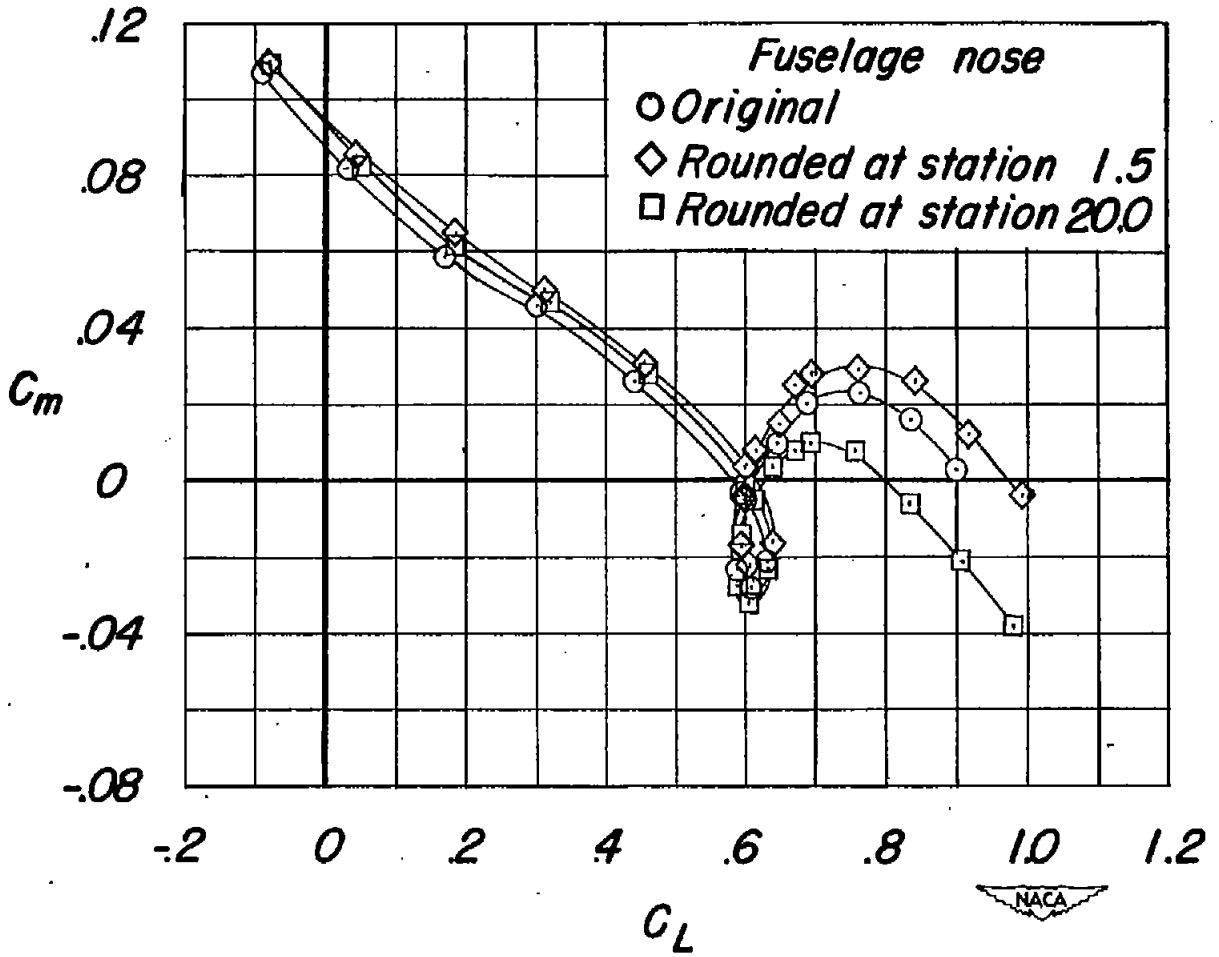

Figure 17.- Effect of altering the fuselage-nose configuration on the longitudinal stability of the model. $i_t = -4^\circ$.

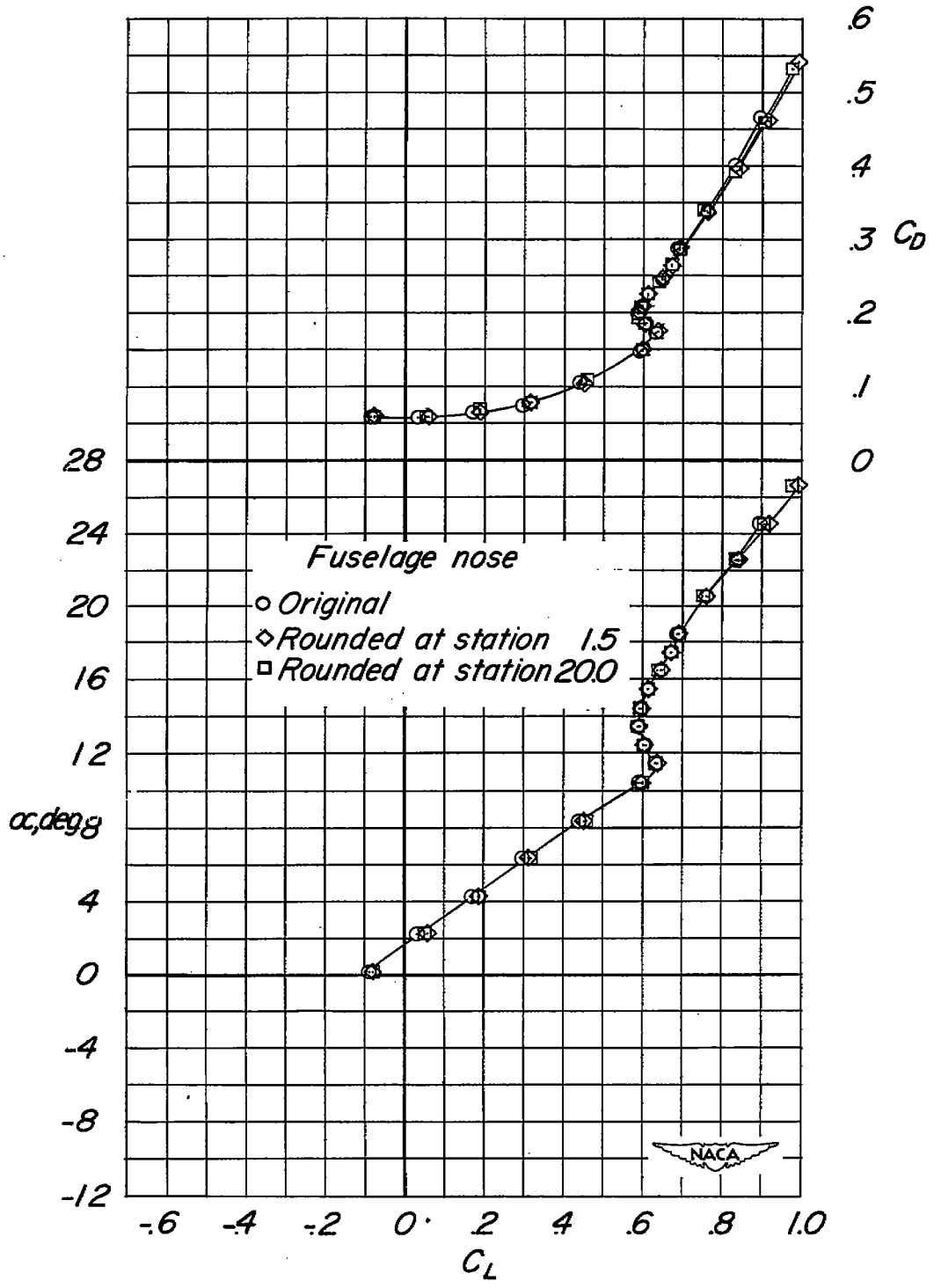

Figure 17.- Concluded.

[redacted]

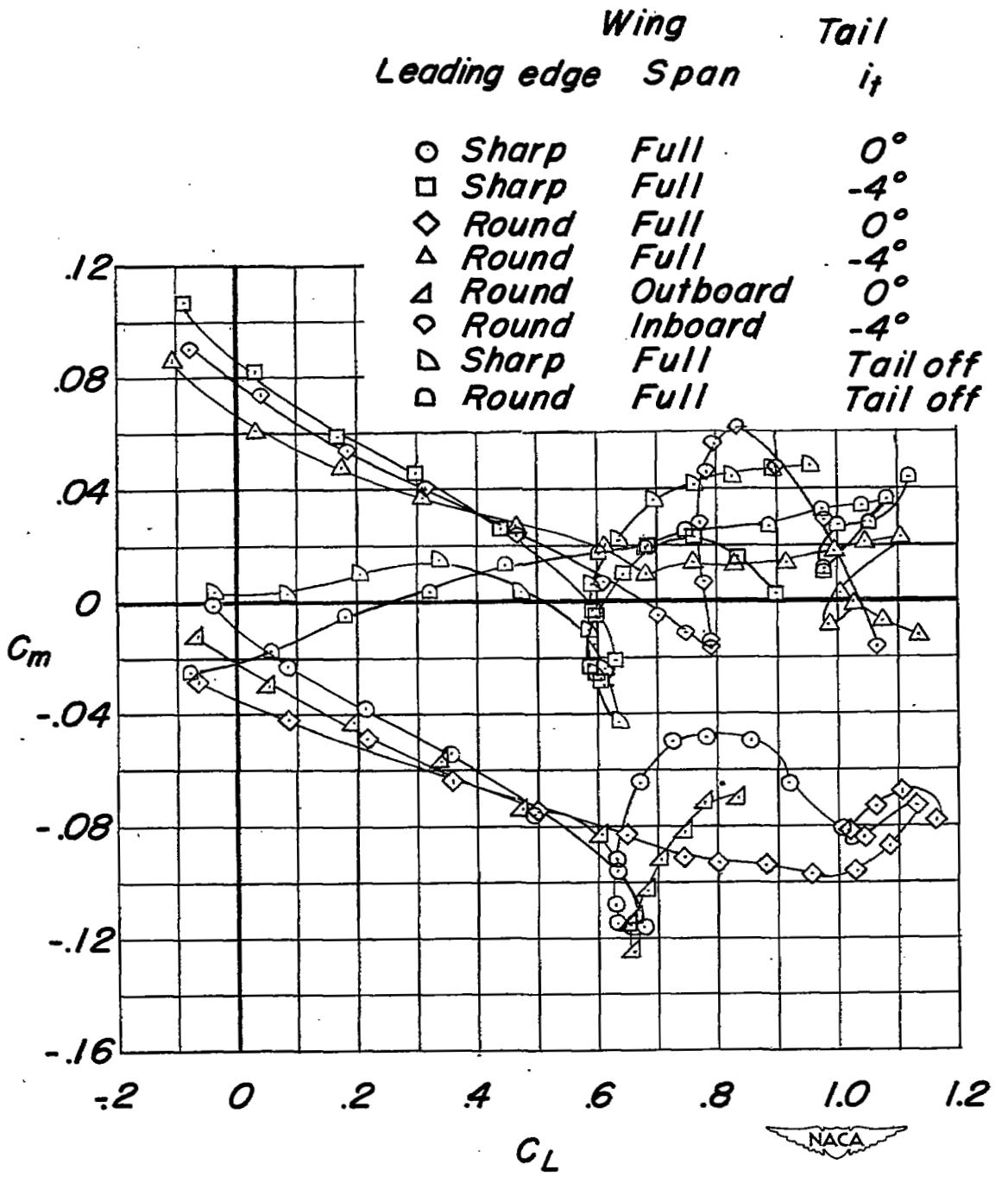

Figure 18.- Effect of rounding the wing leading edge on the longitudinal stability of the model.

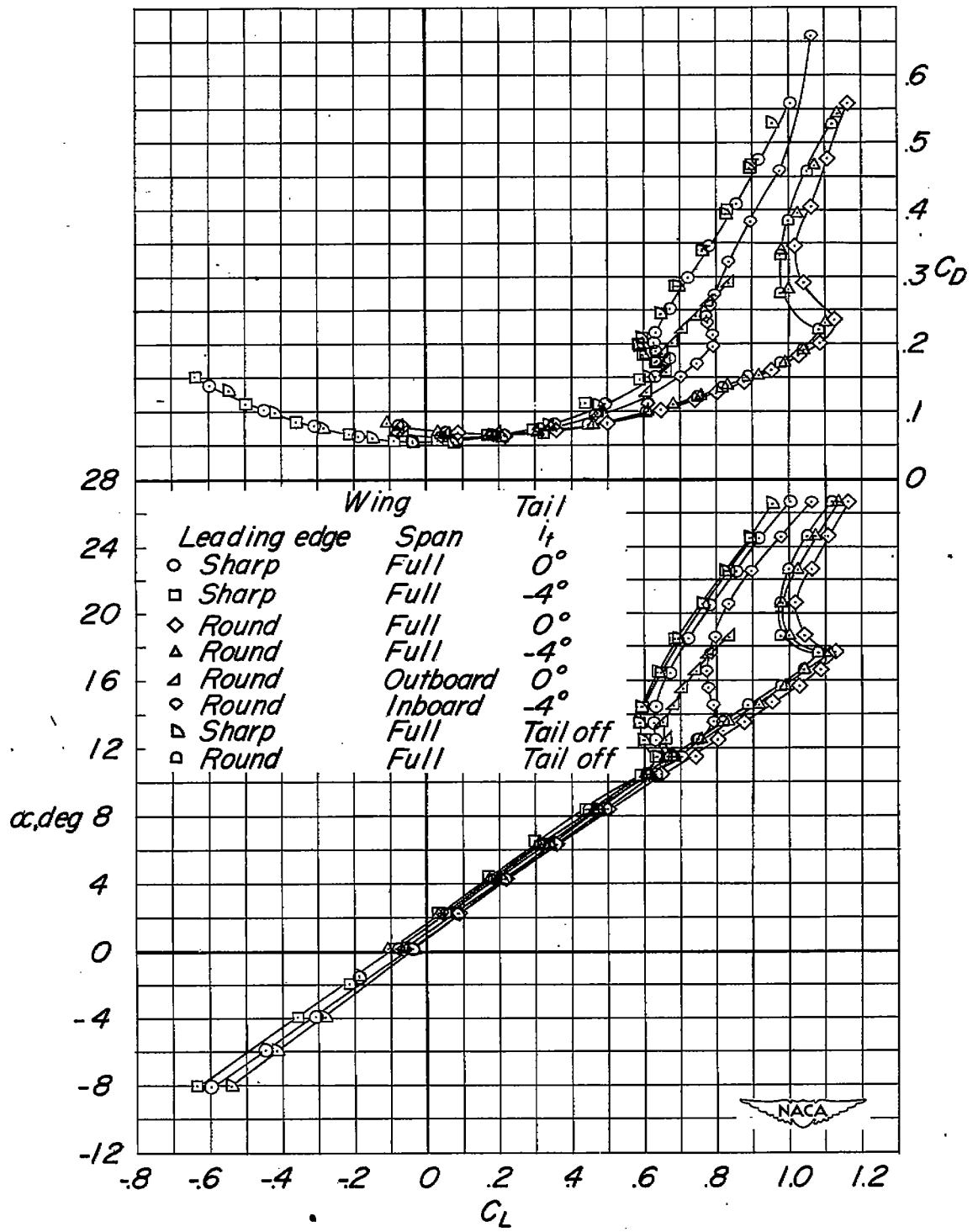

Figure 18.- Concluded.

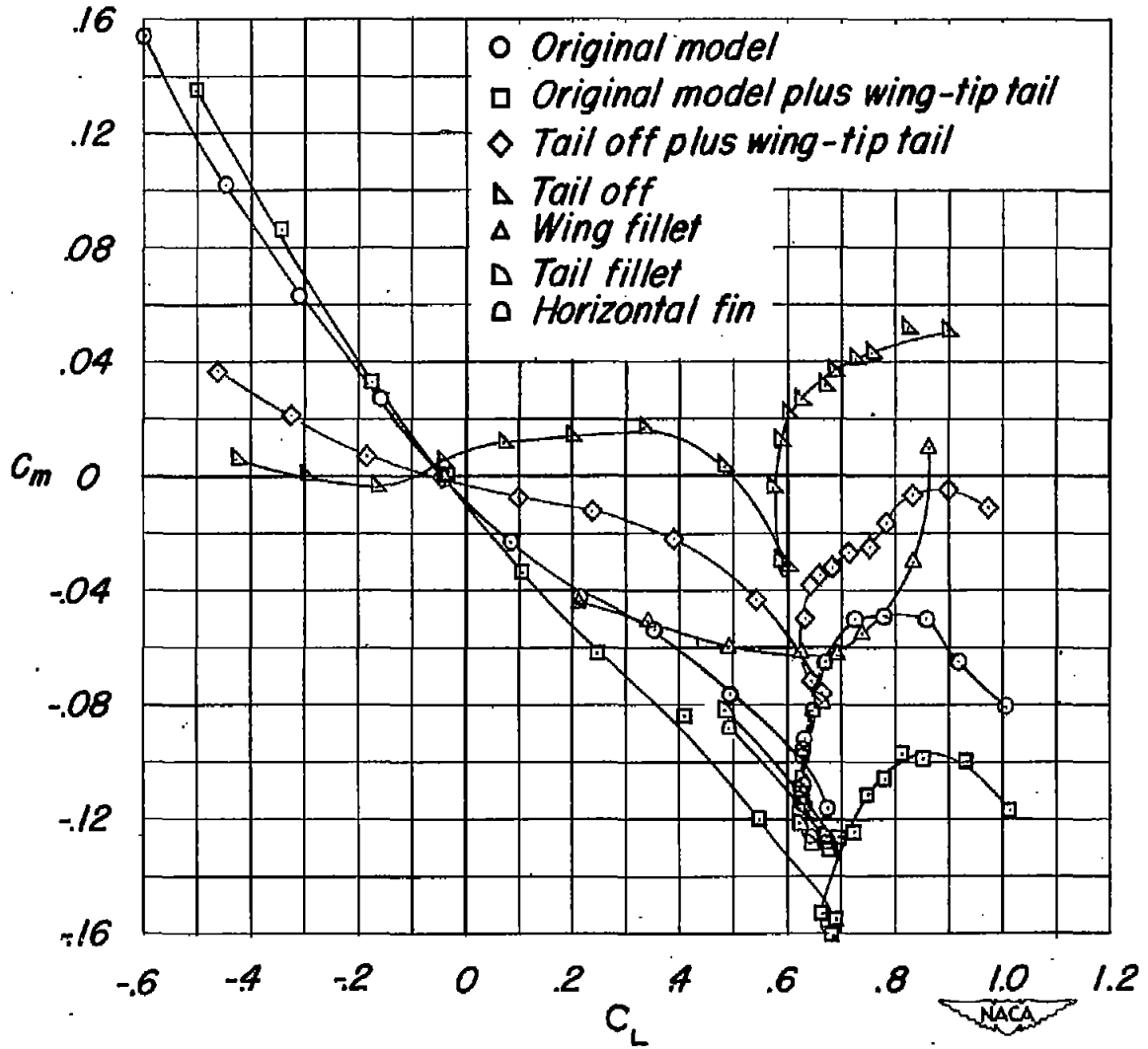

Figure 19.- Effect of auxiliary fillets and a wing-tip tail on the longitudinal stability of the model. $i_t = 0^\circ$.

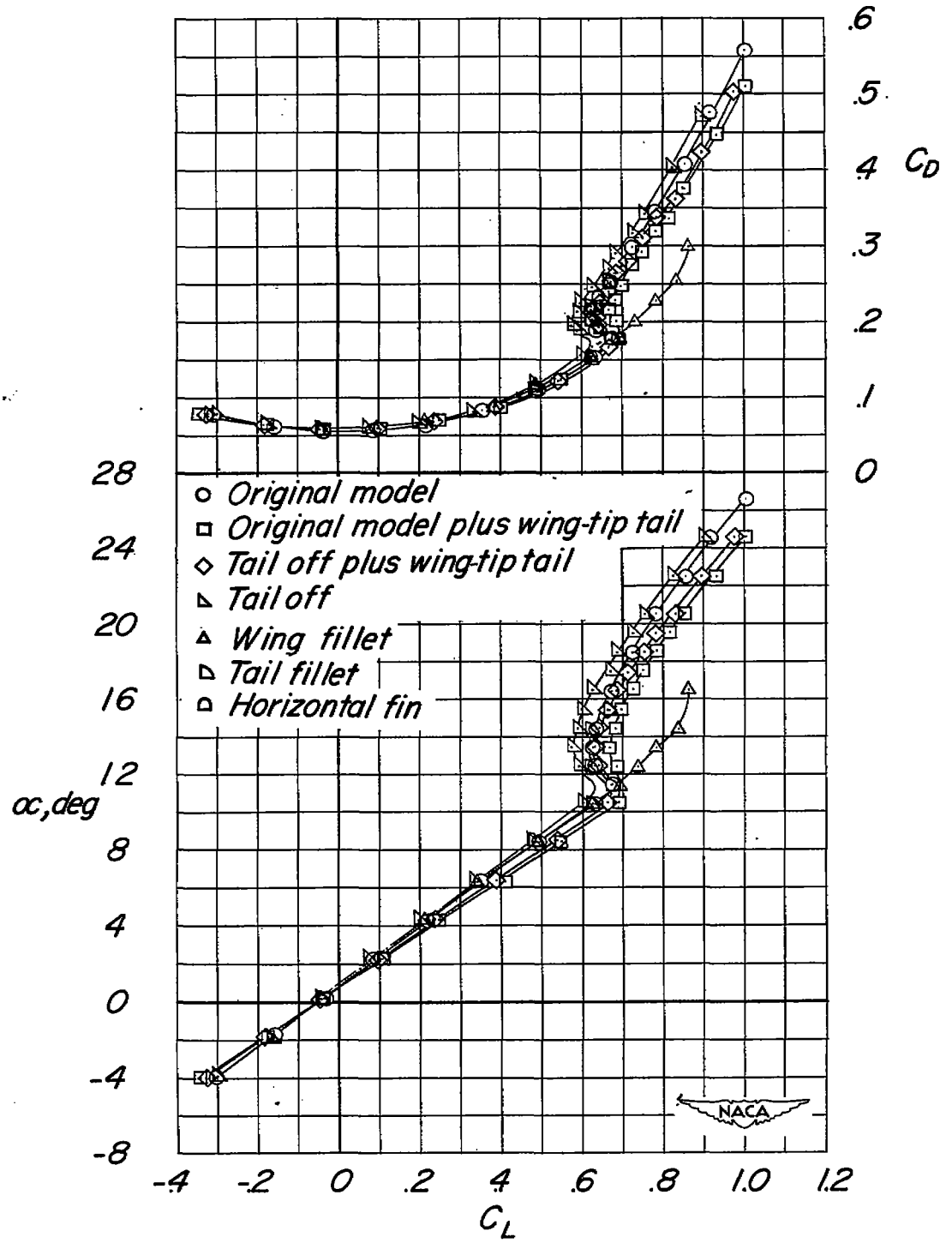

Figure 19.- Concluded.

[redacted]

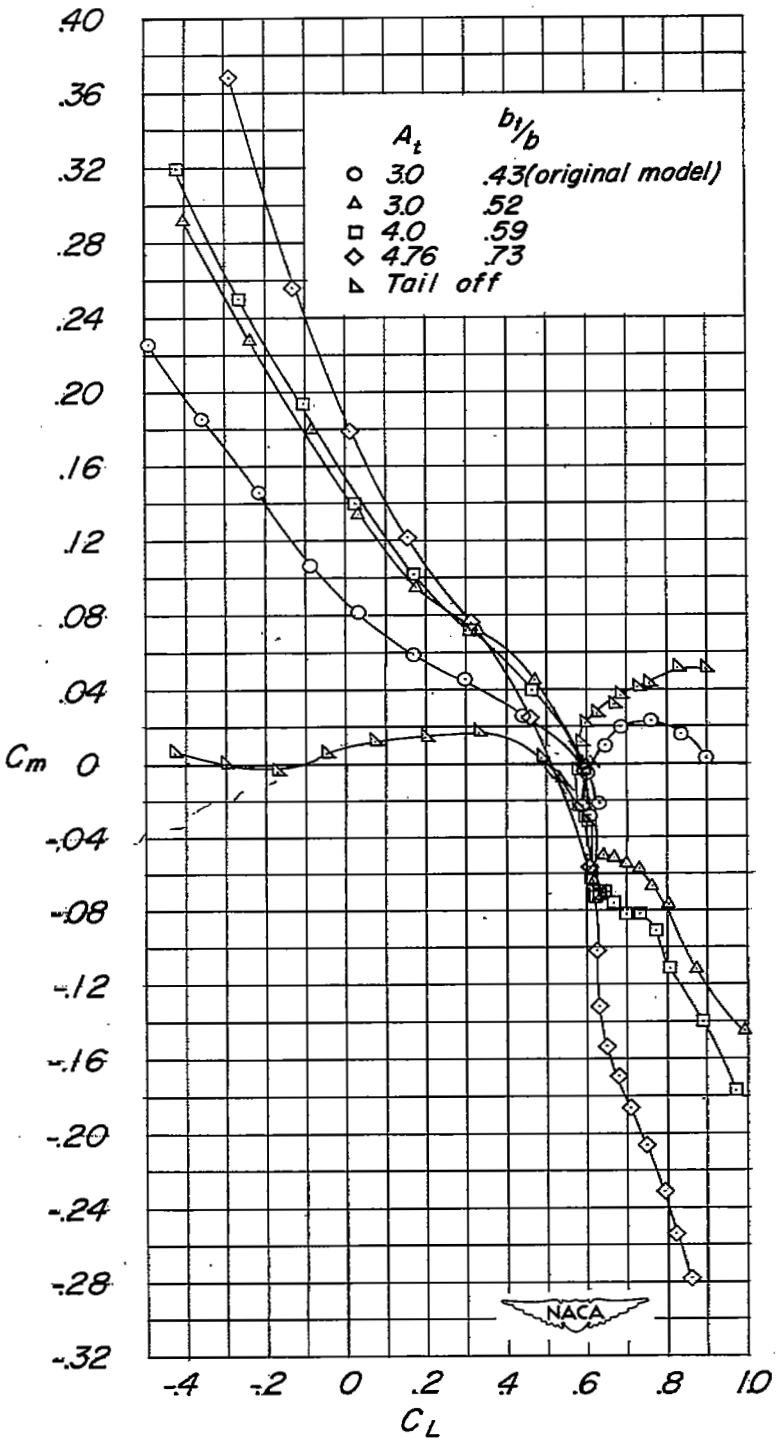

Figure 20.- Effect of various tail arrangements on the longitudinal stability characteristics of the model. $i_t = -4^\circ$.

[redacted]

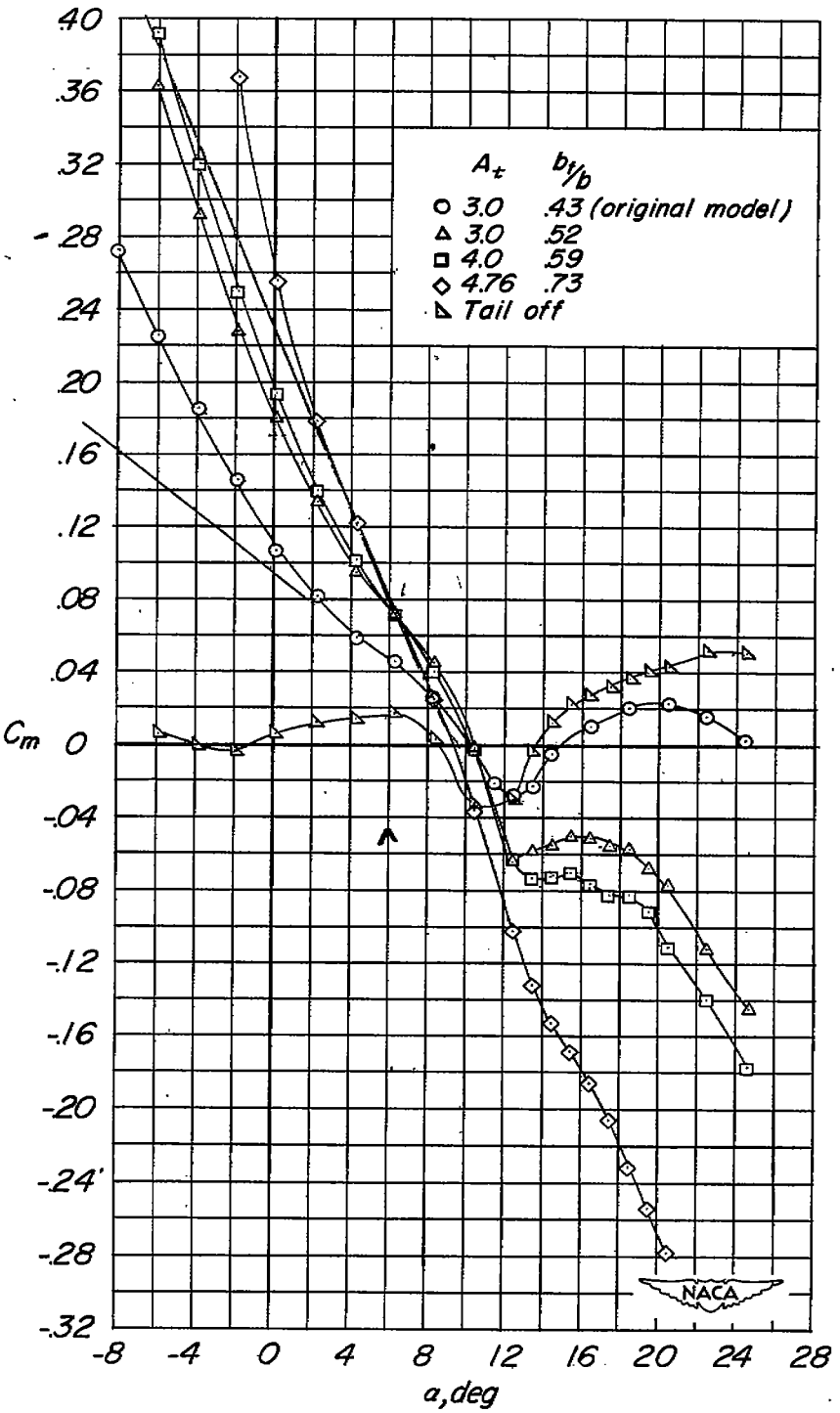

Figure 20.- Continued.

[redacted]

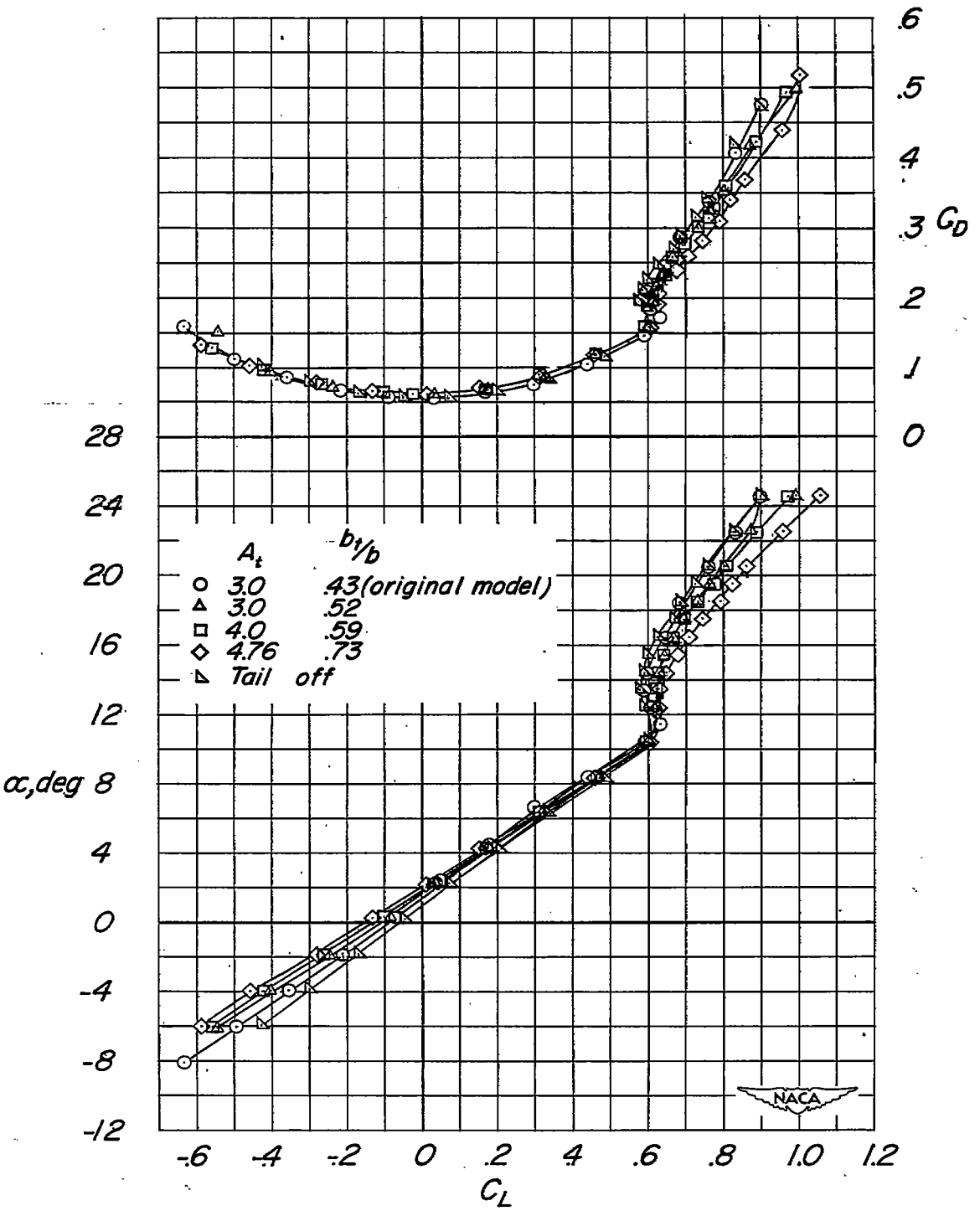

Figure 20.- Concluded.

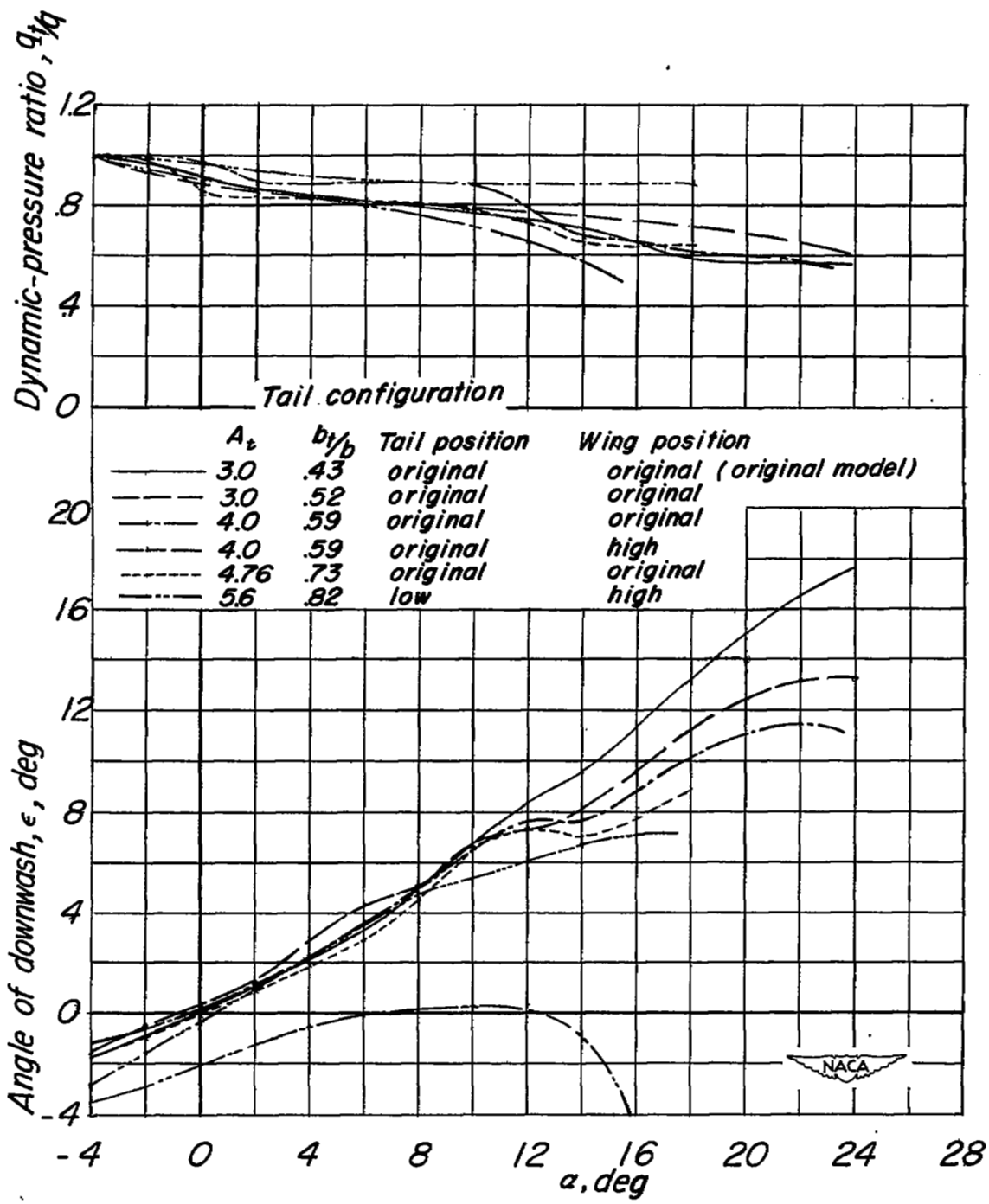

Figure 21.- Effective downwash angles and dynamic-pressure ratio qt/q ıor various tail arrangements of a 0.16-scale model of the Douglas X-3 airplane.

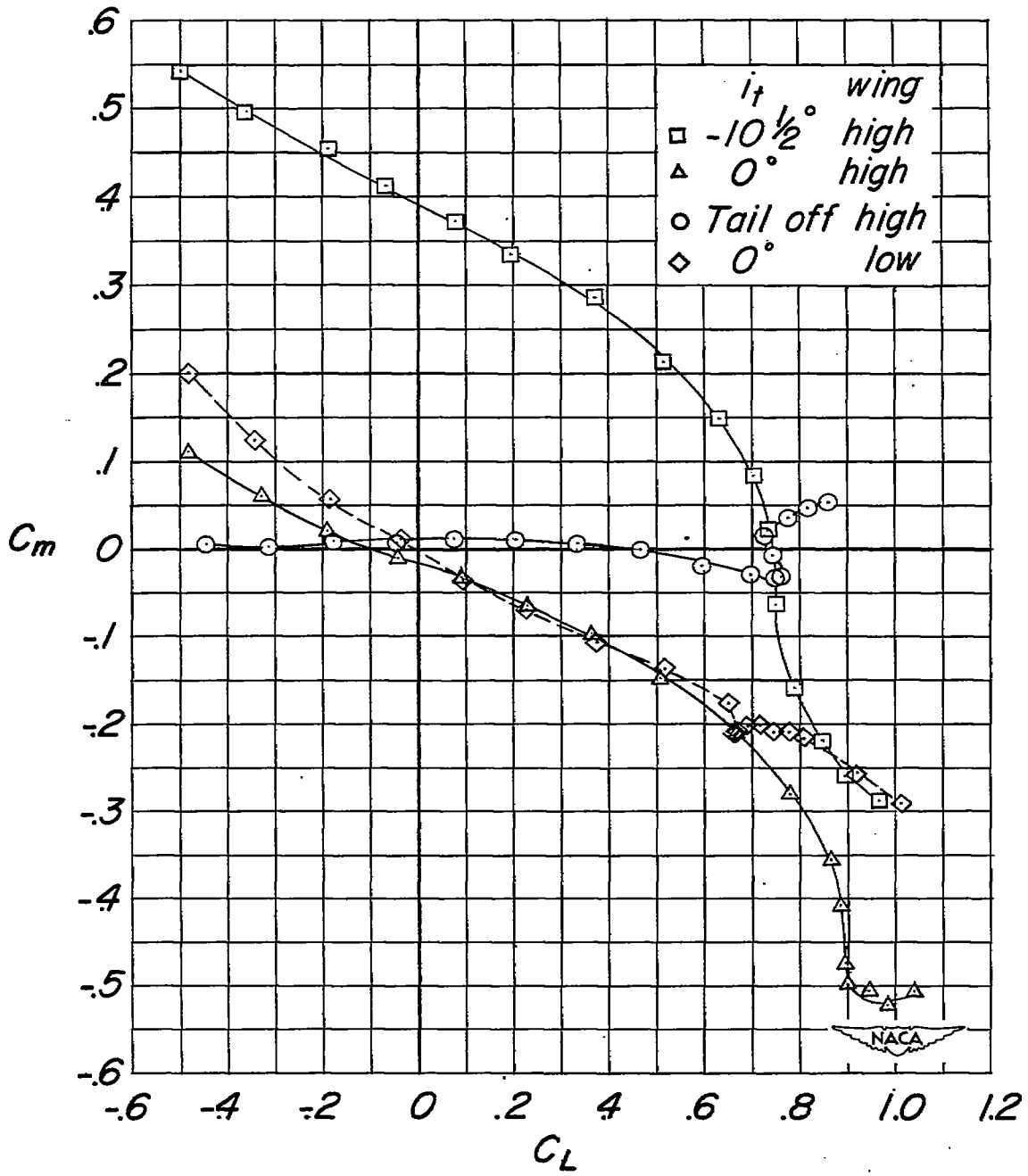

(a) High and low wing with tail of A = 4.0, $\frac{b_t}{b}$ = 0.59.

Figure 22.- Effect of tail location on the longitudinal stability characteristics of the model with high and low wing. Incidence of high wing, 0.33°; incidence of low wing, 0°.

[redacted]

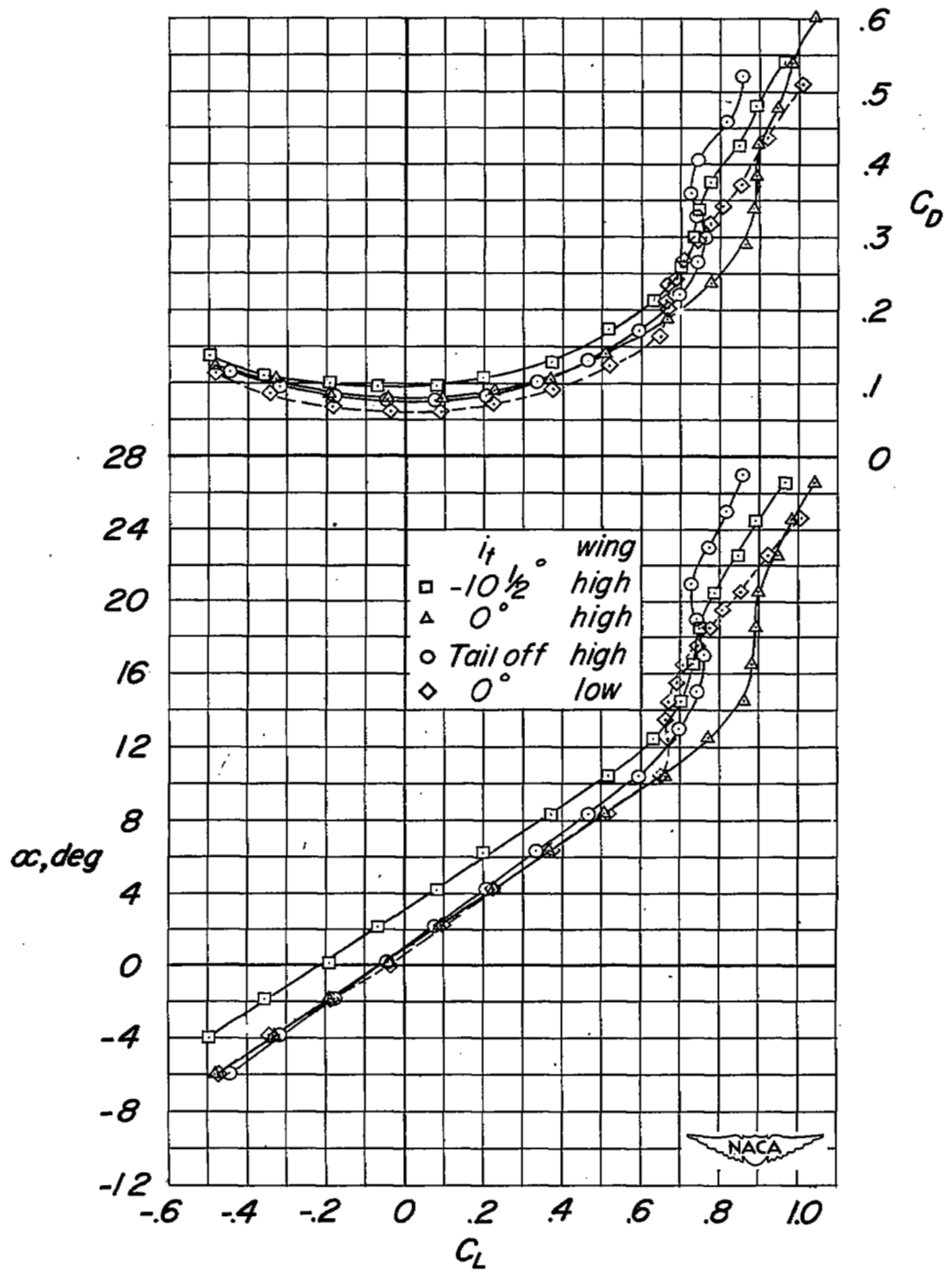

(a) Concluded.

Figure 22.- Continued.

[redacted]

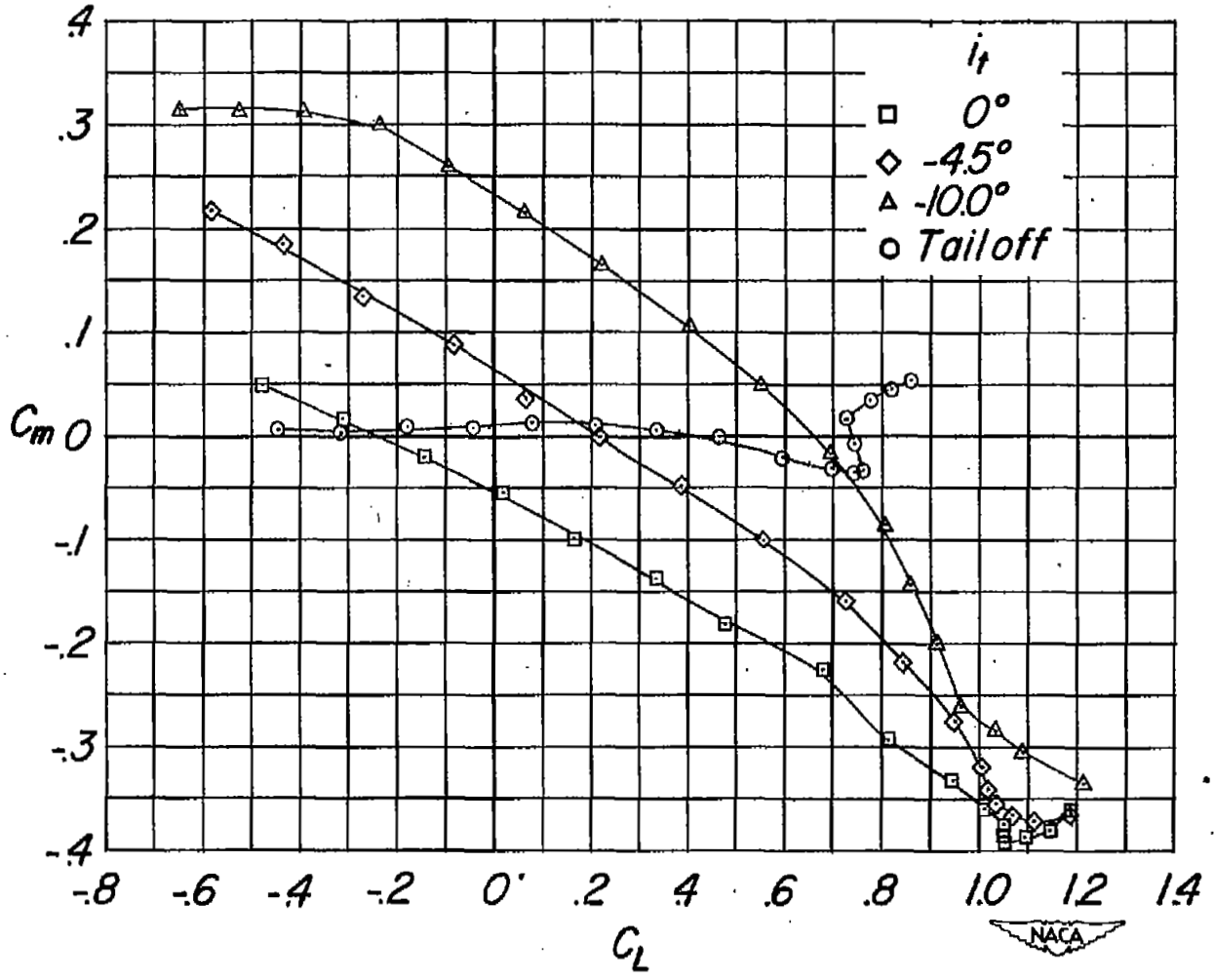

(b) High wing with low tail of A = 5.6, $\frac{b_t}{b}$ = 0.82.

Figure 22.- Continued.

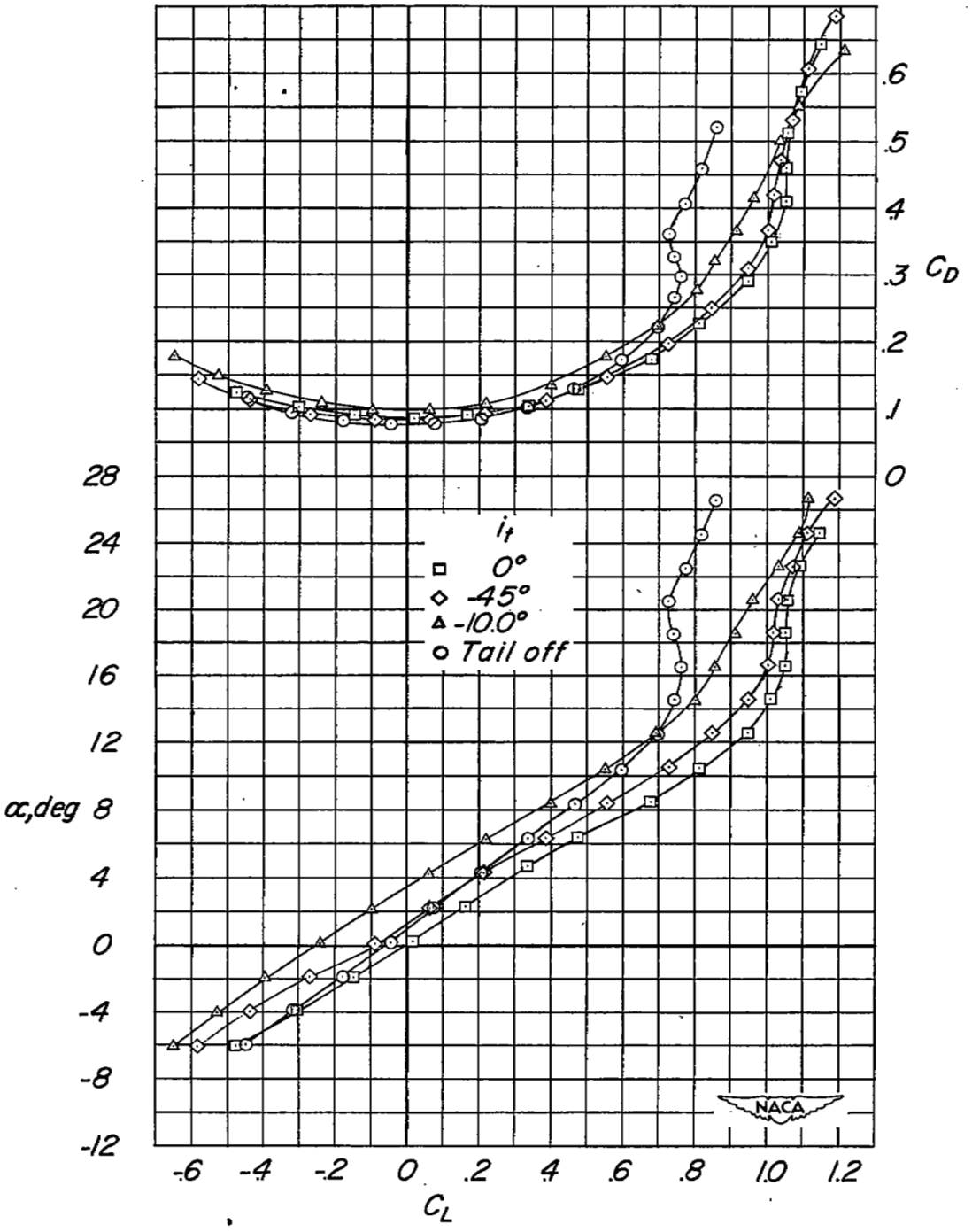

(b) Concluded.

Figure 22.- Concluded.

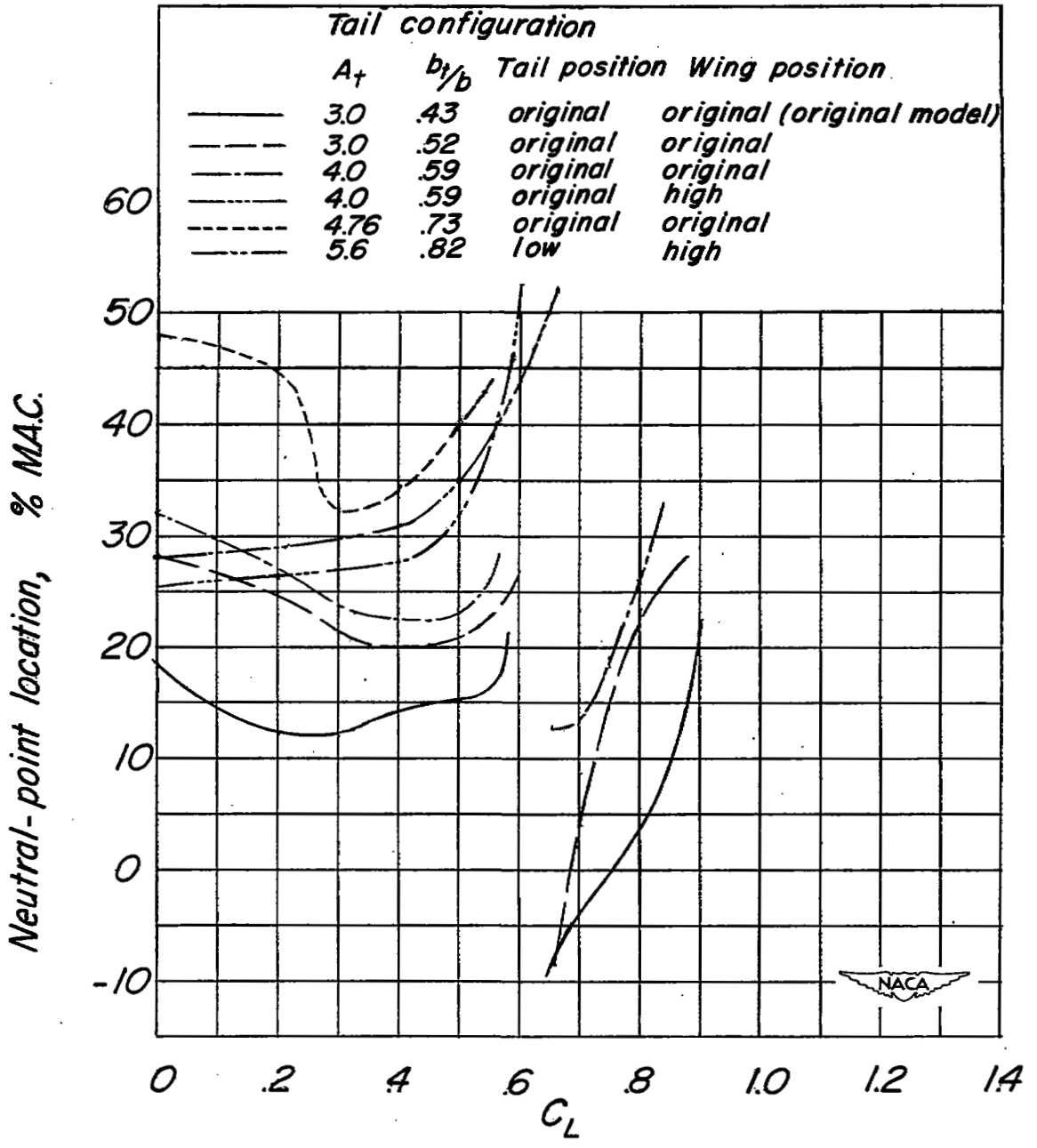

Figure 23.- All-movable-tail fixed neutral points of the Douglas X-3 airplane as determined from wind-tunnel test of a 0.16-scale model.

[redacted]

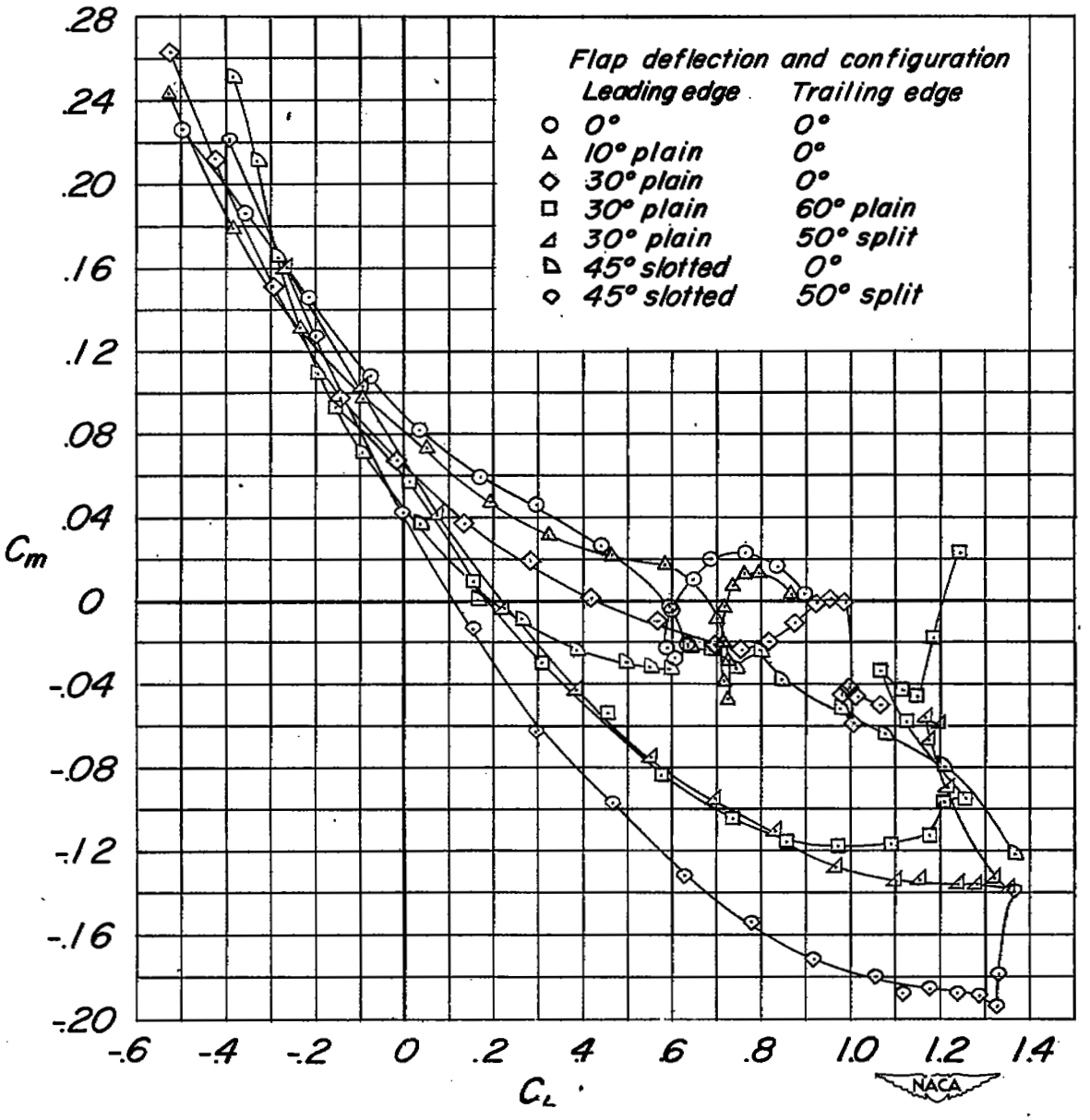

(a) Complete model configuration; $i_t = -4^\circ$.

Figure 24.- Effect of various leading- and trailing-edge flap configurations on the longitudinal stability of the original model.

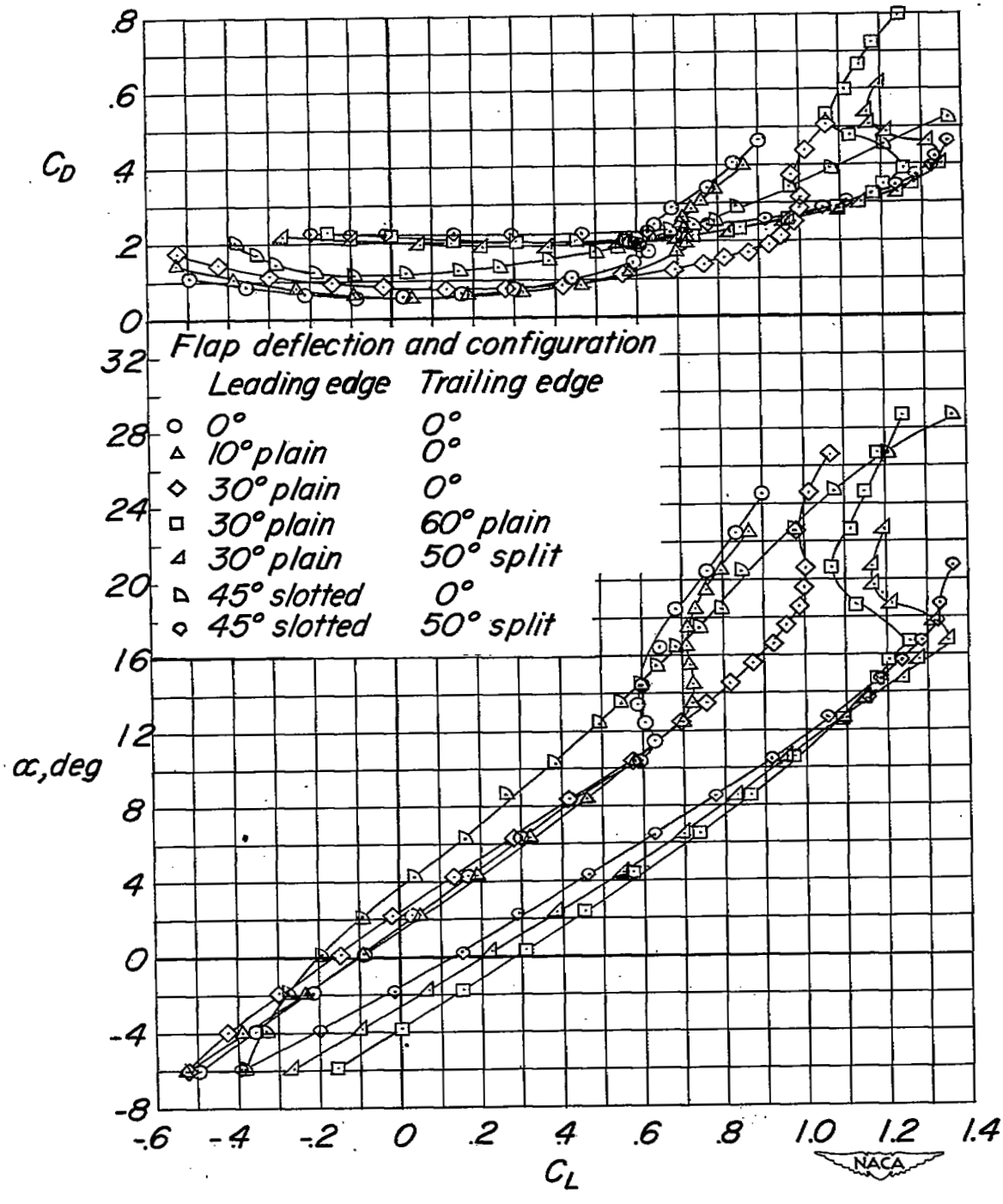

(a) Concluded.

Figure 24.- Continued.

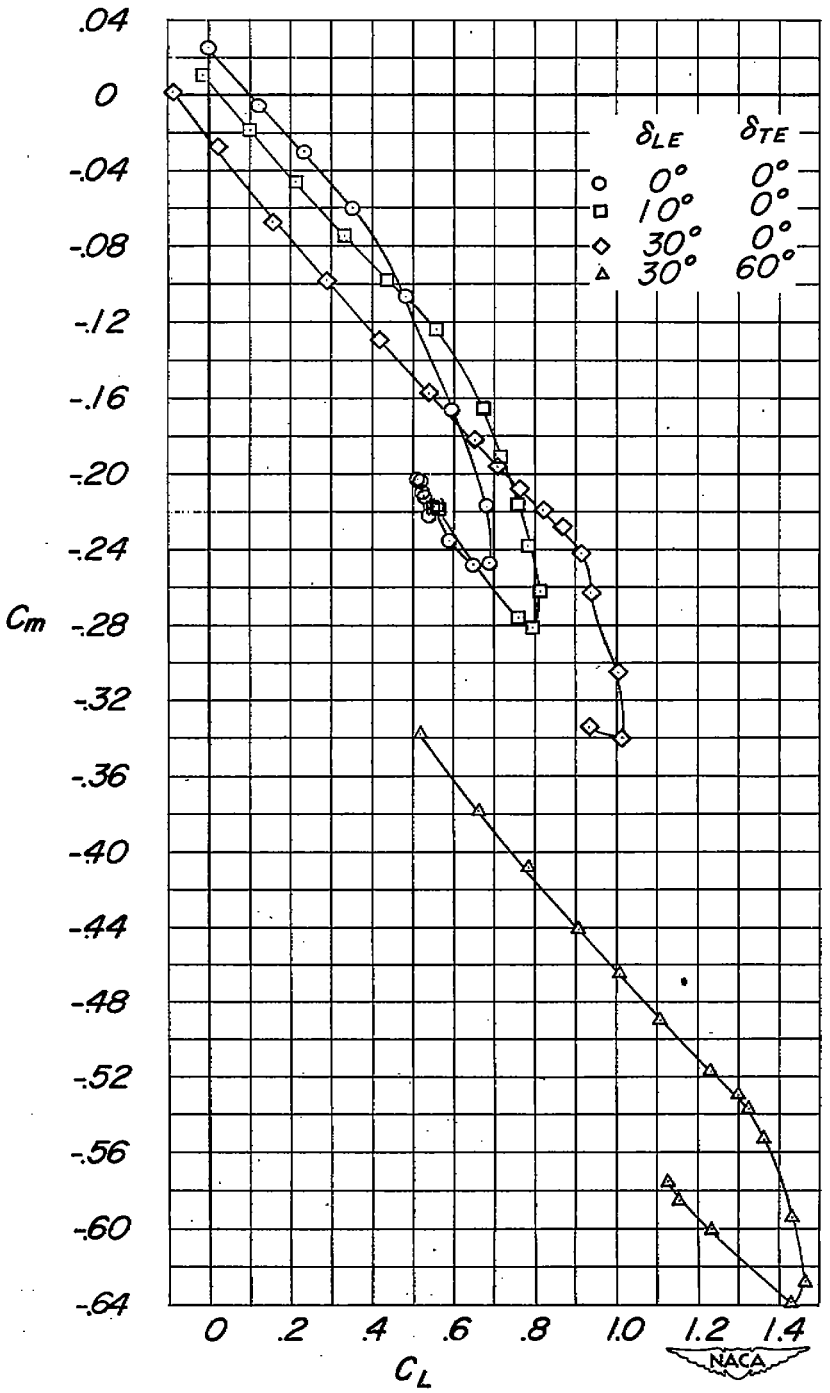

(b) Wing alone; plain flaps.

Figure 24.- Continued.

[redacted]

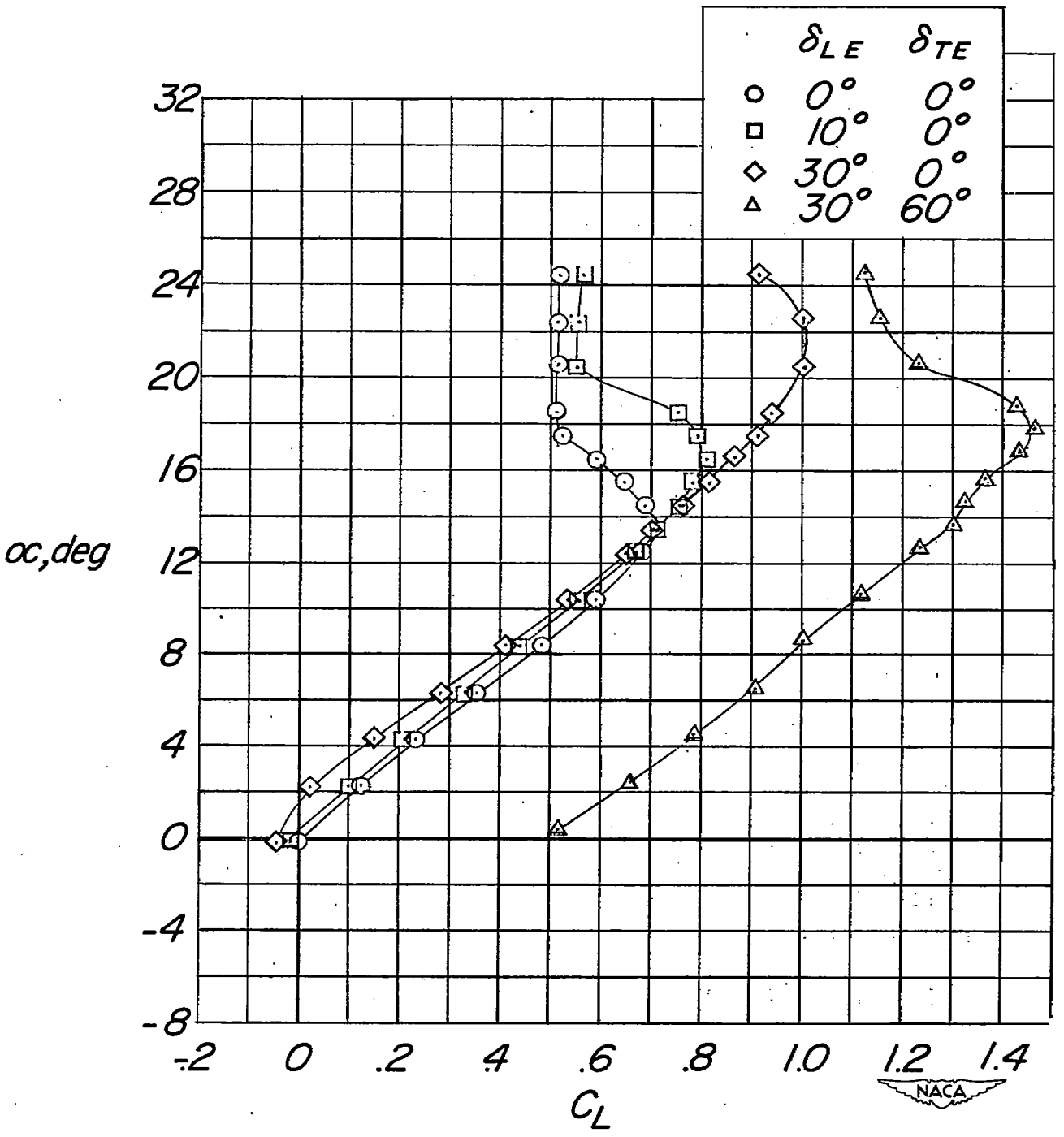

(b) Concluded.

Figure 24.- Concluded.

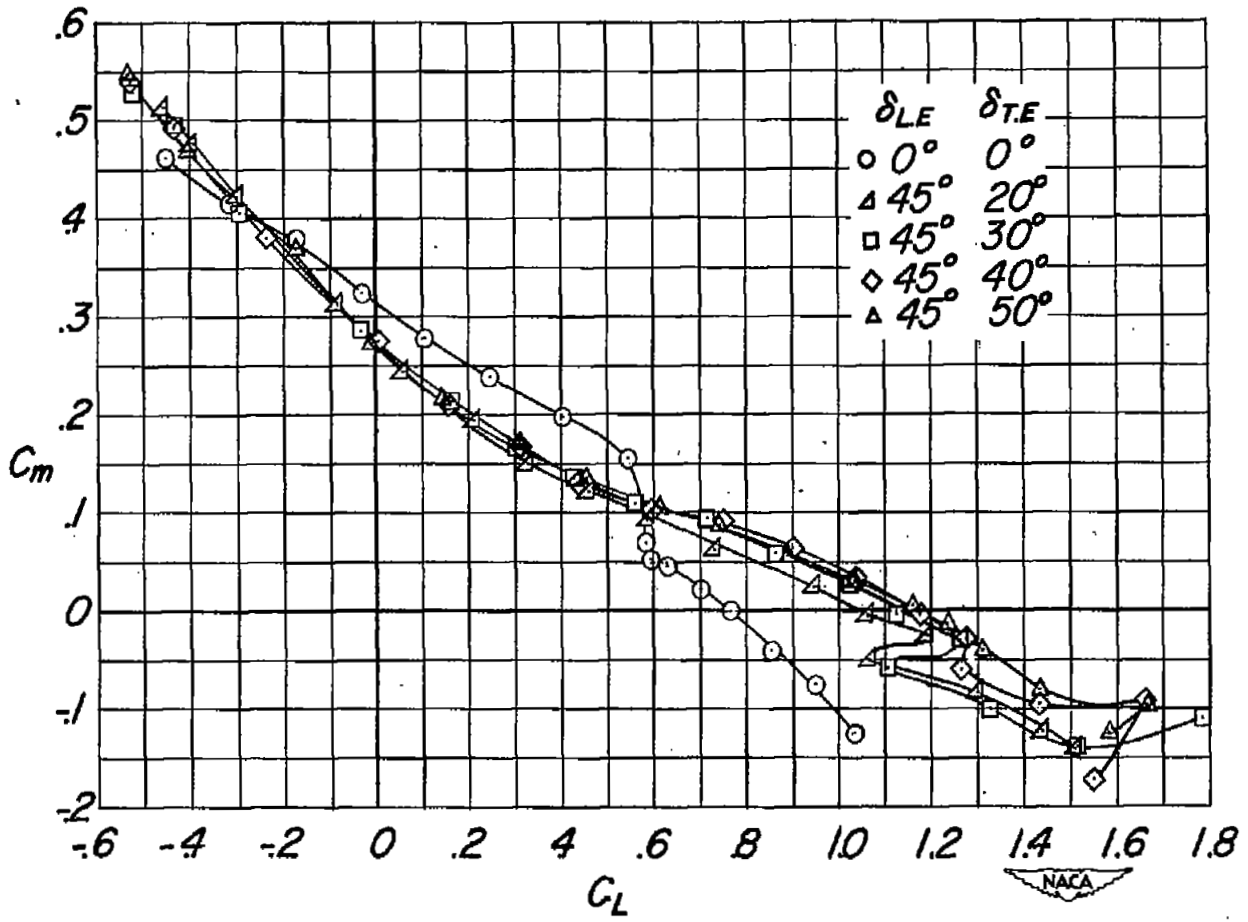

(a) Slotted leading-edge flap; slotted trailing-edge flap; $i_t = -8^\circ$.

Figure 25.- Effect of various leading- and trailing-edge flap configurations on the longitudinal stability characteristics of the model with the $A = 4.0$, $\frac{b_t}{b} = 0.59$ tail.

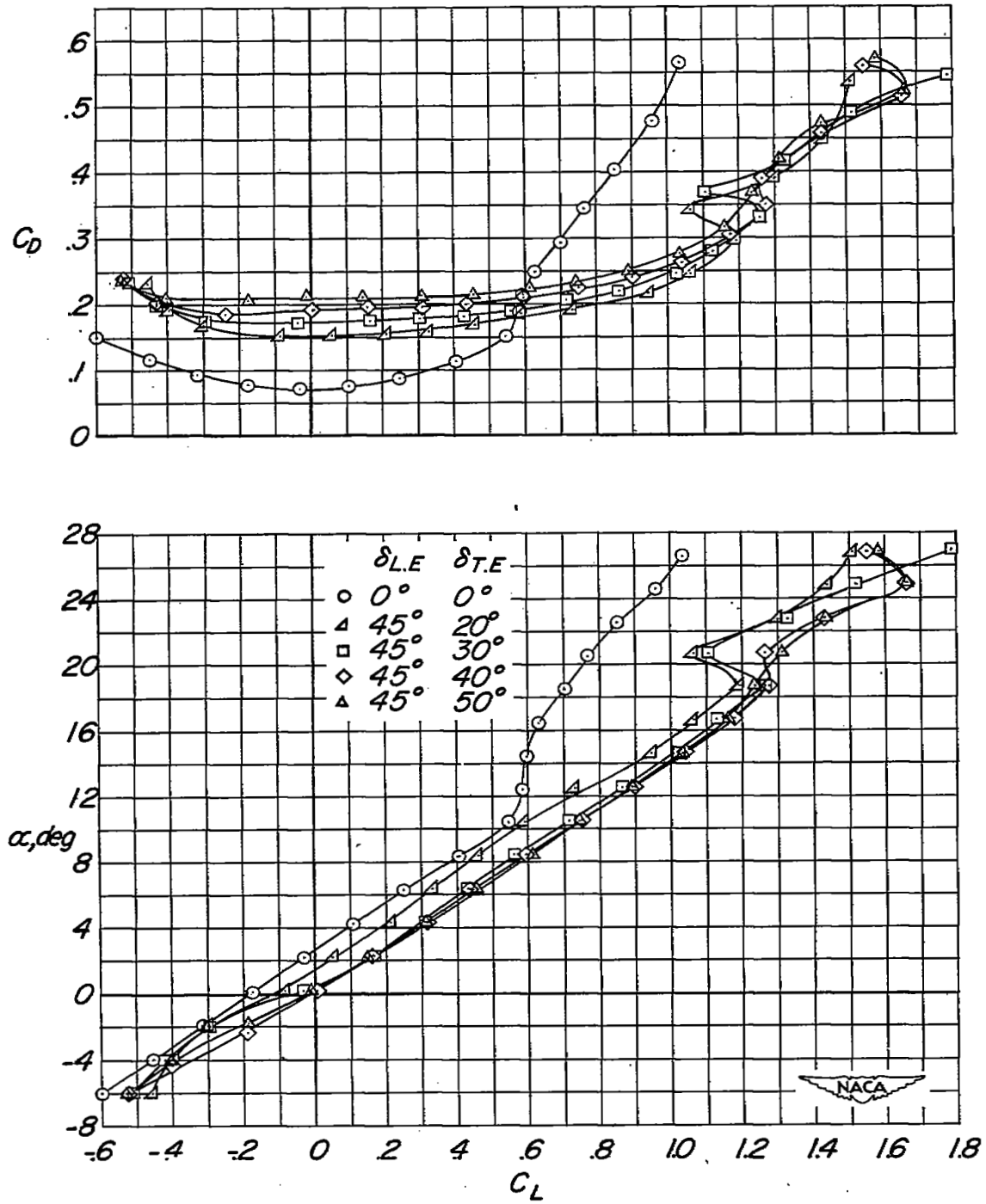

(a) Concluded.

Figure 25.- Continued.

[redacted]

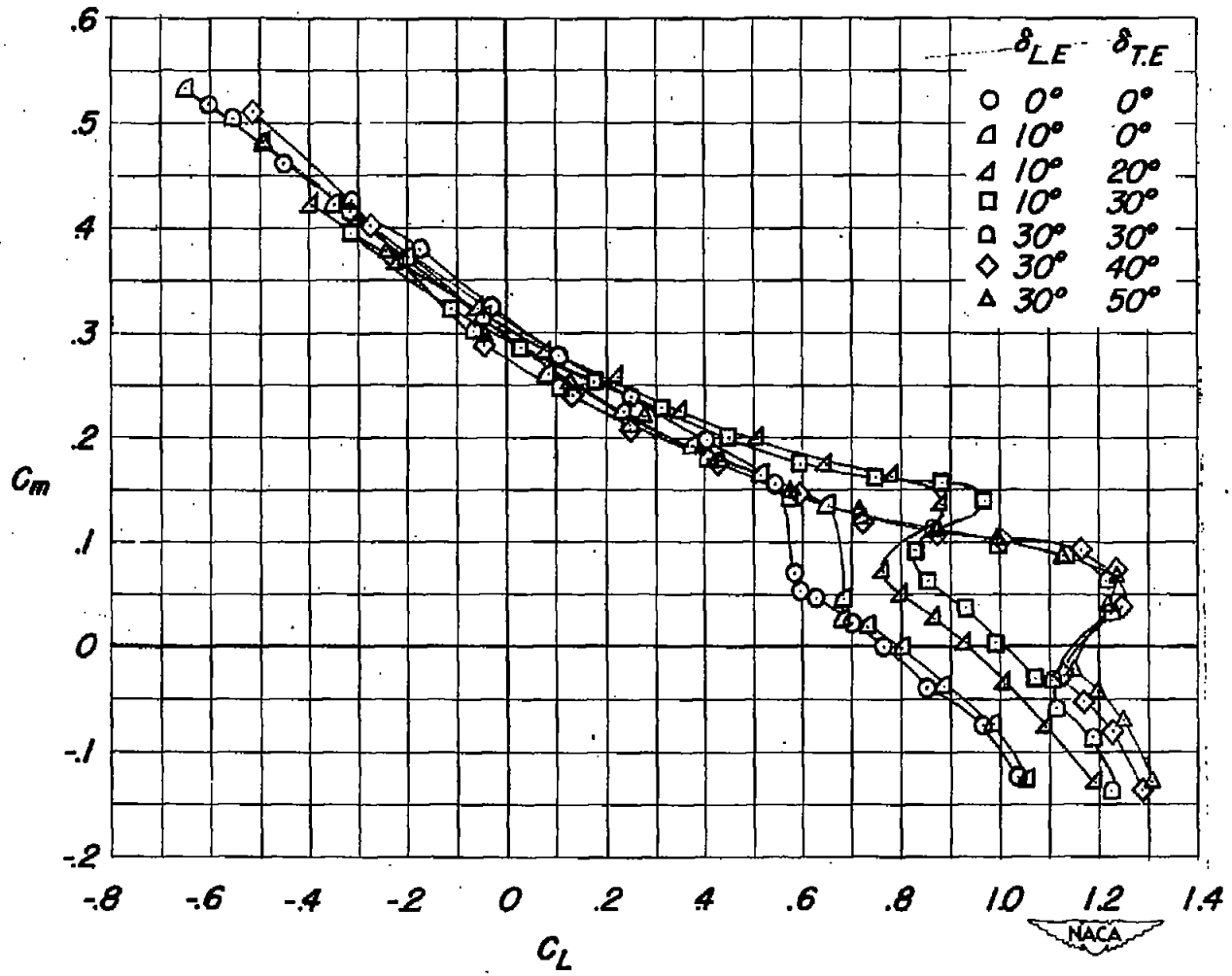

(b) Plain leading-edge flap; slotted trailing-edge flap; $i_t = -8^\circ$.

Figure 25.- Continued.

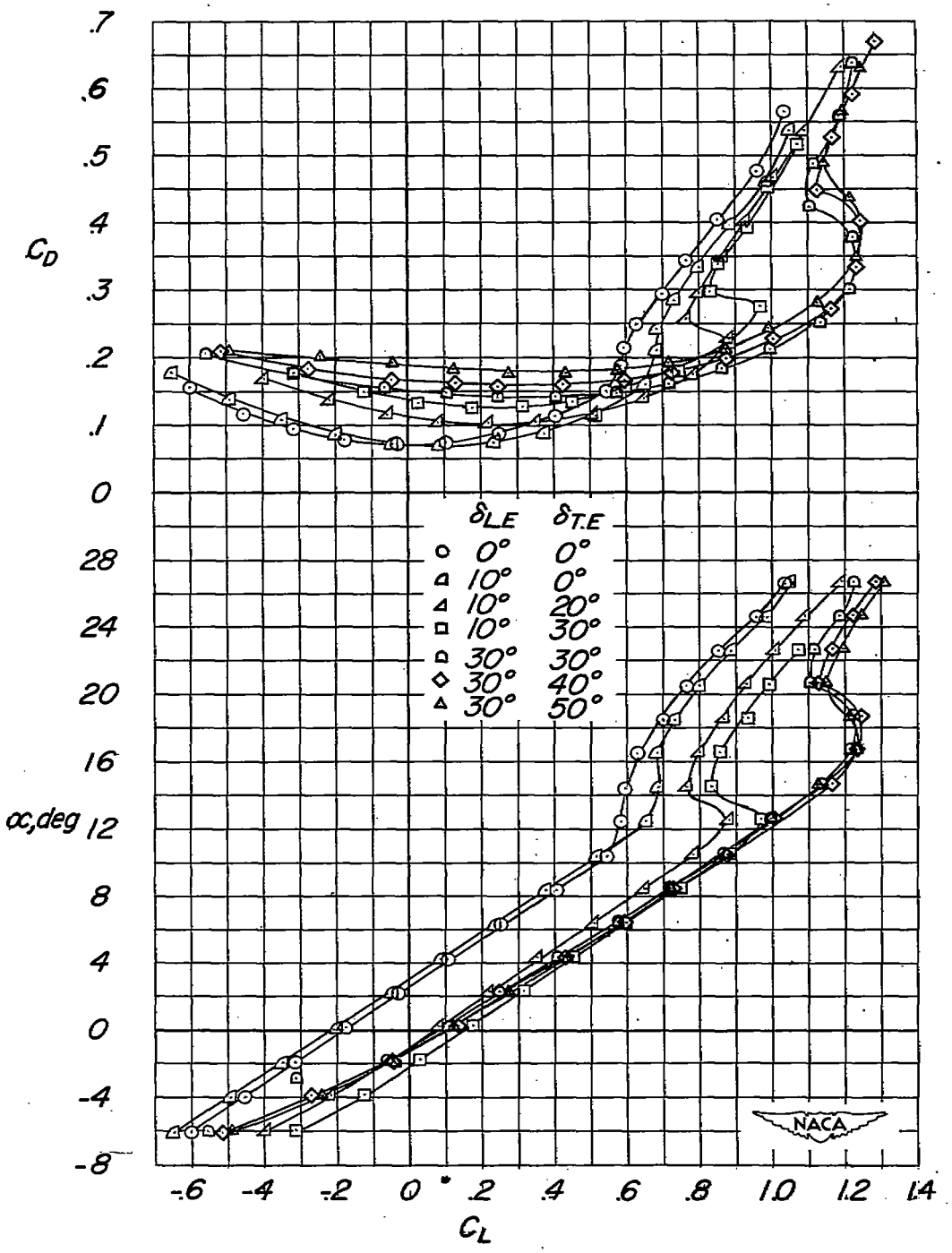

(b) Concluded.

Figure 25.- Continued.

[redacted]

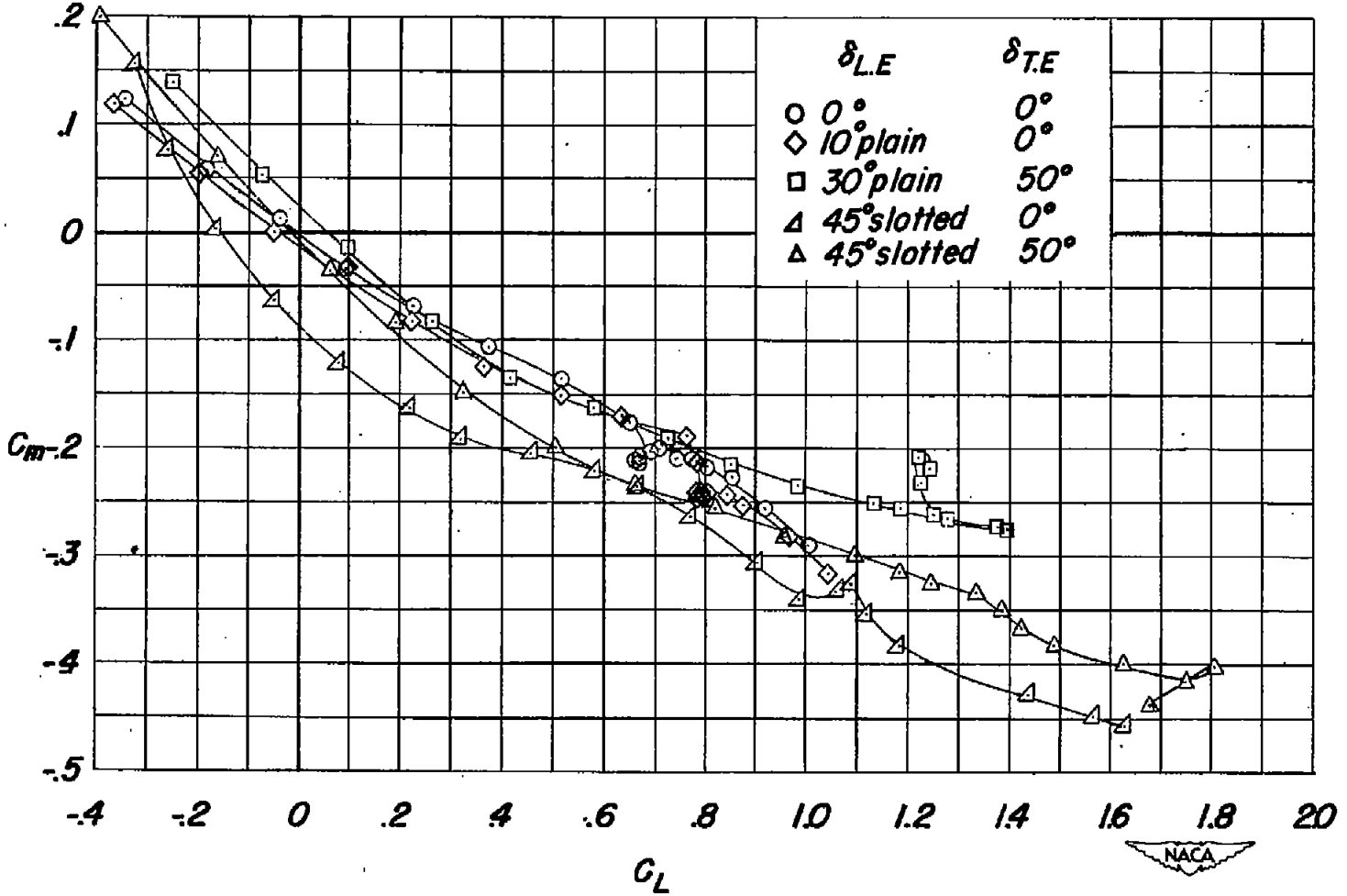

(c) Plain or slotted leading-edge flap; split trailing-edge flap; $i_t = 0^\circ$.

Figure 25.- Continued.

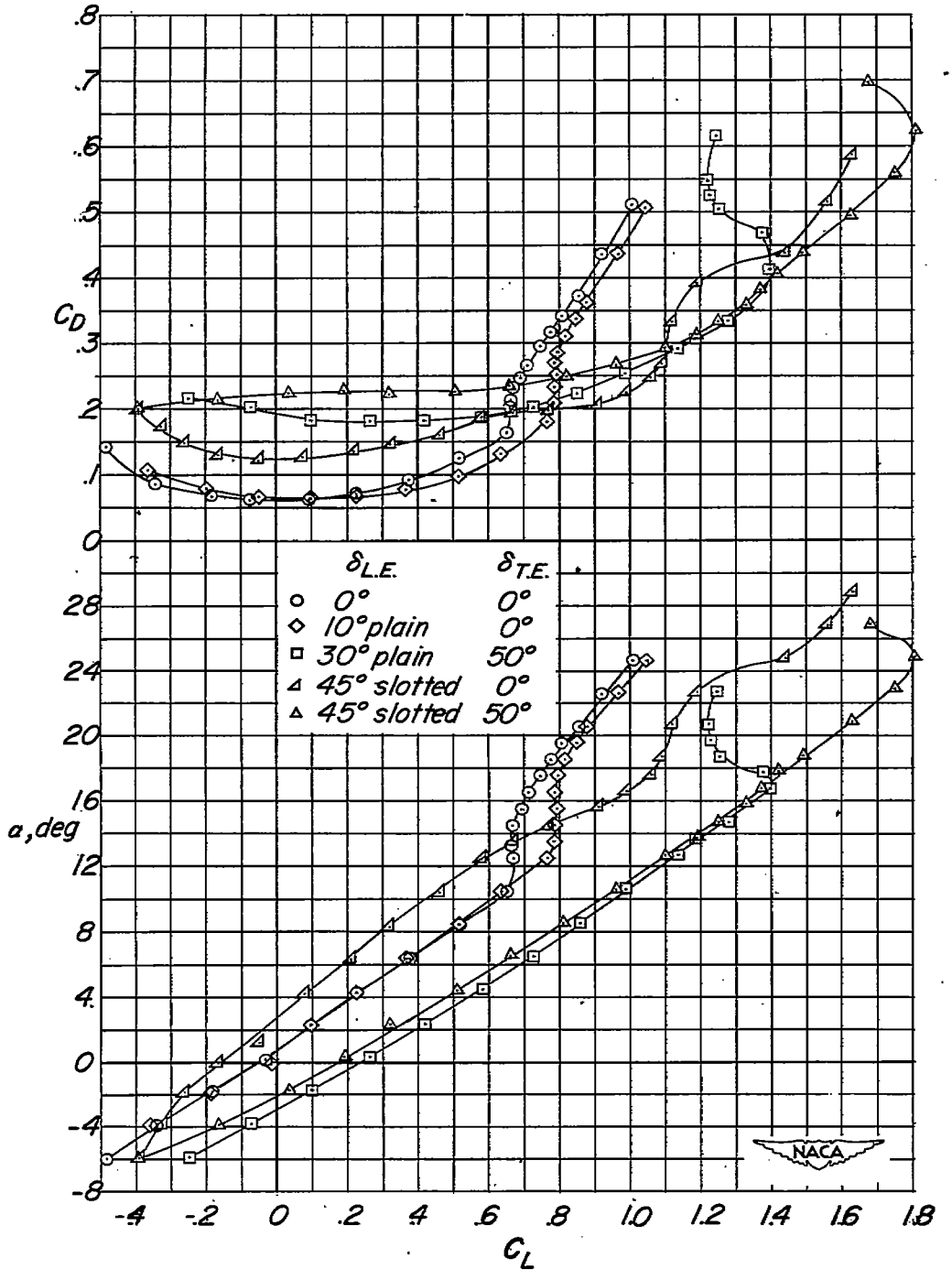

(c) Concluded.

Figure 25.- Concluded.

[redacted]

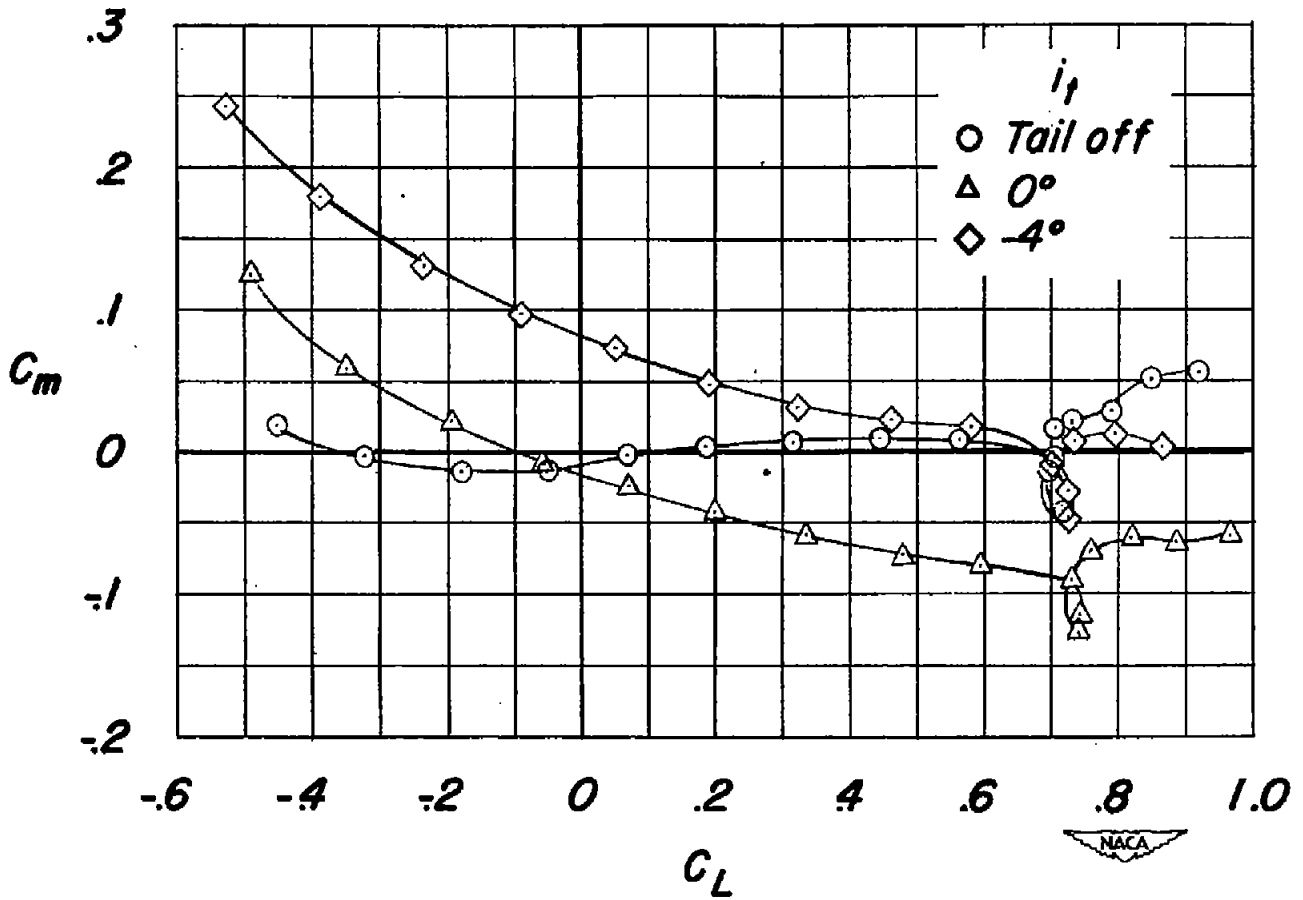

(a) Plain leading-edge flap deflected 10°; trailing-edge flap deflected 0°.

Figure 26.- Effect of various leading- and trailing-edge flap configurations on the tail effectiveness of the model. Original tail configuration.

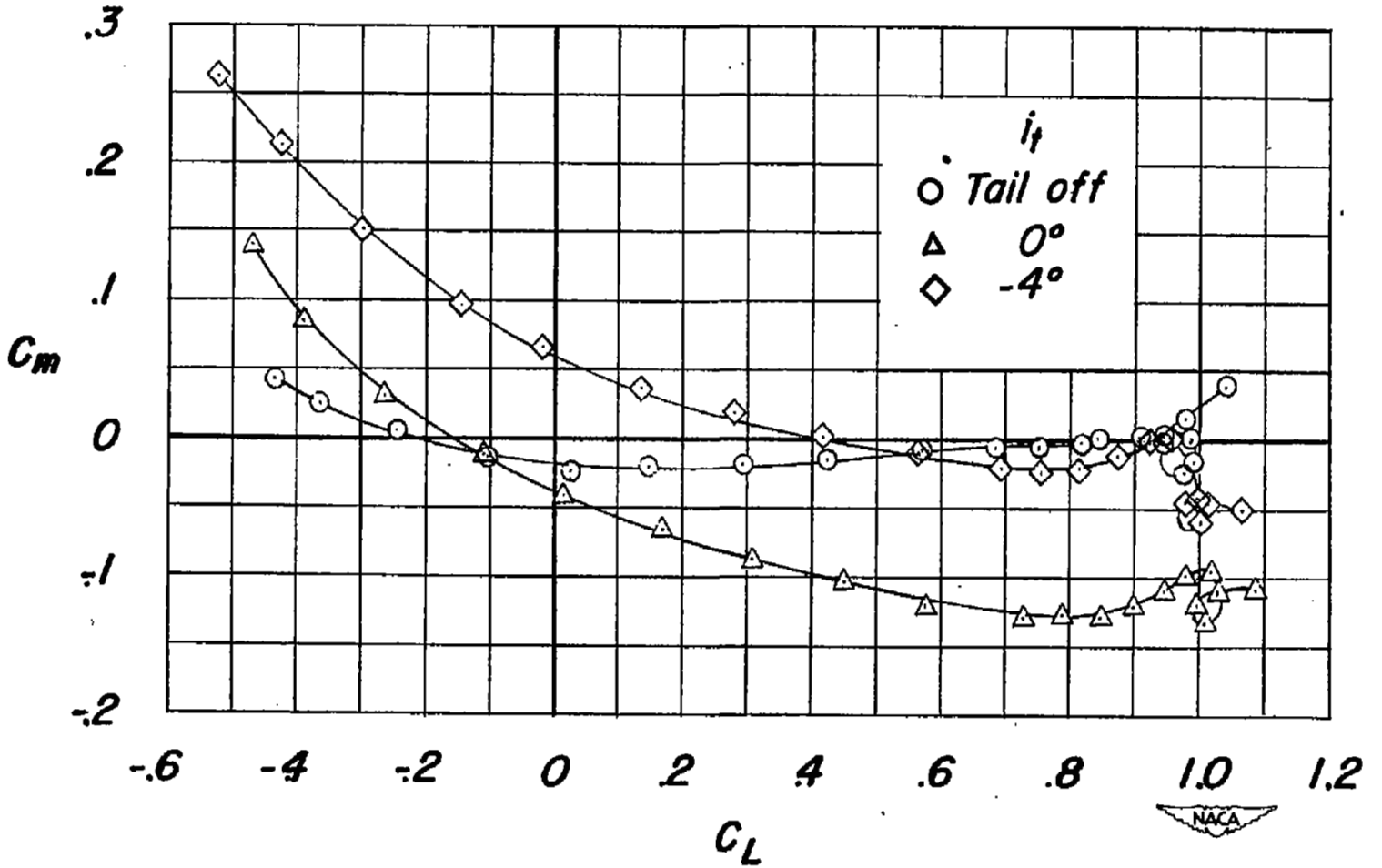

(b) Plain leading-edge flap deflected 30°; trailing-edge flap deflected 0°.

Figure 26.- Continued.

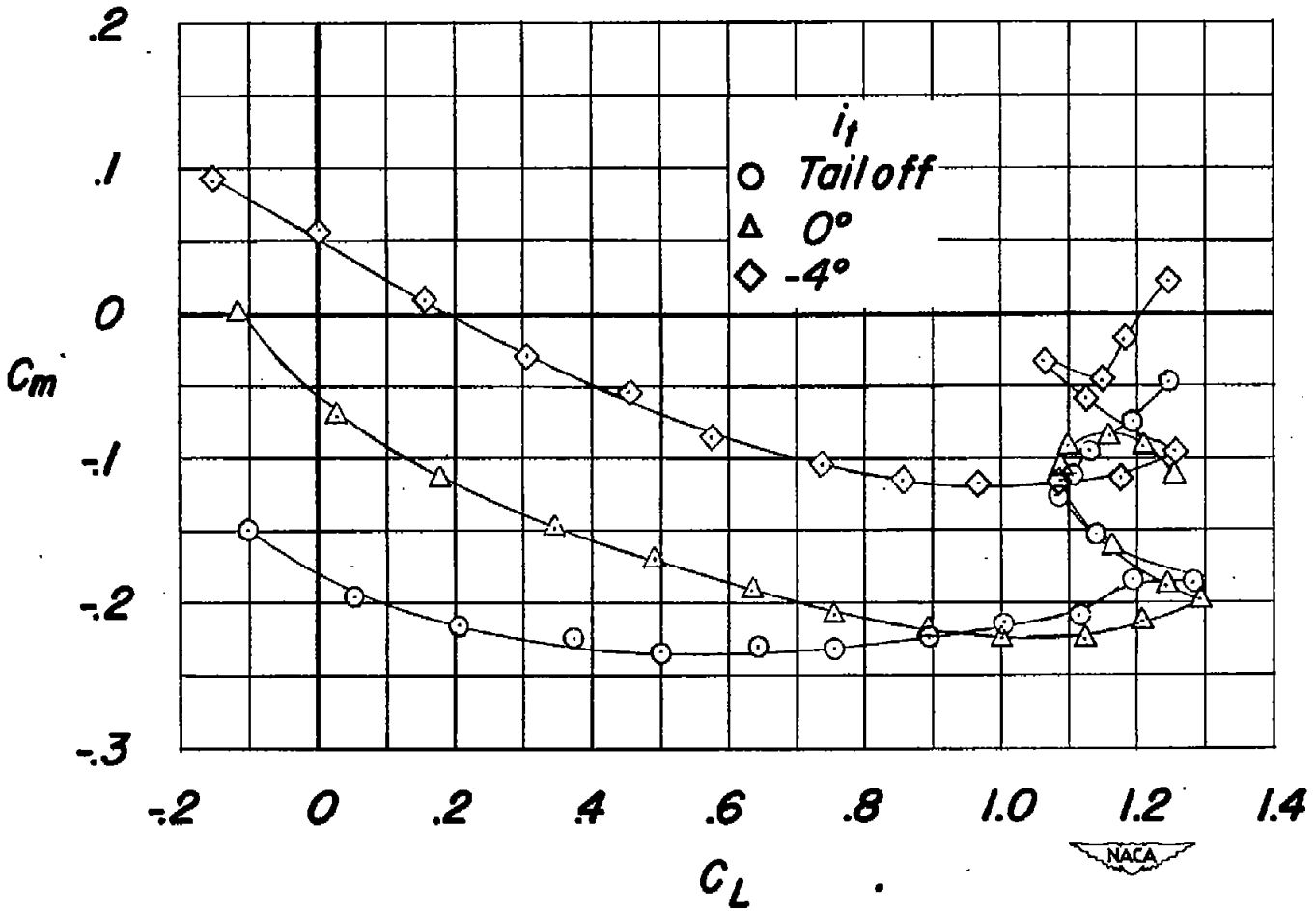

(c) Plain leading-edge flap deflected 30°; plain trailing-edge flap deflected 60°.

Figure 26.- Continued.

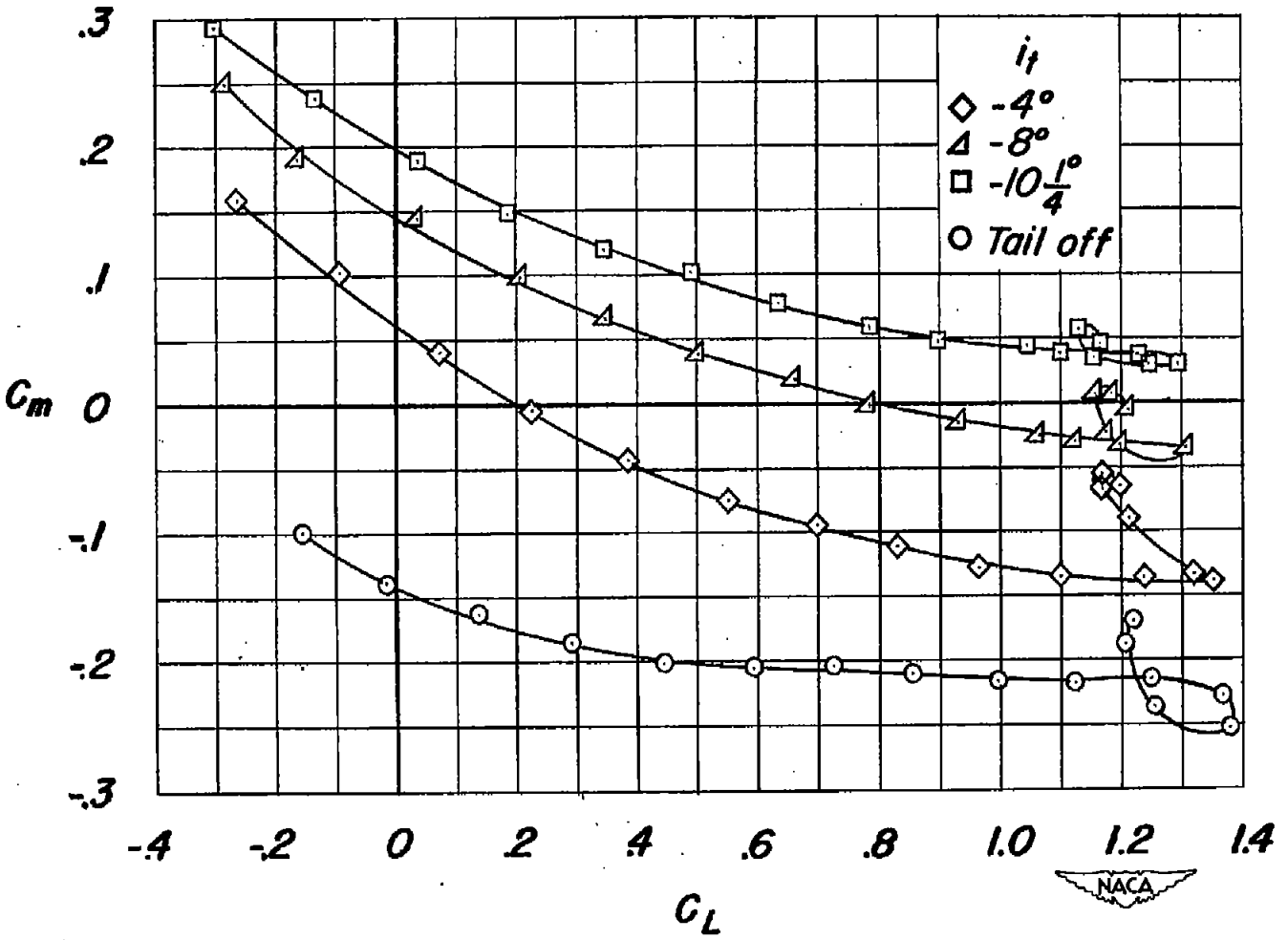

(d) Plain leading-edge flap deflected 30°; split trailing-edge flap deflected 50°.

Figure 26.- Continued.

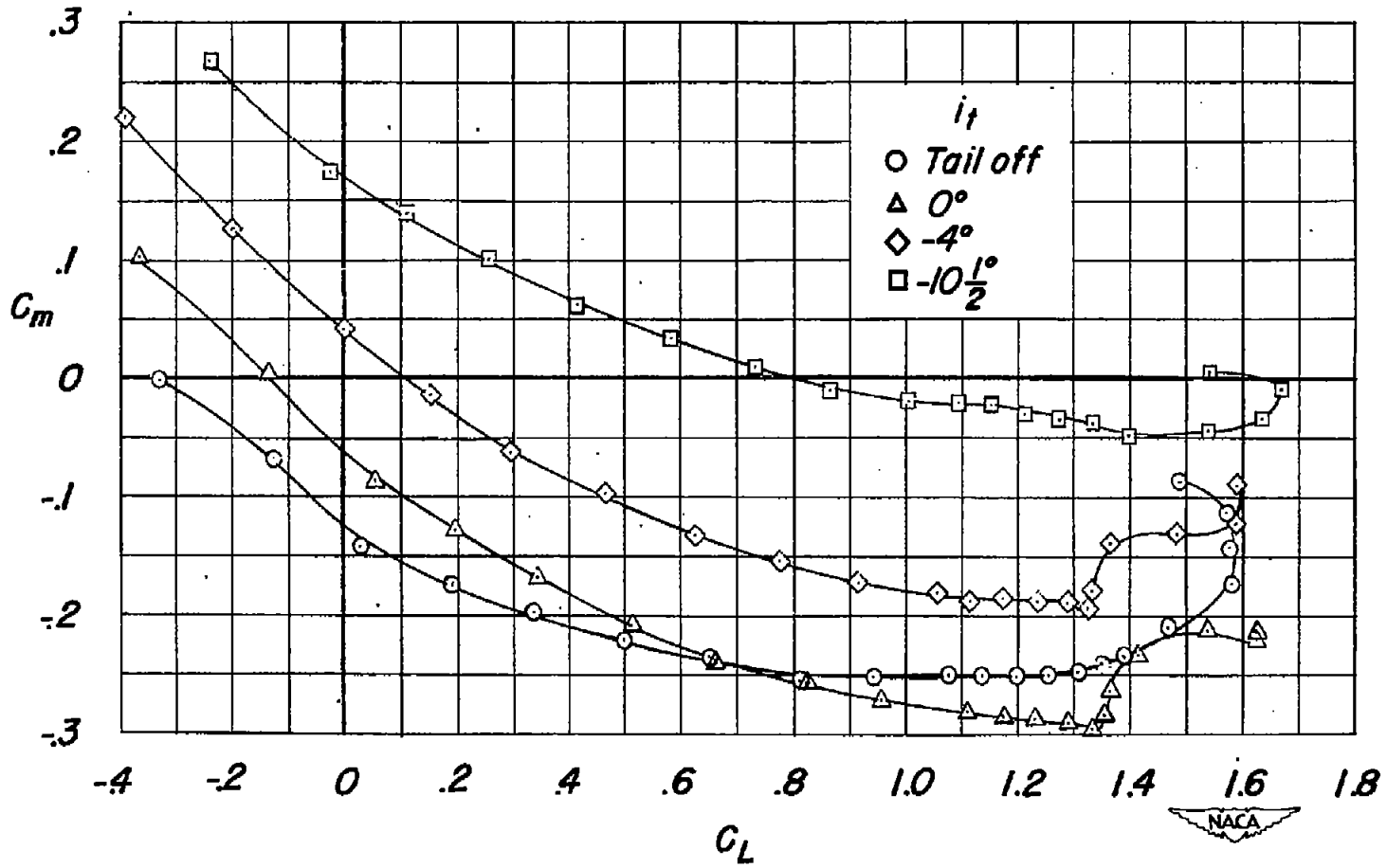

(e) Slotted leading-edge flap deflected 45°; split trailing-edge flap deflected 50°.

Figure 26.- Continued.

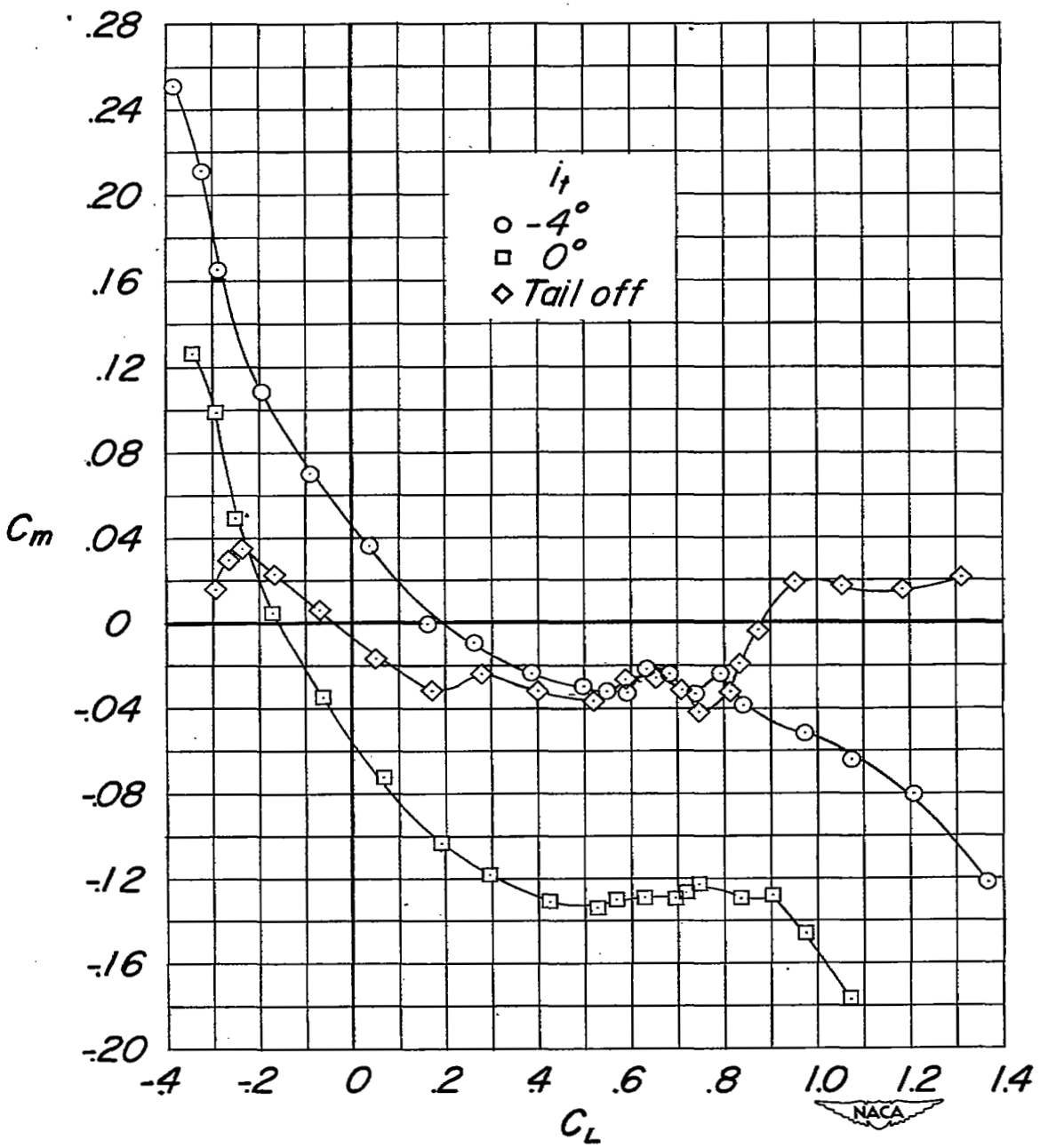

(f) Slotted leading-edge flap deflected 45°; trailing-edge flap deflected 0°.

Figure 26.- Continued.

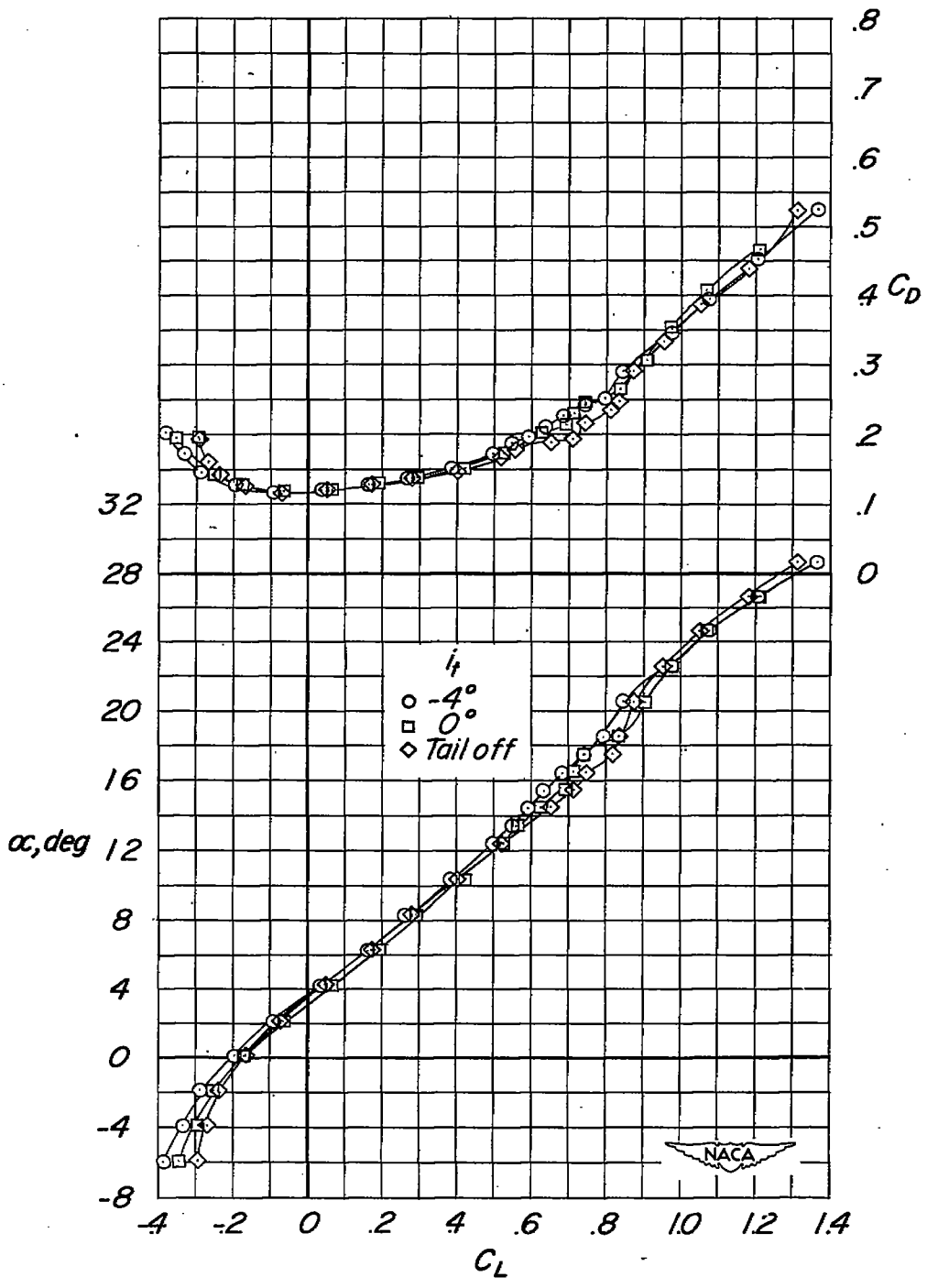

(f) Concluded.

Figure 26.- Concluded.

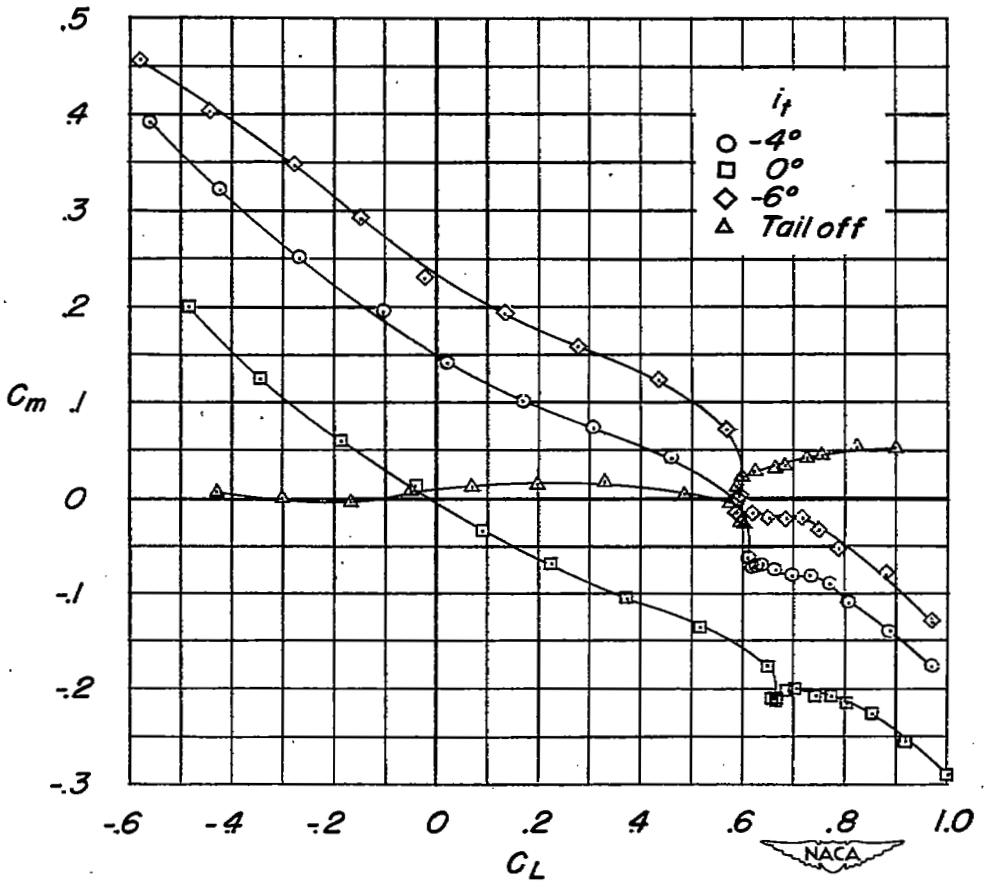

(a) Leading-edge flap deflected 0°; trailing-edge flap deflected 0°.

Figure 27.- Effect of various leading and trailing edge flap configurations on the tail effectiveness of the model with the A = 4.0, $\frac{b_t}{b}$ = 0.59 tail.

[redacted]

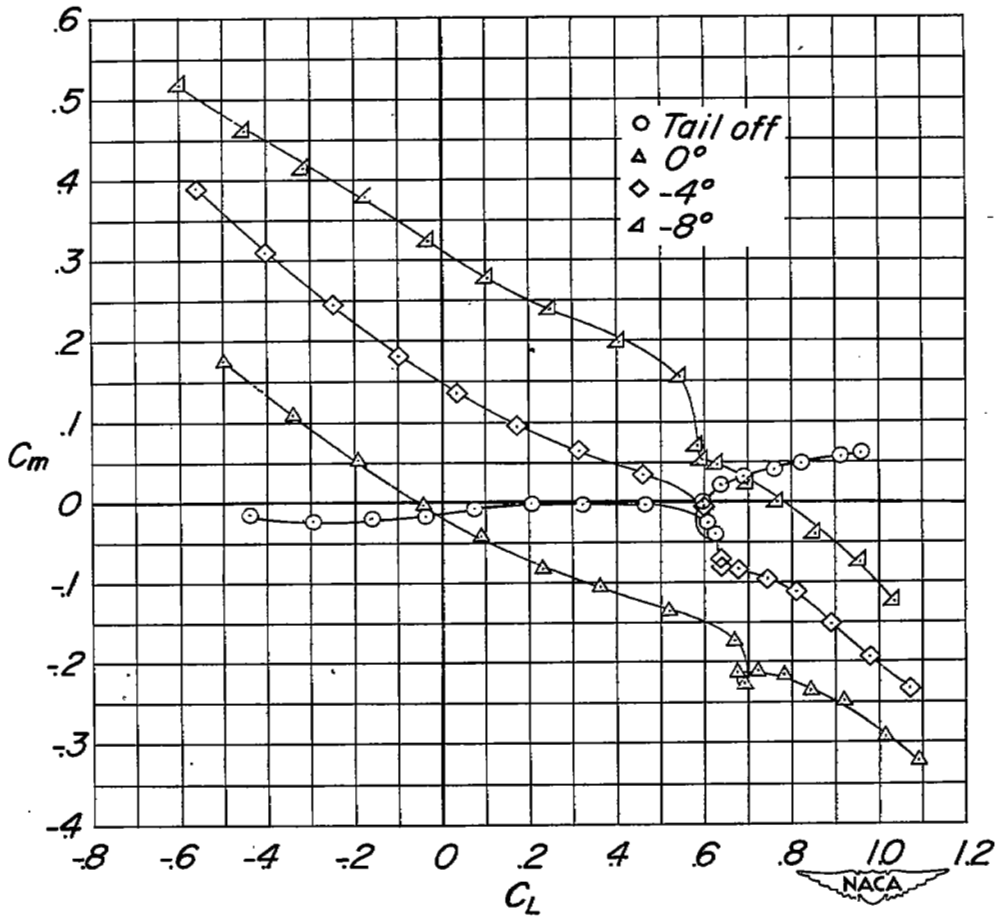

(b) Leading-edge flap deflected 0°; slotted trailing-edge flap deflected 0°.

Figure 27.- Continued.

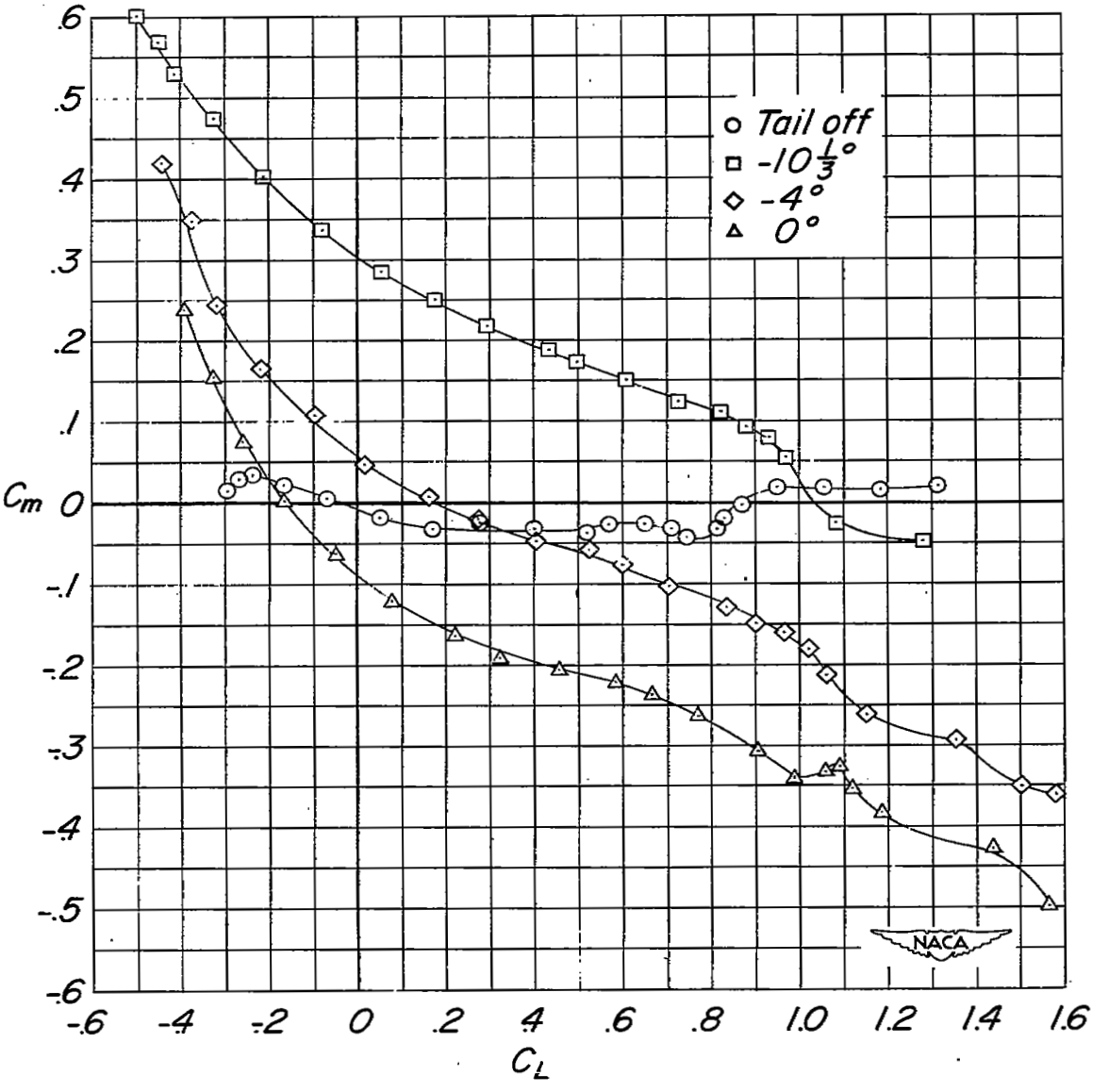

(c) Slotted leading-edge flap deflected 45°; trailing-edge flap deflected 0°.

Figure 27.- Continued.

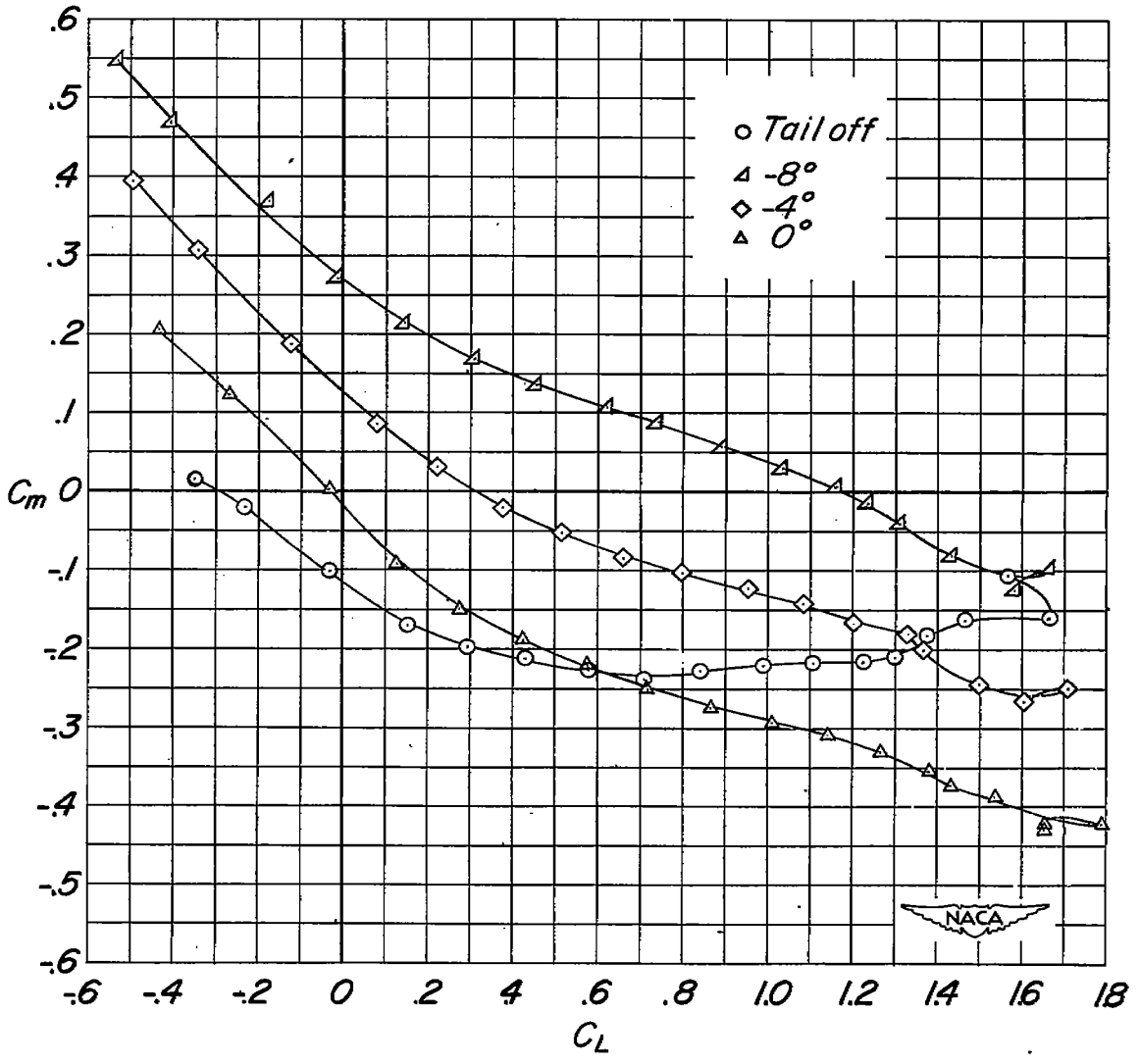

(d) Slotted leading-edge flap deflected 45°; slotted trailing-edge flap deflected 50°.

Figure 27.- Continued.

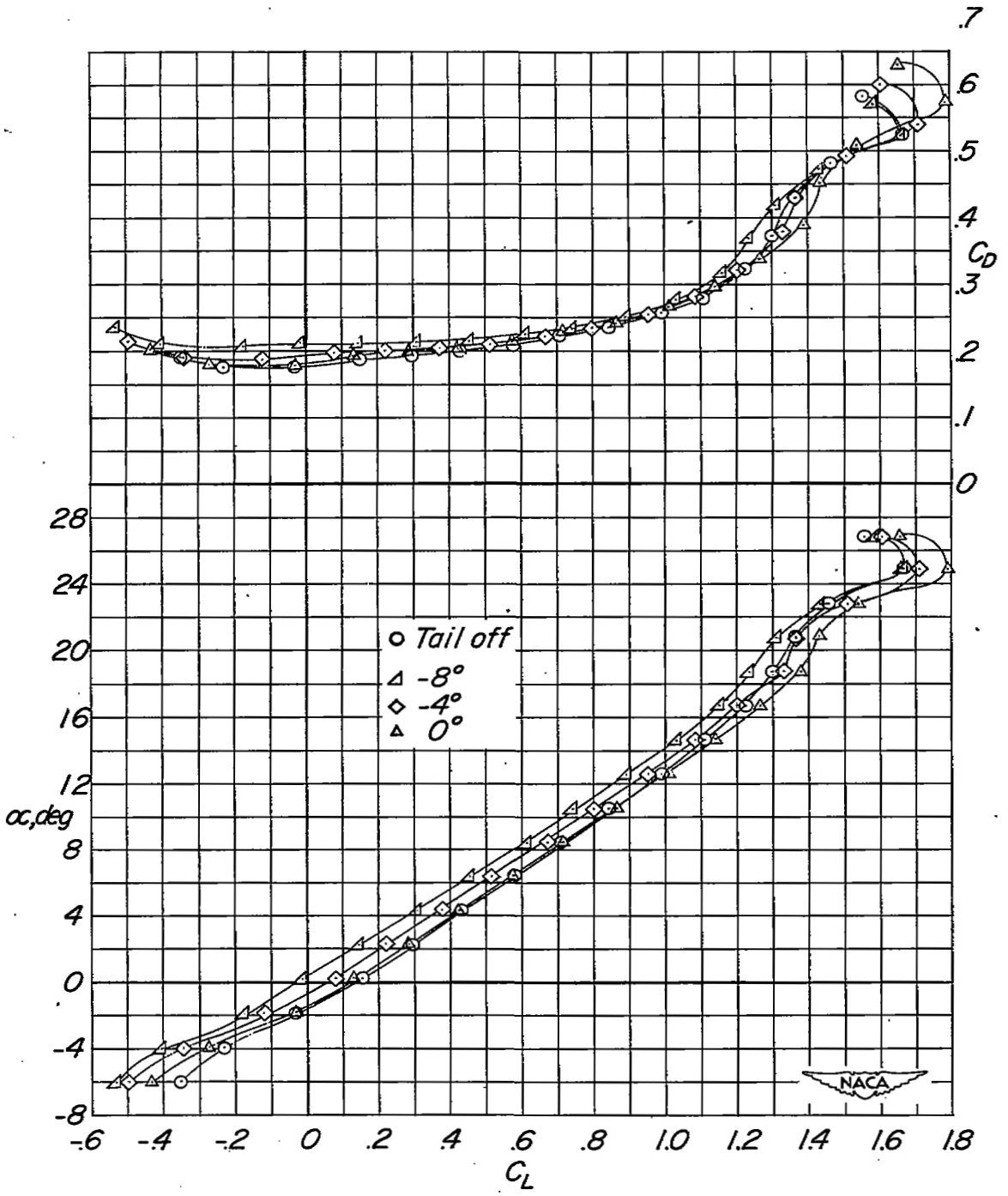

(d) Concluded.

Figure 27.- Continued.

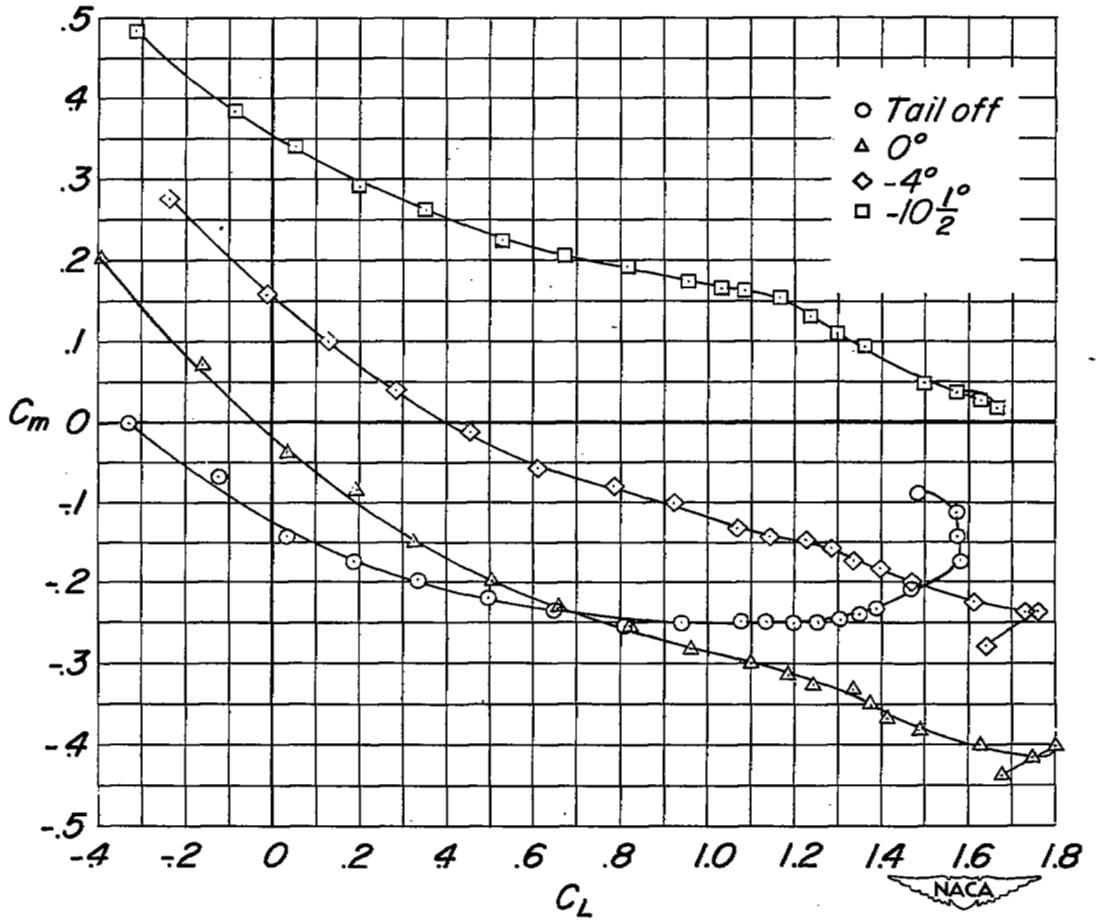

(e) Slotted leading-edge flap deflected 45°; split trailing-edge flap deflected 50°.

Figure 27.- Continued.

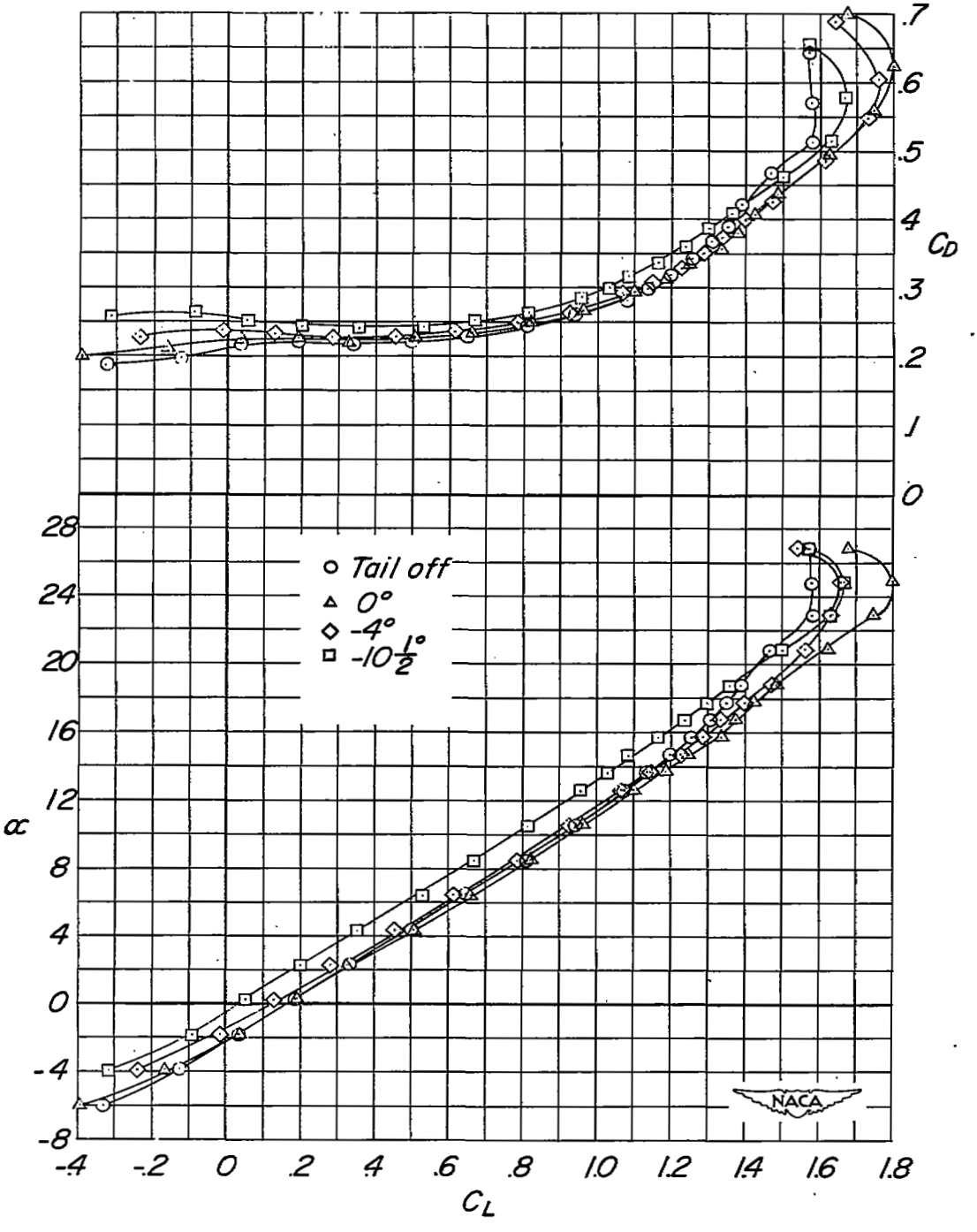

(e) Concluded.

Figure 27.- Continued.

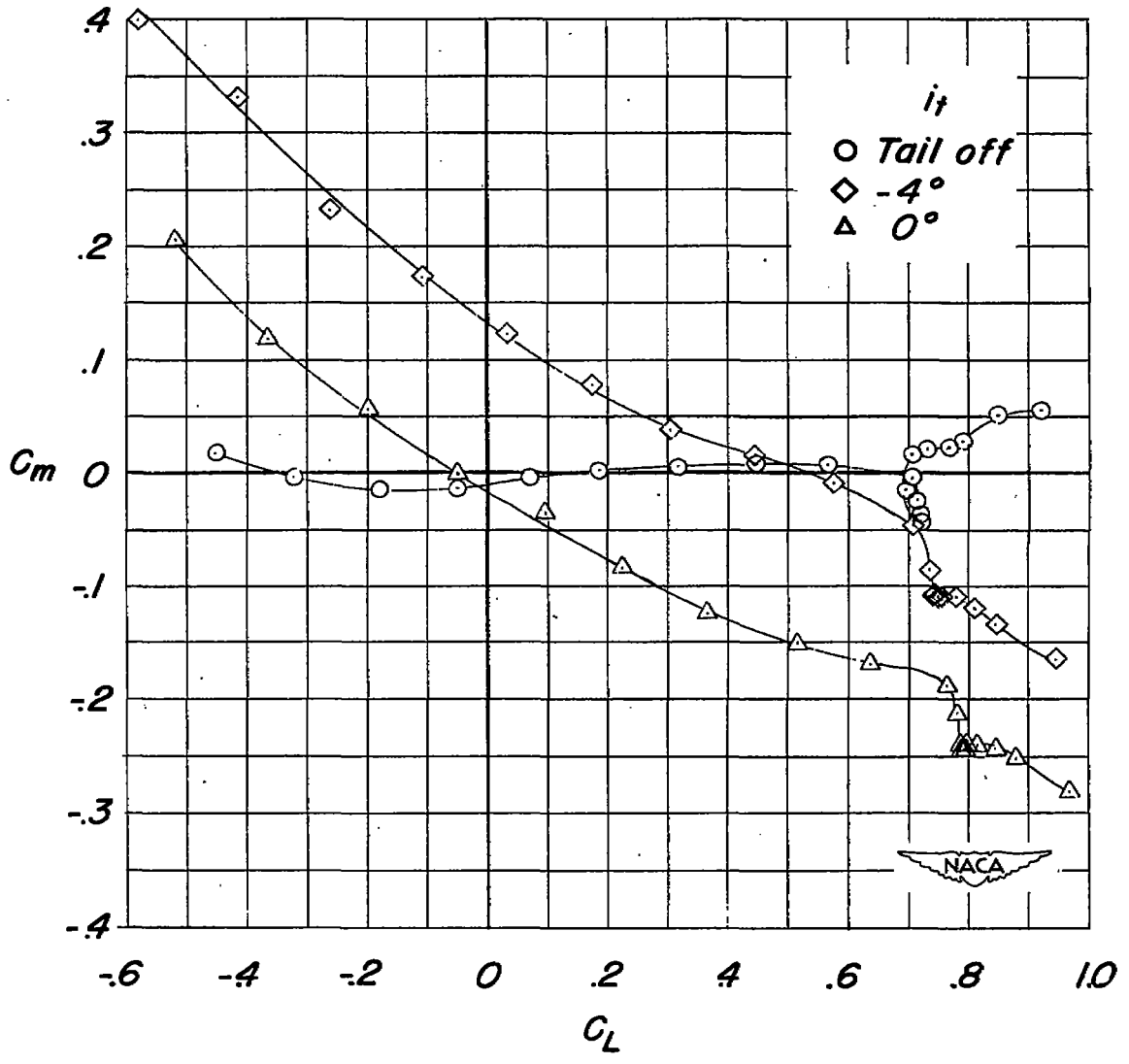

(f) Plain leading-edge flap deflected 10°; trailing-edge flap deflected 0°.

Figure 27.- Continued.

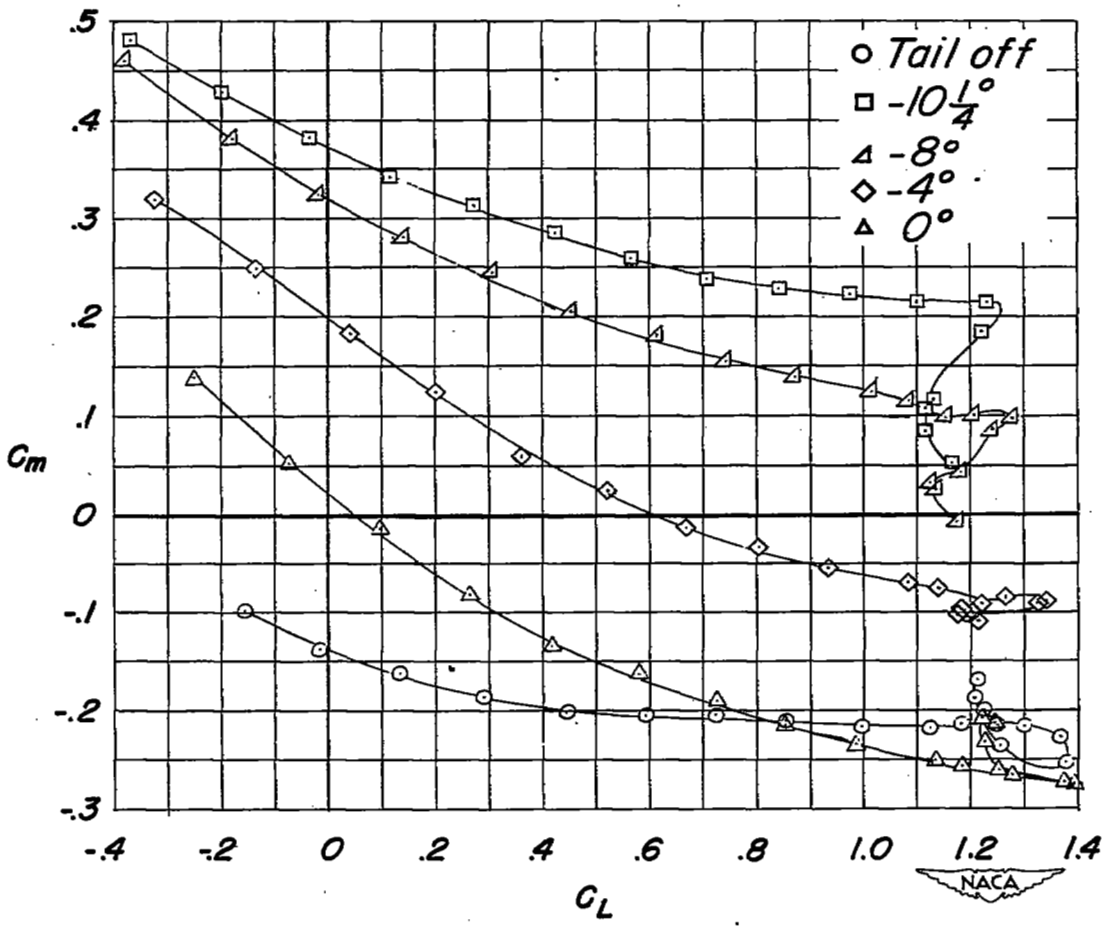

(g) Plain leading-edge flap deflected 30°; split trailing-edge flap deflected 50°.

Figure 27.- Continued.

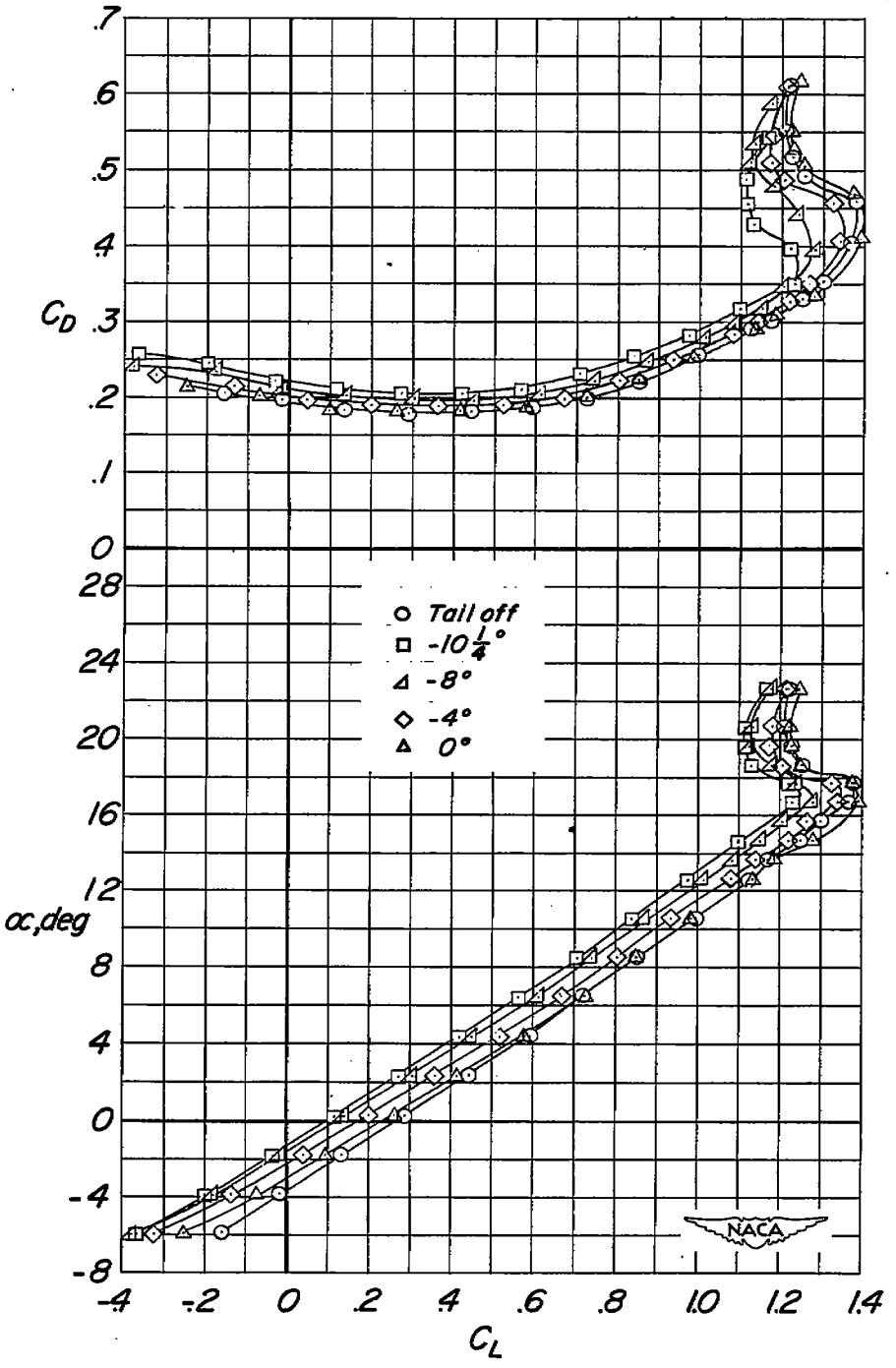

(g) Concluded.

Figure 27.- Continued.

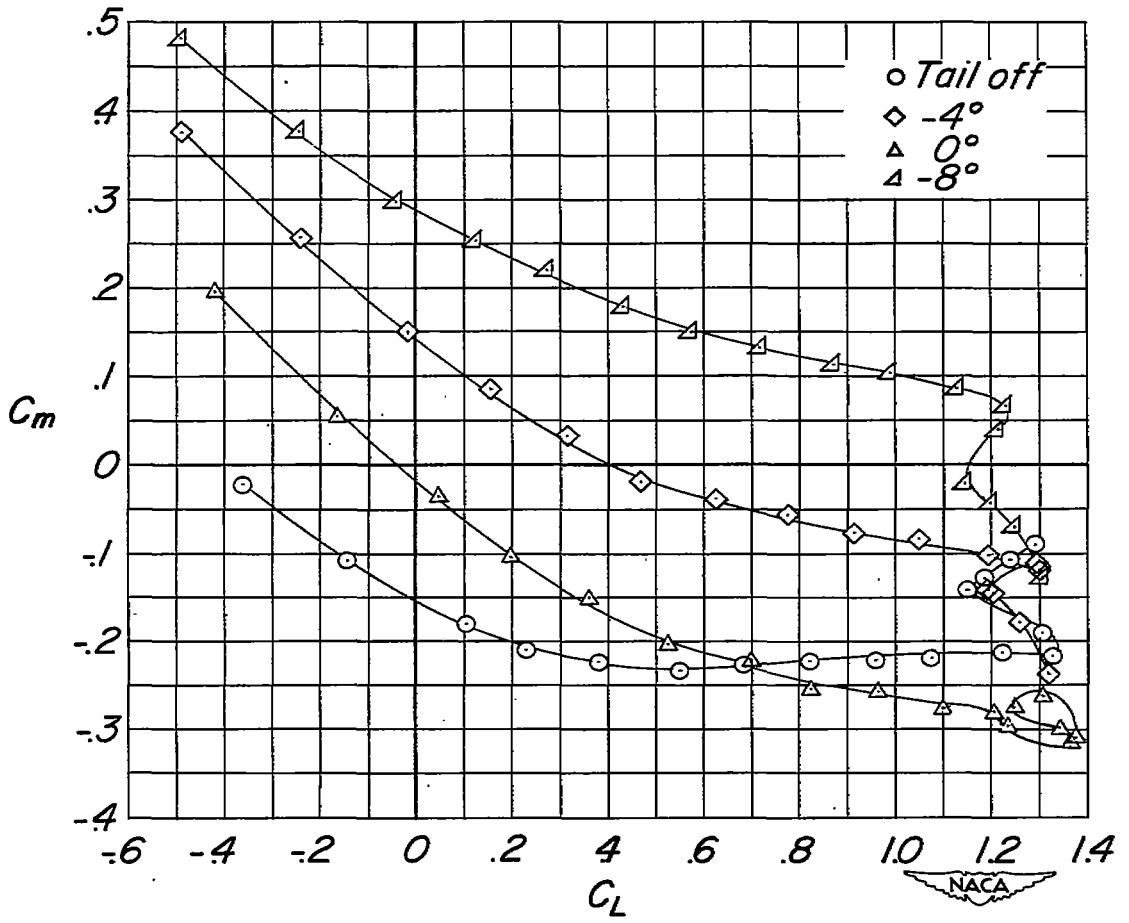

(h) Plain leading-edge flap deflected 30°; slotted trailing-edge flap deflected 40°.

Figure 27.- Concluded.

[redacted]

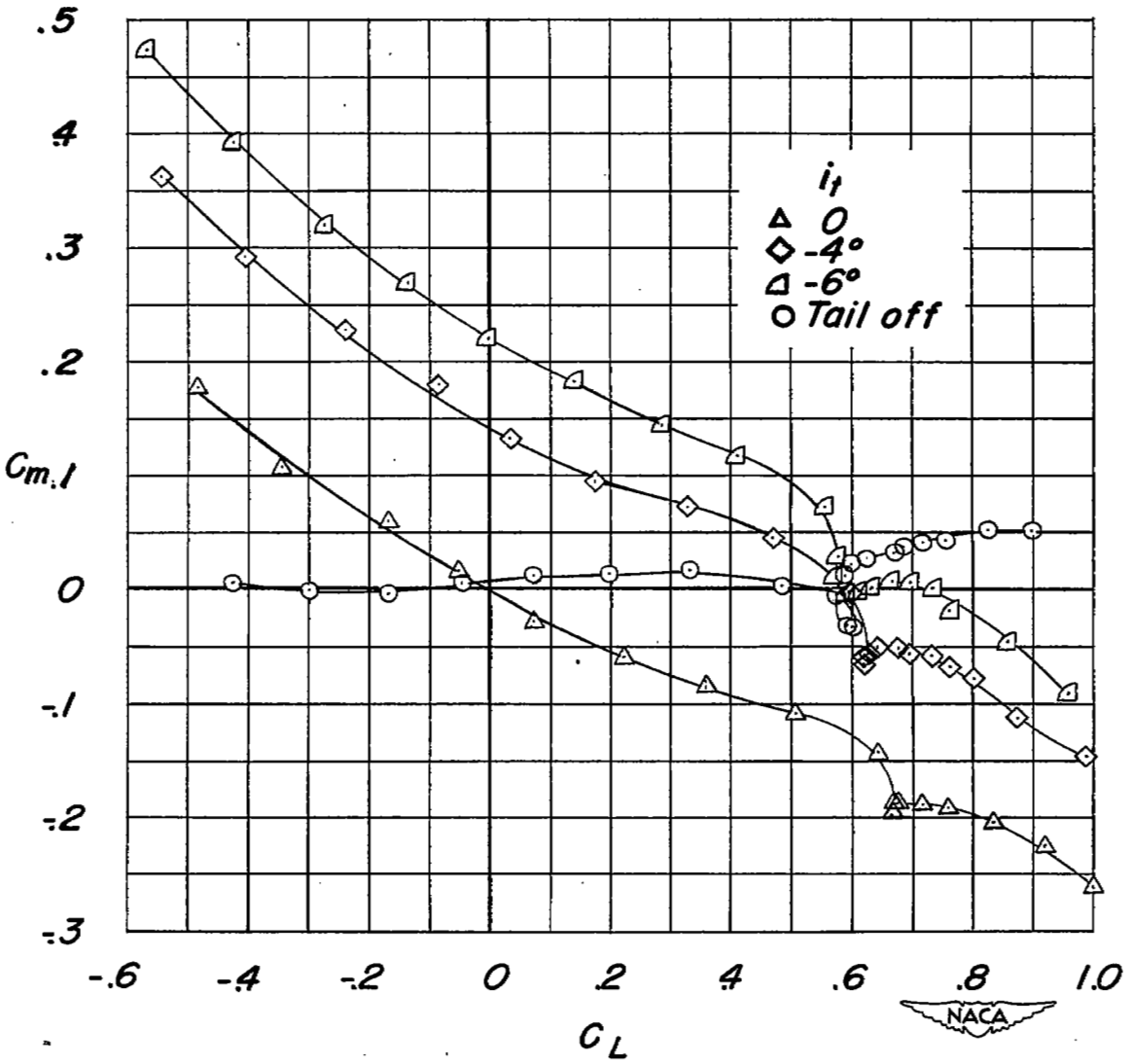

(a) Leading-edge flap deflected 0°; trailing-edge flap deflected 0°.

Figure 28.- Effect of various leading- and trailing-edge flap arrangements on the tail effectiveness of the model with the A = 3.0, $\frac{b_t}{b}$ = 0.51 tail.

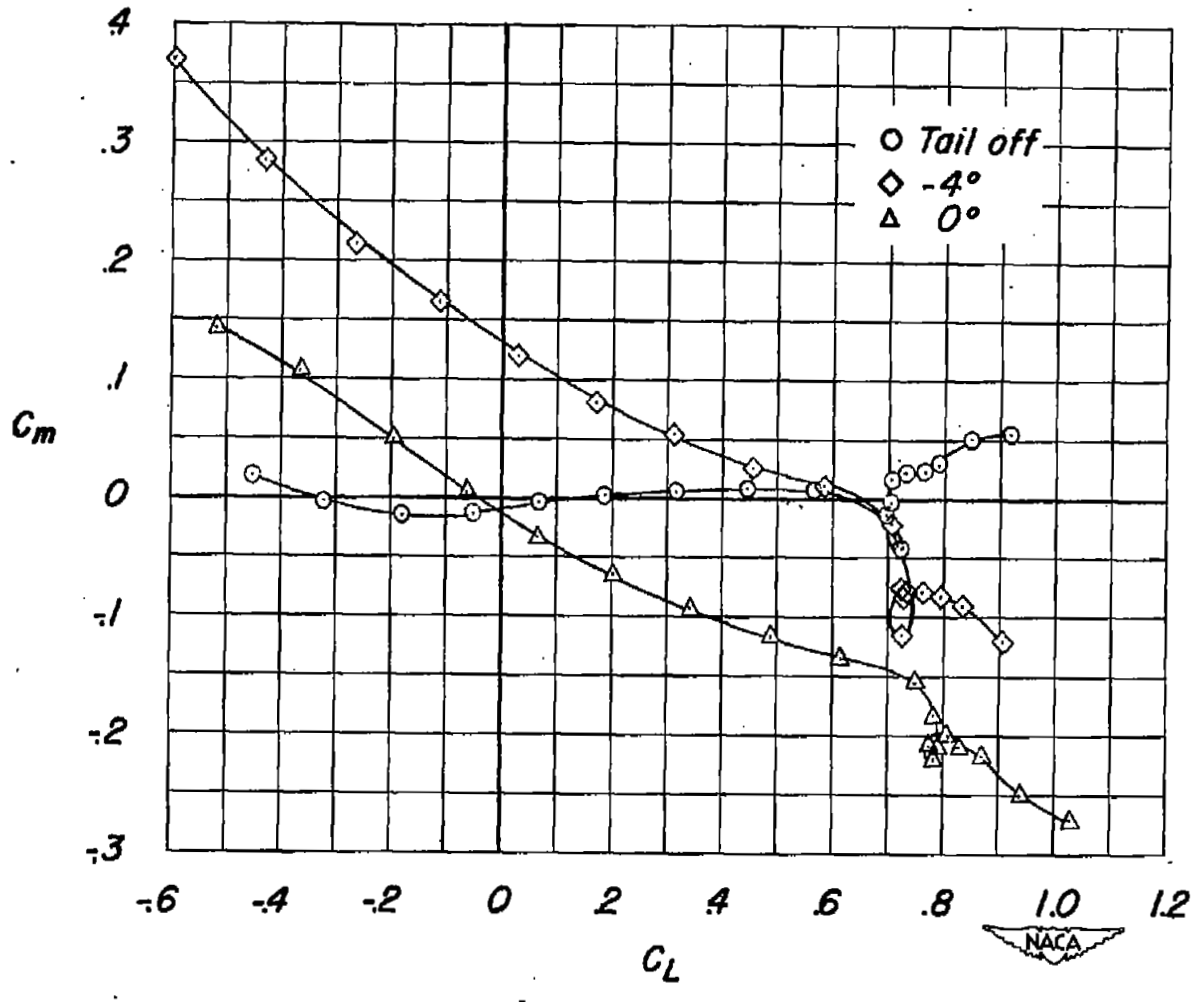

(b) Plain leading-edge flap deflected 10°; trailing-edge flap deflected 0°.

Figure 28.- Continued.

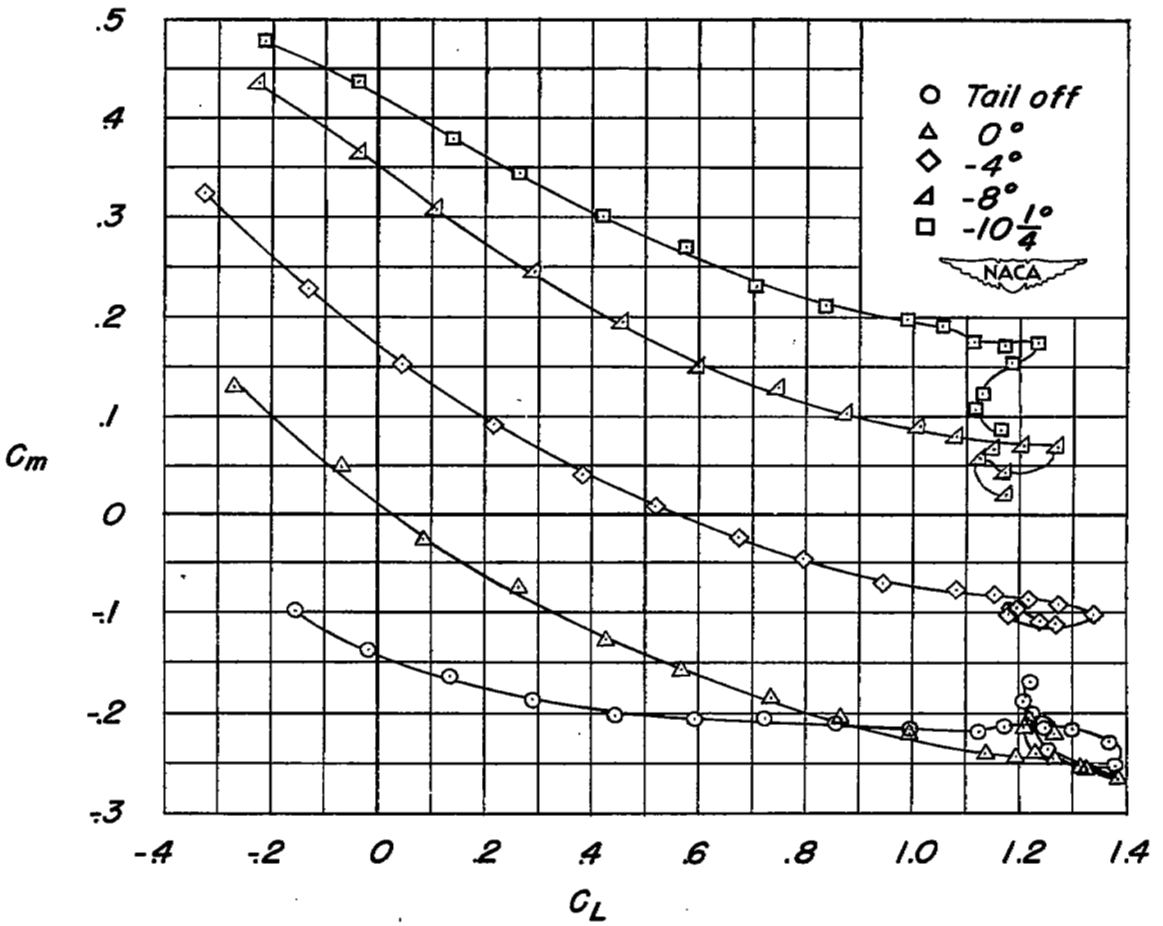

(c) Plain leading-edge flap deflected 30°; split trailing-edge flap deflected 50°.

Figure 28.- Concluded.

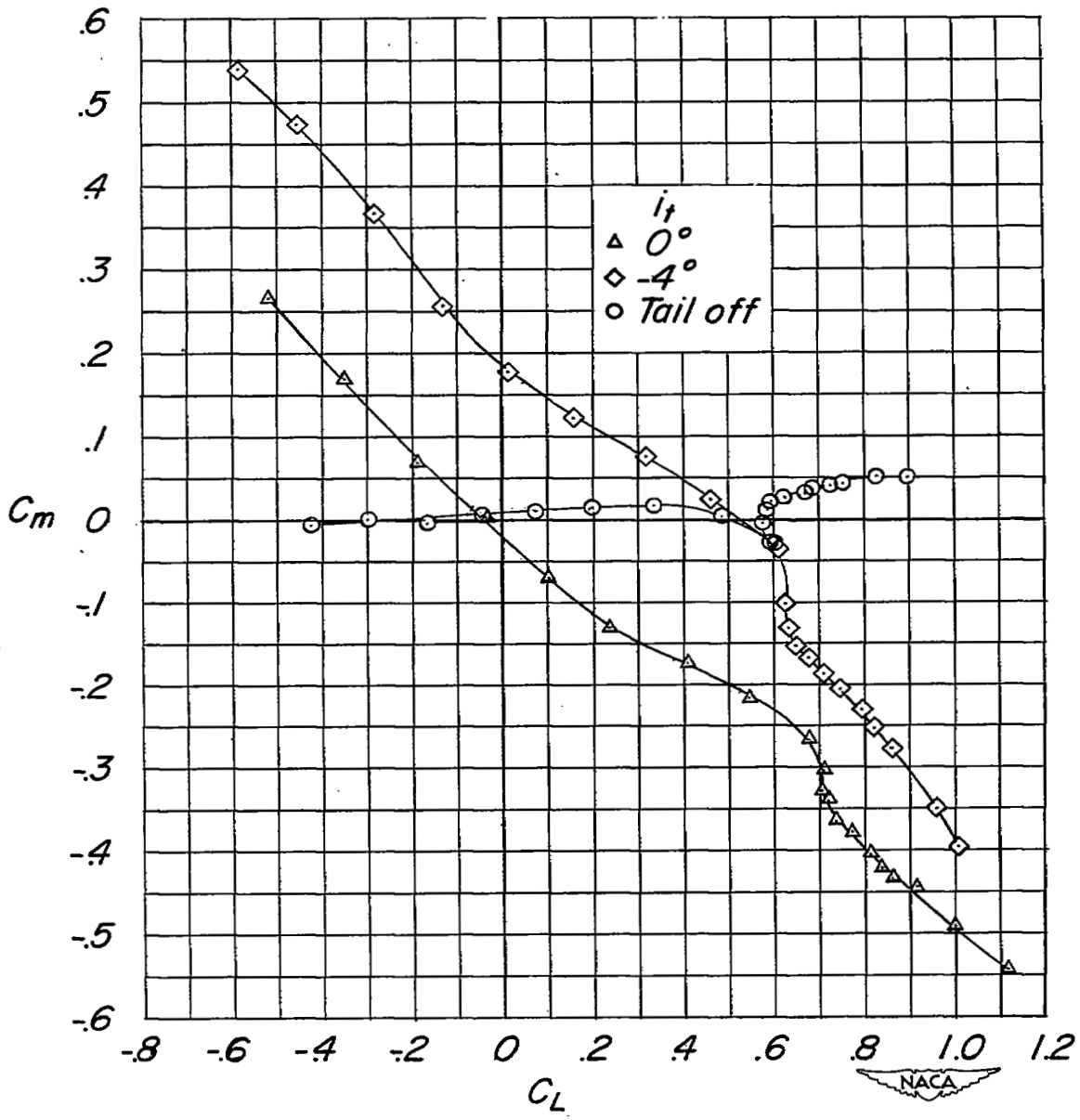

(a) Leading-edge flap deflected 0°; trailing-edge flap deflected 0°.

Figure 29.- Effect of various leading- and trailing-edge flap arrangements on the tail effectiveness of the model with the $A = 4.76$, $\frac{b_t}{b} = 0.73$ tail.

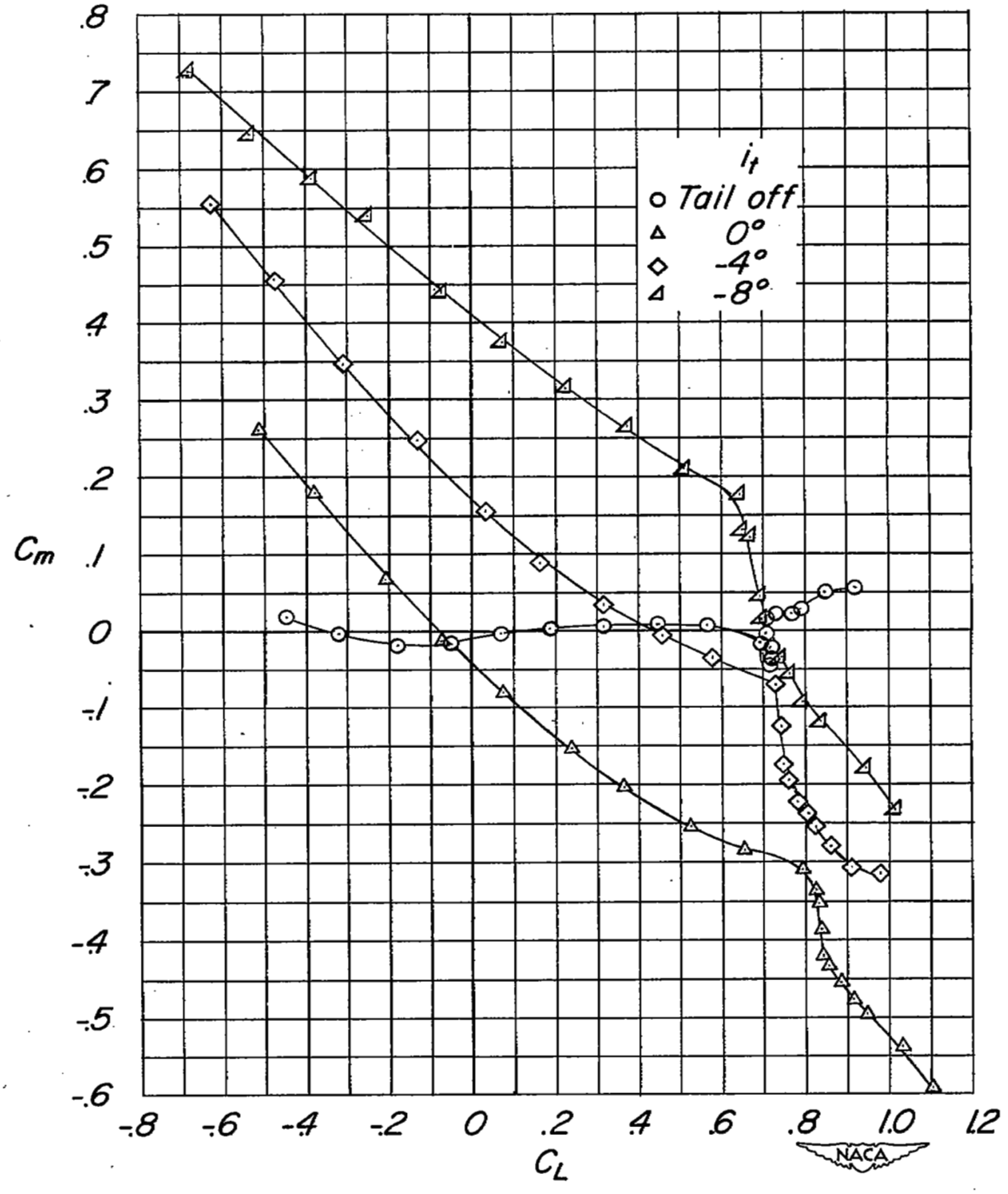

(b) Plain leading-edge flap deflected 10°; trailing-edge flap deflected 0°.

Figure 29.- Continued.

[redacted]

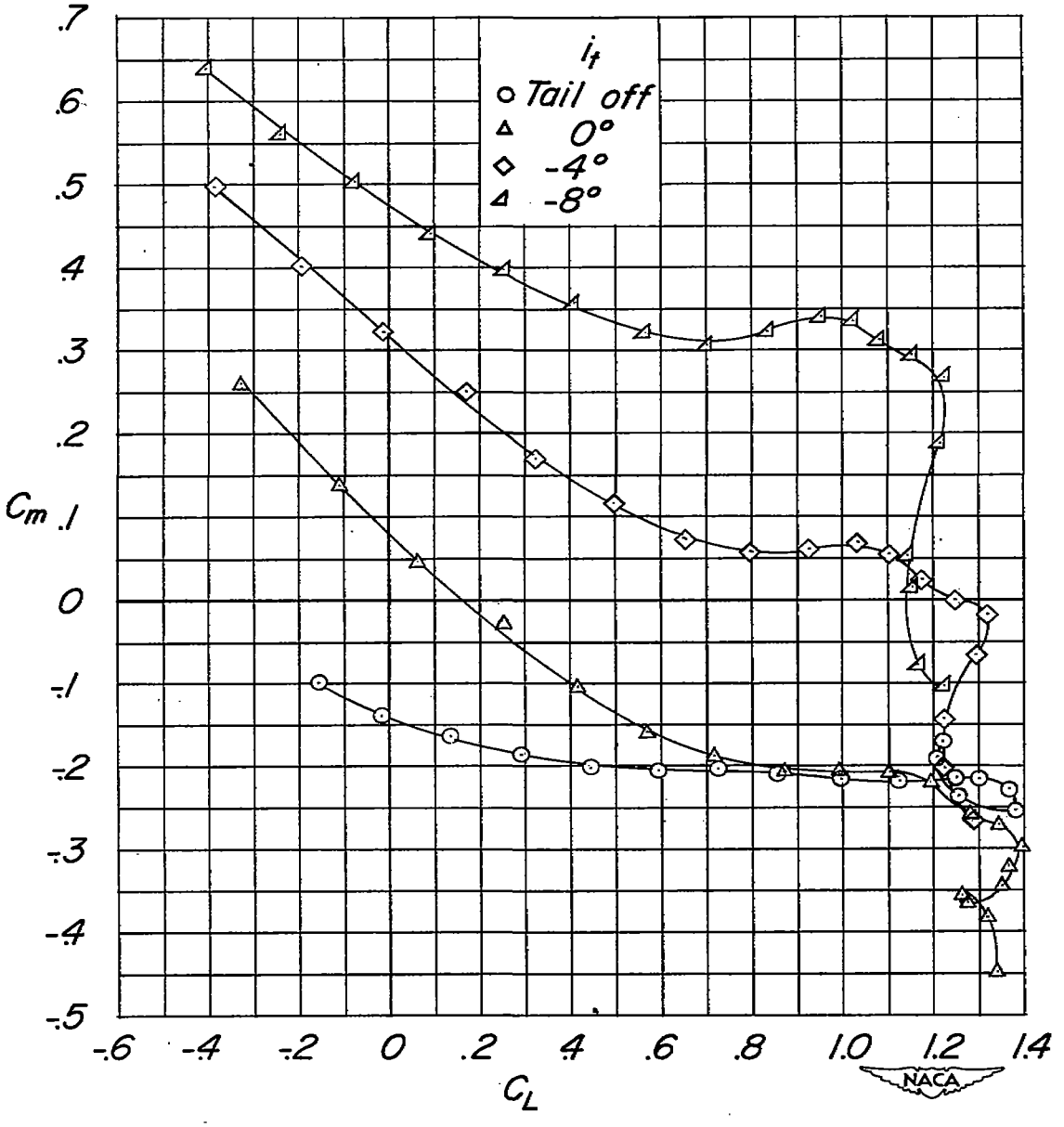

(c) Plain leading-edge flap deflected 30°; split trailing-edge flap deflected 50°.

Figure 29.- Concluded.

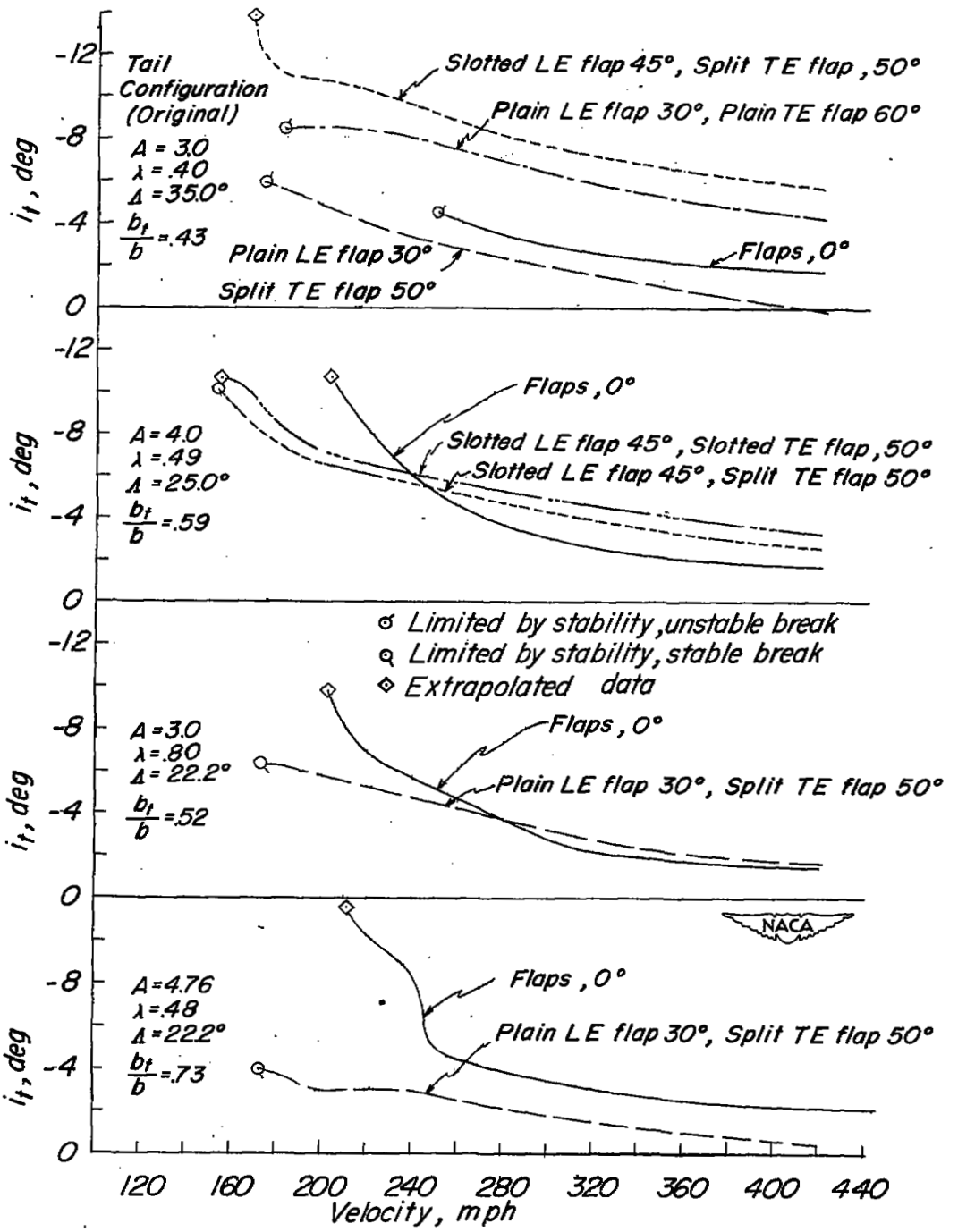

Figure 30.- Effect of various flap arrangements on the variation of horizontal-tail incidence with indicated airspeed of the airplane for steady flight conditions. Wing loading, 100 pounds per square foot.